ERBIUM-ZIRCONIA-YTTRIA-ALUMINUM CO-DOPED FIBER FOR AMPLIFIER AND NANOMATERIAL BASED ULTRAFAST LASER APPLICATIONS

ARNI MUNIRA BINTI MARKOM

DEPARTMENT OF ELECTRICAL ENGINEERING
FACULTY OF ENGINEERING
UNIVERSITY OF MALAYA
KUALA LUMPUR

2016

ERBIUM-ZIRCONIA-YTTRIA-ALUMINUM CO-DOPED FIBER FOR AMPLIFIER AND NANOMATERIAL BASED ULTRAFAST LASER APPLICATIONS

ARNI MUNIRA BINTI MARKOM

THESIS SUBMITTED IN FULFILMENT OF THE REQUIREMENTS FOR THE DEGREE OF DOCTOR OF PHILOSOPHY

DEPARTMENT OF ELECTRICAL ENGINEERING
FACULTY OF ENGINEERING
UNIVERSITY OF MALAYA
KUALA LUMPUR

2016

UNIVERSITY OF MALAYA

ORIGINAL LITERARY WORK DECLARATION

Name of Candidate: ARNI MUNIRA BINTI MARKOM

Matric No: KHA 120046

Name of Degree: DOCTOR OF PHILOSOPHY

Title of Project Paper/Research Report/Dissertation/Thesis ("this Work"): ERBIUM-ZIRCONIA-YTTRIA-ALUMINUM CO-DOPED FIBER FOR AMPLIFIER AND NANOMATERIAL BASED ULTRAFAST LASER APPLICATIONS

Field of Study: Electronic Engineering (Photonics)

I do solemnly and sincerely declare that:

(1) I am the sole author/writer of this Work;
(2) This Work is original;
(3) Any use of any work in which copyright exists was done by way of fair dealing and for permitted purposes and any excerpt or extract from, or reference to or reproduction of any copyright work has been disclosed expressly and sufficiently and the title of the Work and its authorship have been acknowledged in this Work;
(4) I do not have any actual knowledge nor do I ought reasonably to know that the making of this work constitutes an infringement of any copyright work;
(5) I hereby assign all and every rights in the copyright to this Work to the University of Malaya ("UM"), who henceforth shall be owner of the copyright in this Work and that any reproduction or use in any form or by any means whatsoever is prohibited without the written consent of UM having been first had and obtained;
(6) I am fully aware that if in the course of making this Work I have infringed any copyright whether intentionally or otherwise, I may be subject to legal action or any other action as may be determined by UM.

Candidate's Signature Date:

Subscribed and solemnly declared before,

Witness's Signature Date:

Name:

Designation:

ABSTRACT

The tremendous growth in telecommunications traffics increased the demand for very high speed, large capacity and long-haul transmission systems. Therefore, a new optical amplifier is required to overcome the limitations of conventional erbium-doped fiber amplifier. Besides optical amplifier, another interest is on pulsed lasers. Pulsed lasers have expanded an incredible attention in recent years as a possible replacement to high-cost and bulk solid state lasers especially for ultrafast technology with pulse duration down to the femtosecond and attosecond region which led to many diverse applications. In this work, a new Zirconia-Yttria-Aluminum co-doped Erbium-doped fiber (Zr-EDF) was investigated as gain medium for amplifier and pulsed laser applications. The fiber is heavily doped with erbium concentration with absorption pump power around 80 dB/m at 980 nm and was fabricated by using modified chemical vapour deposition (MCVD) process. For amplifier application, this fiber can be used to obtain an efficient gain and noise figure for both single- and double-pass configurations. For instance, at optimum length of 1 m for double pass amplifier, the highest gain of 40.3 dB was achieved at 1560 nm with noise figure less than 6 dB for the specific region. Moreover, a high flat-gain of 38 dB with gain fluctuation of ± 1.5 dB was successfully obtained within 1530 to 1565 nm wavelength. The new Zr-EDFA also performed better compared to the amplifiers configured with the previous Zr-EDF with a lower erbium concentration, conventional bismuth-based EDF (Bi-EDF) and the commercial silica-based EDF (Si-EDF). Pulsed Zr-EDF lasers (Zr-EDFLs) were also demonstrated by using various passive methods. A bright and dark pulse Zr-EDFL were delivered by using nonlinear polarization rotation (NPR) technique to generate dual-wavelength with pulse duration of 27 ns and repetition rate of 14.1 MHz. Q-switched pulsed laser was realized by using thulium-doped fiber (TDF) as solid state saturable absorber (SA) fiber. Bright solitons were also obtained by using high nonlinearity SAs of carbon nanotubes (CNTs) and graphene oxide with the

generation of ultrashort pulse duration of 770 fs and 600 fs, respectively. Finally, mode-locked Zr-EDFLs operating in dark pulse regime were successfully demonstrated using three types 2D nanomaterials SAs; graphene oxide, graphene film and black phosphorus as the mode-locker.

ABSTRAK

Pertumbuhan hebat di dalam laluan telekomunikasi menyebabkan permintaan tinggi kepada kelajuan tinggi, kapasiti besar dan sistem penghantaran yang jauh. Oleh itu, penguat optik yang baru diperlukan untuk menyelesaikan masalah terhad yang dihadapi oleh penguat gentian erbium-dop yang biasa. Selain itu, laser denyut juga merupakan bidang yang menarik perhatian ramai. Laser denyut berkembang dan mendapat perhatian kerana kemampuannya sebagai pengganti barangan pukal keadaan pepejal dan harga yang mahal terutamanya kepada teknologi ultralaju dengan denyut masa dari femtosaat and attosaat di mana ia membawa kepada pelbagai jenis bahagian aplikasi. Gentian Erbium Zirconia Yttria Aluminium ko-dop (Zr-EDF) yang baru dikaji sebagai pengantara pengganda diperincikan untuk aplikasi penguat dan laser denyut. Gentian ini mempunyai penumpu kedopan erbium yang sangat tinggi dengan kuasa penyerapan pam di antara 80 dB/m di 980 nm dan difabrikasi menggunakan kaedah pengewapan pemendapan kimia (MCVD). Bagi aplikasi penguat, fiber ini mampu digunakan untuk mendapatkan gandaan dan angka hingar yang berkesan untuk kedua-dua jenis konfigurasi iaitu tunggal dan ganda dua. Sebagai contoh, dengam penggunaan panjang fiber yang optimum di konfigurasi ganda dua, gandaan tertinggi 40.3 dB dikecapi di 1560 nm dengan angka hingar di bawah 6 dB. Tambahan pula, gandaan seragam yang tinggi sebanyak 38 dB dengan kadar naik turun ± 1.5 dB berjaya didapati dari gelombang 1530 ke 1565 nm. Zr-EDF baru ini juga menunjukkan prestasi yang lebih baik berbanding Zr-EDF lama dengan kedopan erbium yang lebih rendah, gentian tapak-bismuth erbium-dop (Bi-EDF) dan gentian komersial tapak-silika erbium-dop (Si-EDF). Laser denyut Zr-EDF (Zr-EDFL) juga dapat didemonstrasi dengan pebagai kaedah pasif. Laser denyut cerah dan gelap ditunjukkan dengan menggunakan kaedah putaran pengutuban taklinear (NPR) untuk menghasilkan dua-gelombang dengan denyut masa 27 ns dan kadar pengulangan 14.1 MHz. Laser denyut Q-suis pula ditunjukkan dengan menggunakan gentian thulim-dop

(TDF) sebagai keadaan padu gentian penyerap tepu. Soliton cerah pula dapat dikenalpasti dengan menggunakan penyerap tepu taklinear yang tinggi iaitu karbon tiub nano (CNTs) dan graphene oksida dengan pembentukan denyut masa yang sangat singkat iaitu 770 dan 600 fs sahaja. Akhir sekali, Zr-EDFL mod-kunci yang beroperasi di kawasan gelap berjaya didemonstrasi menggunakan tiga jenis bahan nano dua-dimensi (2D) sebagai penyerap tepu iaitu graphene oksida, graphene filem dan phosphorus hitam sebagai mode-pengunci.

ACKNOWLEDGEMENTS

Alhamdulillah, to the Most gracious and the Most merciful of the almighty Allah, I finally finishing my PhD studies.

First of all, my deepest appreciation is to my main supervisor, Prof. Dr. Sulaiman Wadi Harun for the valuable guidance, encouragement, patience and knowledge throughout my PhD journey. The continuous help and support for all my researches activity until the thesis completion. My appreciation is also to my co-supervisor, Prof. Dr. Harith Ahmad for his guide and support.

Special thanks for my beloved parents, Hj Markom and Hjh Maimun with your never ending praying and supports. Parents is not someone that we can choose, it was gifted by Allah, and I'm glad for having you as my parents. May Jannah is the only place that you will belong. To my dear lovely kids, Fahmi, Faheem and Fateha, the stars may stop twinkling, but my love for you is never fading. My appreciation is also to my husband and my siblings especially angah, thank you for the understanding, supports and motivation.

My sincere gratitude and appreciation is also for the members of Photonic Research Centre (PRC): Kak Sin Jin, Ajib, Arman, Kak Wati, Anas, An, Taufiq, Rafis, Zaimas, Ila, Kak Asiah, En.Faizal and Afiq for the help and knowledge shared in research activities. I am extremely thankful to be one of your friends with the joy and fun despite the ups and downs that we face during our journey.

My sense of gratitude to one and all, directly or indirectly, have lent their help and kindness in this venture. Finally, to the Universiti Teknologi MARA (UiTM) for providing me the Tenaga Pengajar Muda (TPM) sponsorship.

TABLE OF CONTENTS

CHAPTER 5: MODE-LOCKED FIBER LASER WITH 2D NANOMATERIALS

LIST OF FIGURES

LIST OF TABLES

LIST OF SYMBOLS AND ABBREVIATIONS

Aeff	:	Effective Area
$\emptyset_{NL}$	:	Fluctuating Refractive Index
AC	:	Autocorrelator
Al	:	Aluminium
ASE	:	Amplified Spontaneous Emission
Bi-EDF	:	Bismuth-based Erbium-doped Fiber
BP	:	Black Phosphorus
c	:	Speed of Light
CGLE	:	Complex Ginzburg-Landau Equation
CNTs	:	Carbon Nanotubes
CW	:	Continuous Wave
dB	:	Decibel
DCF	:	Dispersion Compensating Fiber
DSF	:	Dispersion Shifted Fiber
DWDM	:	Dense Wavelength Division Multiplexing
EDF	:	Erbium-doped Fiber
EDFA	:	Erbium-doped Fiber Amplifier
Er^{3+}	:	Erbium
FBG	:	Fiber Bragg Grating
FWHM	:	Full Width Half Maximum
FWM	:	Four-Wave Mixing
G	:	Gain
GFF	:	Gain Filtering Filter
GOSA	:	Graphene Oxide Saturable Absorber
GVD	:	Group Velocity Dispersion
HNLF	:	Highly Nonlinear Fiber
$h\nu$	:	Photon Energy
MoS_2	:	Molybdenum disulfide
NF	:	Noise Figure
NLSE	:	Nonlinear Schrödinger Equation
NOLM	:	Nonlinear Loop Mirror
NPR	:	Nonlinear Polarization Rotation
OSA	:	Optical Spectrum Analyzer

OSC	:	Oscilloscope
OSNR	:	Optical Signal-to-Ratio
PC	:	Polarization Controller
PD	:	Photodiode
PDI	:	Polarization Dependent Controller
Pin	:	Input Power
Pout	:	Output Power
Pr^{3+}	:	Praseodymium
RF	:	Radio Frequency
RFSA	:	Radio Frequency Spectrum Analyzer
SA		Saturable Absorber
SBS		Stimulated Brillouin Scattering
SEM	:	Scanning Electron Microscope
SMF	:	Single Mode Fiber
SOA	:	Semiconductor Optical Amplifier
SOP	:	State of Polarization
SPM	:	Self-Phase Modulation
SRS	:	Stimulated Raman Scattering
TBP	:	Time Bandwidth Product
TDM	:	Time Division Multiplexing
Te^{3+}	:	Terbium
TLS	:	Tunable Laser Source
Tm^{3+}	:	Thulium
WDM	:	Wavelength Division Multiplexing
XPM	:	Cross Phase Modulation
Y	:	Yttria
Yb^{3+}	:	Ytterbium
Zr^{4+}	:	Zirconium
Zr-EDF	:	Zirconia-based Erbium-doped Fiber
B_m		Birefringence Degree
E_p	:	Pulse Energy
I	:	Intensity of Light
Is	:	Saturation Intensity
L	:	Length of Fiber
n	:	Refractive Index

n_0	:	Linear Refractive Index
n_2	:	Nonlinear Refractive Index
P	:	Nonlinear Polarization
α_0	:	Linear Absorption Coefficient
α_{us}	:	Un-saturable Absorption
β_2	:	Group Velocity Dispersion Parameter
γ	:	Nonlinear Coefficient
$\delta\omega$	:	Frequency Chirping
ε_0	:	Vacuum Permittivity
λ	:	Wavelength
σ	:	Absorption Cross Section
τ	:	Recovery Time
τ_p	:	Pulse Width or Pulse Duration
χ	:	Linear Susceptibilities

CHAPTER 1: INTRODUCTION

1.1 Background

In 1917, when no one else had ever conceived of the possibility, Albert Einstein proved the existence of stimulated emission. It was the beginning for the evolution of laser technology that almost 100 years ago. Another breakthrough when the first laser was invented in 1960 at Hughes Laboratories by using ruby crystal in a shape of cube in a laser (Maiman, 1960). The main difference between laser and other light sources is, it produces a coherent photons of light where all the photons emits at the same magnitude, directions and phase, splendid in focusing a tight spot. This events finally granted the practical lightwave communication system to be realized worldwide in 1978.

The basic motivation to develop a new system in communications is to increase transmission capacity and distance, so that more information with very fast speed can be delivered around the world. The first installed optical fiber networks are used for transmitting telephony signals at approximately 6 Mb/s over distances around 10 km in the late of 1970s. It then significantly increased during 1980s to provide networks carrying beyond terabits per second over distances of hundreds of kilometres. At early 1990s, demand increases for hungry services transmission such as database queries, online shopping, blogging, high definition interactive video, remote education, worldwide social media and Grid computing.

To overcome the never-ending demand for high transmission bandwidth that ranging from home-based computer users to a large businesses and research group, telecommunications companies worldwide improved the capacity of fiber networks by adding more independent signal-carrying wavelength on individual fiber, and thus enhances the transmission speed of information that being carried by each wavelength. To date, a joint group of researcher from Netherlands and US, boost the fastest network

in the world that capable to carry 255 tera-bits per second data of information into one single glass fiber. Technically, the fiber competent enough to transfer 1 TB hard drive only in 31 milliseconds (Lichtenauer, 2009).

Optical amplifier is an enabling technology for the modern communication system based on dense wavelength division multiplexing (DWDM). It is required to extend the transmission bandwidth more than thousand kilometres without regeneration and external devices such as repeater for each wavelength. The amplifier is used to counterbalance for a fiber loss over the long haul transmission. The limitation of loss has commonly been overcome using repeaters which is first need to convert in electrical signal and then regenerated by using a transmitter. It was a complex and expensive for multi-channel communication systems such as DWDM. Thus, amplifiers is outstanding alternative to extend the system capacity, which amplifies the signal without the need converting in electrical signal. Moreover, it also provide low loss communication links compared to radio or electrical cables. As comparison to copper cable, optical fibers are immune to electromagnetic interference, lighter and cheaper with the same capacity of data information. Optical links are more reliable and capable to support future applications due to inherently large available capacity. These advantages improves the performance of telecommunication system, worldwide.

In general, there are four amplifier applications. The first is as in-line amplifiers that very important in long haul systems. The use of an amplifier is particularly fascinating for multichannel lightwave systems since it able to amplify all the channel simultaneously. Second is to enhance the transmitter power by insertion an amplifier just after transmitter. This amplifiers are known as power booster or power amplifier, as their key goal is to boost the transmitted power. A power amplifier could extend the transmission distance over thousands kilometres depend on the gain amplifier and fiber loss. Third is optical preamplifiers which are frequently used to increase the sensitivity

of receiver. Finally, the last amplifier is for compensating distribution losses in local area network.

To date, research focus to find the best solution to provide an amplifier with a flat gain characteristic. To amplify all wavelengths by nearly the same amount of gain, the double-peak nature of erbium gain spectrum forces one to pack all wavelengths near one of the gain peaks. As a result, the number of channels is limited not only by the amplifier bandwidth but also by the spectral non-uniformities. Thus, several techniques for gain-flattening have been established for this purpose such as the choice of host material, the choice of pump power level or by using spectral filtering at output of amplifier. This thesis will focus on evaluating a newly developed Zirconia-Yttria-Aluminum-based Erbium-doped fiber (Zr-EDF) to provide a high average flat-gain in a wideband region ranging from C- to L-band with an acceptable noise figure. Besides amplifier applications, the fiber will also be evaluated for fiber laser applications.

1.2 Overview on Recent Development of Pulsed Fiber Laser

Today, optical fiber plays an important role for communication application as well as various types of industries such as medical, military, aerospace, civil, geotechnical and many more engineering works. This is due to their efficiency, reliability and many other advantages. They are immune to many interferences such as electrometric interference, radio-frequency interference and crosstalk and could provide cost effective, compact size and design of devices. They are also flexible for bending or connecting to other link, low power loss, and very high security due to no leakage of light and extremely difficult to tap or break the fiber without people get noticed from it. One of the breakthroughs of fiber-optic technology is its applications in fiber lasers. Fiber lasers were first developed in the early 1960's. They operated at wavelengths of about 1 μm with just a few milliwatts (mW) of output power (Maiman, 1960; DeCusatis, 2013).

Fiber lasers have grew a remarkable interest in recent years as a possible replacement to high-cost, bulk solid state lasers. For high power applications, cladding pumped fiber lasers pumped by inexpensive diodes present simpler, lower cost and more compact solutions, in the fields of micro-machining, laser range finding, communication, remote sensing, biomedical imaging, medical surgery and surgical marking. Pulsed fiber lasers that operate in Q-switched or mode-locked regimes, emitting short pulses and ultrashort pulses on the order of nanoseconds (ns) to femtoseconds (fs), at repetition rates of kHz to MHz, respectively, possess specific advantages over continuous wave (CW) operation. They enables cleaner ablation of materials in micro-machining and medical surgeries, and precise measurement in remote sensing and laser range finding (Bass et al., 2009; Ramaswami, Sivarajan & Sasaki, 2009). Furthermore, pulsed lasers have extensive applications ranging from industry to optical communication.

Various laser configuration setups generate pulses with different and distinctive pulse characteristics. Hence, separately this laser setup can be designed to accommodate for each applications. For instance, pulsed laser with high peak intensity and high pulse energy is applicable for micromachining and drilling which useful for medical, electronic and automotive industries. In the medical field, pulsed laser is used in eye and dental surgeries whereas in electronic semiconductor industry, it used to mark information such as logo, manufactured date and batch number. Meanwhile, optical communication based on ultrafast fiber laser is commonly used for high speed and long distance network. Millions of computers are connected as people can communicate worldwide, freely. Ultrafast fiber laser is desired due to its high reliability, simple fabrication and resonator, least footprint and cost effective for large and most industrial applications. Multiplexing with Wavelength Division Multiplexing (WDM) is effectively offers a further boost in fiber transmission capacity. The basic operation of WDM is to use multiple wavelengths to transmit several independent information simultaneously over the same fiber.

Moreover, soliton pulse is desired for ultra-long haul transmission and was effectively employed and extend the distance more than one million km (Nakazawa et al., 1991). Two popular techniques to generate pulsed laser, there are active and passive pulsing methods. However, passive mode-locking is preferable for ultrashort pulsed laser, essentially due to the utilization of saturable absorber (SA) which modulates the resonator much faster than any electronic modulator that is required for an active mode-locking. The benefits of passive mode-locking are simple and compact design system, cost effective, robustness and ultrashort pulse formation. This thesis work is intended to explore passive pulsing approaches as well as the formation of different pulse profiles.

1.3 Problem Statement

Recent years, the tremendous growth in traffic telecommunications motivate researchers to develop highly efficient performance of fiber amplifier, which capable to increase the capacity transmission for WDM networks. An extensive researches had accomplished on erbium-doped fiber amplifier (EDFA) by using various types of host and co-dopant materials such as alumina, silica, phosphate, bismuth and telluride to improve the overall performance of amplifier including the gain, noise figures and cost of the devices (Bass et al., 2009; Digonnet, 2001; Agawal, 2007). So far, these materials demonstrate different qualities that bring a significant effect on the amplifier performance. Some materials have a wide transmission bandwidths that capable to amplify a further distance in transmission systems. Others offer high erbium concentration doping with minimal damaging effects such as concentration quenching and cluster generation, which is occurs in a short gain medium for compact devices. Commonly, this type of materials are also have minimal loss and thus, it improved the overall efficiency of amplifier.

In a choice of glass hosts, many researchers have focused on high silica glass owing to its proven reliability and compatibility with conventional fiber-optic components. Recently, lanthanum co-doped bismuth based erbium-doped fibers (Bi-EDFs) have been extensively studied for use in compact amplifiers with a short piece of gain medium (Harun et al., 2010). However, this type of fiber cannot be spliced with a standard single-mode fiber (SMF) using the standard splicing machine owing to the difference in melting temperature. Previously, a wideband erbium-doped fiber amplifier (EDFA) is demonstrated using a new type of erbium-doped fiber (EDF), which is fabricated in a ternary glass host, zirconia–yttria–alumina (Zr–Y–Al) co-doped silica fiber. With a combination of both Zr and Al, we could achieve a high erbium doping concentration of 2800 ppm in the glass host without any phase separations of rare-earths (Harun et al., 2011). It is found that a zirconia-based EDFA (Zr-EDFA) can achieve a better flat-gain value and bandwidth, as well as lower noise figure than the conventional Bismuth-based EDFA (Paul et al., 2010).

On the other hand, demand for ultrafast technology is never ending due to the development of fiber laser technology which offers compact and robust source with pulse width down to the femtosecond and attosecond region. Ultrafast fiber laser is desired due to its high reliability, simple fabrication and resonator, least footprint and cost effective for large and most industrial applications. Ultrashort pulses can be generated using passive or active technique, where passive mode-locking is preferable for ultrashort pulsed laser, essentially due to the utilization of saturable absorber (SA) which modulates the resonator much faster than any electronic modulator that is required for an active mode-locking. To date, the most versatile saturable absorber is based on semiconductor materials. However, they require complex manufacturing techniques, such as metal–organic chemical vapour deposition and molecular beam epitaxy. Therefore, researchers are working to discover more alternative material to compete this drawback.

In this thesis, a new Zr-EDF with high erbium concentration is proposed and developed to improve the attainable gain and reduces the noise figure of EDFA. An efficient Zr-EDFA with an improved gain is demonstrated using the new gain medium. Besides optical amplifier application, highly doped gain medium is also required for fiber laser applications. Here, various pulsed fiber lasers are also demonstrated using newly developed nanomaterials based passive SAs.

1.4 Research Objectives

Amplifier and pulsed laser are essential for long distance data transmissions in optical fiber communication systems. Thus, this PhD work aims to design and demonstrate practical amplifier and pulsed fiber lasers by using an improved Zr-EDF as a gain medium. To achieve this, several objectives have been outlined to guide the research route:

1. To characterize the optical characteristics of the enhanced Zr-EDF for both amplifier and pulsed laser applications.

2. To optimize and demonstrate an efficient optical amplifiers using the Zr-EDF as the gain medium.

3. To demonstrate both pulsed fiber lasers using the Zr-EDF as the gain medium in conjunction with the conventional passive techniques such as nonlinear polarization rotation (NPR), thulium fiber and carbon nanotubes (CNT) saturable absorbers.

4. To generate passively mode-locked Zr-EDFL using new 2D materials based saturable absorbers such as graphene oxide, graphene film and black phosphorus.

1.5 Thesis Overview

This thesis is organized into six chapters to comprehensively demonstrate an amplifiers applications for both single and double pass configurations and the generation of pulsed laser by using several new methods. Chapter 1 is the brief introduction about the background and motivation of this study. The aim and research objective of this study are also highlighted in this chapter. Chapter 2 describes a detail literature review, theoretical background and fundamental principles of erbium-doped fiber amplifier (EDFA), relevant nonlinear effects that occurring in optical fiber and fiber lasers.

Chapter 3 describes on the fabrication and characterization of a new Zr-EDF with a higher erbium concentration. Then, the performance of the Zr-EDFA is investigated and demonstrated for both single-pass and double-pass configurations for different active fiber lengths and pump powers in order to determine the optimize design. The performance of the enhanced Zr-EDFA is also compared with the use of the conventional Zr-EDF and other high concentration EDFs such as Bismuth-based EDF (Bi-EDF) and commercial IsoGainTM I-25 silica based EDF. Chapter 4 proposes and demonstrates Zirconia based Erbium-doped fiber lasers (Zr-EDFLs) operating in both Q-switched or mode-locked regimes are demonstrated using three different passive techniques. These techniques are NPR, thulium fiber and single-walled carbon nanotubes SAs.

Chapter 5 proposes and demonstrates various mode-locked fiber lasers using the newly developed Zr-EDF in conjunction with new SAs based on 2D nanomaterials. Three new SAs based on graphene oxide, graphene and black phosphorus (BP) are developed and used in this study. Finally, chapter 6 summarize all the research findings for this PhD work. A future work is also proposed in this chapter.

CHAPTER 2: LITERATURE REVIEW ON FUNDAMENTAL OF FIBER AMPLIFIER AND PULSED LASER

2.1 Introduction

Bringing 21st century, the fast-growing internet traffic dominates the worldwide communications since it becomes essential to everyday of human life. With the deployment fiber-to-the-home, this shows that the optical communication system is capable to support high data rates such as trillions bits of information carrying capacity in transmission bandwidth. Furthermore, optical nonlinearity gives a significant improvement which resulted the transmission distance to be spanned to longer distance and higher data rates. The evolvement of optical communication is mainly due to the rapid progress in the development of optical devices such as optical amplifiers (Harun et al., 2011; Ahmad, Shahi & Harun, 2010), optical switching (Heebner & Boyd, 1999) and wavelength converter (Olson et al., 2000; Yoo, 1996).

Moreover, the fiber optic communication has remarkable advantages such as large information-carrying capacity by using wavelength division multiplexing (WDM) technology. The WDM technology provides terabit per second data rates for transmission bandwidth. Together with WDM components, commercial systems able to transport more than 100 channels in a single optical fiber (Bobrovs et al., 2009). Hence, the connected systems can be improved continuously without additional of a new device, which makes it promising to construct a cost effective WDM systems as well as much greater capacity (Azadeh, 2009). The increment of number of channels in such systems will eventually result in the usage of more optical signal de-multiplexing components which will introduce losses to the system. Furthermore, when transmits over long distances, the signal is extremely attenuated. To overcome this, optical engineers need to perform optical power budget analysis to ensure that the transmitted signal is detectable at the

receiver. As for the choice of optical amplifier, erbium-doped fiber amplifiers (EDFA) is preferable due to high power transfer efficiency from pump to signal power, wide spectral amplification with flatter gain, low noise figure and suitable for long-haul applications.

Besides optical amplifier, another breakthrough of fiber-optic technology is fiber lasers. Fiber lasers have expanded a tremendous attention in recent years as a possible replacement to high-cost, bulk solid state lasers. To date, many works have been focused on developing ultrashort pulsed fiber lasers operating in either Q-switched or mode locked regimes. This chapter presents a thorough literature reviews on various topics such as optical amplifier, EDFA, nonlinear effects, fiber lasers, Q-switching and mode-locking mechanism, which are related to this thesis.

2.2 Optical Amplifiers

In long haul fiber optic communication systems, optical fiber loss is the factor that limits the transmission of signal across large distance. This causes signal to degrade as it propagates down the optical fiber. Then, a repeater, an electronic device, was developed to overcome signal degradation by amplifying the signal along the optical fiber so that signal can be amplified and thus can propagate further down the optical communication link. The operation of a repeater is described in Figure 2.1. The repeaters produce a clean amplified signal but it is complex and expensive device. It provides amplification in electrical domain based on regeneration of the signal where optical signal is converted to electrical signal first for amplification. Here, the electrical signal is also processed to remove the effect of dispersion. The electrical signal is then converted back to optical domain and is ready for retransmission down the fiber. The amplification of optical signal using regenerator involves signal conversion from the optical domain to electrical and back to the optical domain.

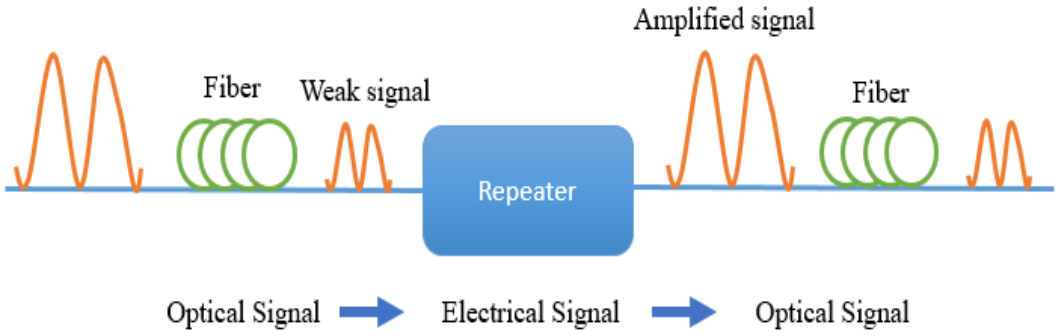

Figure 2.1: An electronic repeater basic operation

Later on, an optical amplifier is introduced where signal amplification is carried out in the optical domain itself. Optical amplifier is insensitive to bit rates and modulation format and thus provides the flexibility where optical transmission system can be easily upgraded without the need to replace amplifiers (Bass et al., 2009). This significantly revolutionized the long distance communication network which led to many diverse applications. Generally, optical amplifiers that are widely used nowadays can be categorized into three, which are based on semiconductor optical amplifier (SOA), rare-earth doped fiber amplifier and nonlinear optical amplifier. SOA is popular due to their small 14-pin butterfly package for booster applications, but it suffer from large noise figures and narrow bandwidth. Nonlinear amplifier such as Raman amplifier is preferable in many choices due to high gain and wideband transmission link with very little noises. The working principle for nonlinear optical amplifier is different compared to SOA and rare-earth doped amplifier where it is based on photon-phonon interaction. However, Raman amplifier requires high intensity pump and long gain medium and is it costlier than rare-earth doped fiber amplifier.

On the other hand, rare-earth elements such as Erbium (Er^{3+}), Praseodymium (Pr^{3+}), Ytterbium (Yb^{3+}), Terbium (Te^{3+}), and Thulium (Tm^{3+}) are doped into silica based fiber to realize an active medium for optical fiber amplifiers. Rare-earth doped fiber

amplifiers are just like a laser diode without feedback and signal is amplified through stimulated emission process. Figure 2.2 shows the operation of rare-earth amplifier where the optical gain accomplished when the amplifier is pumped to excite more ions to the higher state of energy level, this phenomenon known as population inversion. The most popular doped fiber amplifiers is erbium doped fiber amplifier (EDFA) where the emission of Erbium ions fall into the third communication window (1550 nm) where loss is minimum. Besides that, EDFA is cost effective, more reliable, can produce high gain up to 40 dB, minimal noise figure, no coupling loss to the transmission fiber, flexible to be integrated with the fiber devices and telecommunication link, and the gain provided by EDFA is polarization insensitive (Bass et al., 2009; Ghatak & Thyagarajan, 1998; Agrawal, 2007). As EDFA has more advantages compared to the other optical amplifiers, this thesis is focused on developing an efficient and compact EDFA. Besides amplifier application, the Erbium-doped fiber (EDF) is also widely used in fiber lasers.

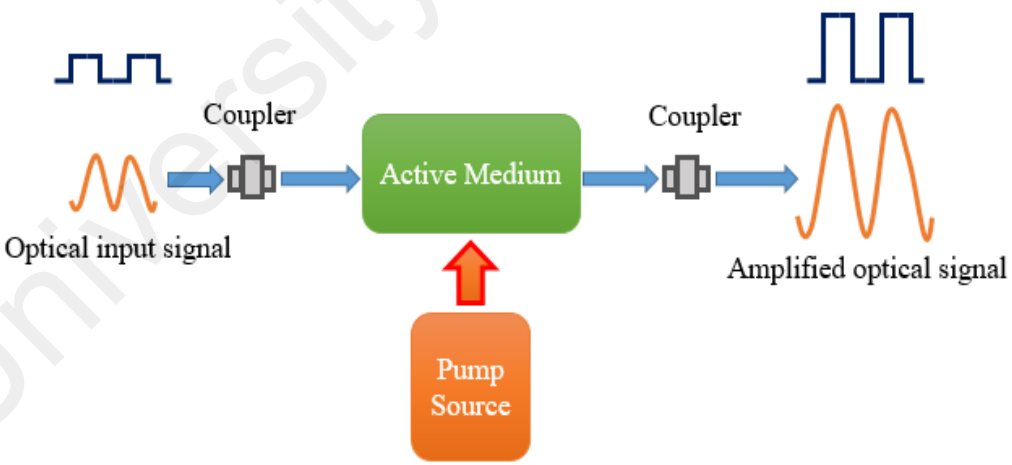

Figure 2.2: Basic operation of optical amplifier

2.3 Erbium-doped Fiber Amplifier (EDFA)

EDFA was invented by Mears et al. (1987) to reduce the cost and complexity of light amplification process in long-haul transmission link. In 1991, the first optical

amplifiers based fiber-optic system was demonstrated by Giles and Desurvire (1991). The carrying information capacity was improved by 100 times compared to the conventional system with electronic amplifiers. Today, EDFA still expanding their applications for worldwide communications with very high speed and large capacity information carrying for many industries including the military, medical, telecommunication, networking and broadcasting (Naji et al., 2011; Bass et al., 2009). Figure 2.3 shows a typical EDFA configuration setup consists of an EDF as the gain medium, optical isolators and couplers. The EDF is pumped bi-directionally with two pumps. One of the pump signal travels in the same direction as the input signal while the other pump signal propagates in the opposite direction to input signal. Isolator is used to prevent any backwards signal from entering the device as well as preventing the amplified spontaneous emission (ASE) noise from disturbing the transmission network. Meanwhile the couplers used are to multiplex input signal with pump signal.

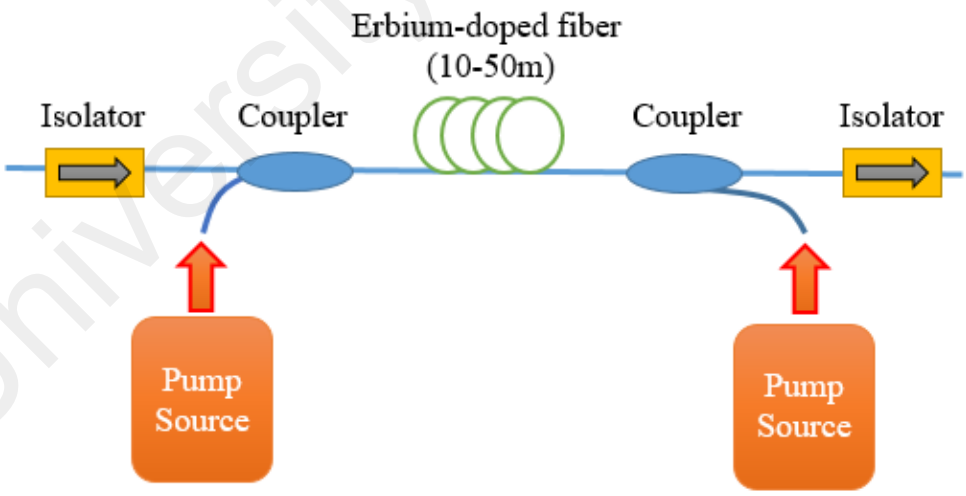

Figure 2.3: Basic configuration setup of EDFA

The EDFA is characterized based on gain and noise figure. The term of gain commonly used to define the strength of amplification in optical amplifiers. The gain, *G* is also known as amplification factor in decibels and it is simply defined as:

$$G\ (dB) = 10\ log_{10}\left(\frac{Pout}{Pin}\right) \quad (2.1)$$

where *Pin* and *Pout* are the input and output powers of the continuous-wave (CW) signal being amplified (Agrawal, 2007). On the other hand, noise figure (NF) is also an important parameter that describes the performance on an optical amplifier. NF comes from ASE noise that originates from the mixing of the desired coherent signal with incoherent ASE signal when gain medium is pumped by laser diode. High NF will lead to the attainment of smaller optical signal-to-noise ratio (OSNR) of amplifier due to spontaneous emission that grow the noise to the desired signal during amplification process. The NF also uses the same unit likes optical gain in decibel (dB) and is written as:

$$NF = \frac{(OSNR)\text{in}}{(OSNR)\text{out}} \quad (2.2)$$

In general, ASE noise can be reduced by providing the highest population inversion, operate in deep saturation regime and by using two or more amplifier stages and by positioning bandpass filter and isolators between the stages. The excellent NF for EDFAs are obtained with the configuration setup that gives the highest population inversions. It is worthy to note that the theoretical lowest value of NF is 3 dB (Bass et al., 2009). The illustration of amplification process within a gain medium is shown in Figure 2.4. When the pump signal travels down the gain medium, it is amplified and random emission is produced along the fiber. Thus, it is essential to provide a gain medium with capabilities to accomplish high population inversion to surpass the ASE noise and lowering the noise figure of amplifier.

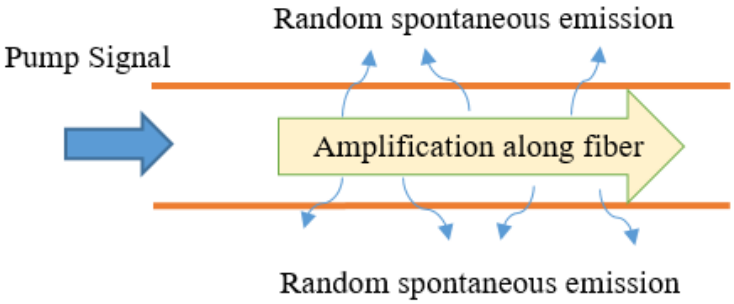

Figure 2.4: Illustration amplification within a gain medium

2.4 Flat-gain Amplifier

Flatness gain is defined as uniform gain for all wavelengths which is crucial for long-haul transmission network with multiple amplifier stages. An EDFA which can maintain the optimum flatness gain over a broad transmission network is highly desirable in WDM systems. It makes the systems to be immune to add/drop multiplexing, link loss change, pump deterioration and network reconfigurations (Kim et al., 1998; Yusoff et al., 2010). When there are obvious fluctuation of gain between signals that transmitted by amplifier, the fluctuation turn out as additional noise and cause depreciation to OSNR at the end of receiver. Thus, the longer transmission distance with many amplifier stages, the larger noise will accumulated, and it degrades the overall performance of WDM system. Therefore, the need of flat-gain EDFA was demanding to maintain a sufficient signal to noise ratio at all wavelengths. Figure 2.5 compares the output gain spectrum after a single and multiple EDFA in long-haul communication system. It shows that the multiple amplifier produces a significant larger gain's fluctuation at the output.

Up to date, a lot of techniques were explored to produce a flat-gain amplifier such as the incorporation of gain filtering filters (GFFs) and Mach-Zehnder filter in the amplifier's device. Filter was used to equalize both of signal power and OSNR performances for multi-wavelength signal over a long transmission distance (Kim et al., 1998). Nevertheless, most of these filters are unpractical due to sensitivity in temperature

changes and the use of external device contributes to the additional losses and cost. Then, a new design of gain clamping was demonstrated by Harun and Ahmad (2003) with the utilization of fiber Bragg grating (FBG) at the end of amplifier's system. This FBG successfully acts as a filter and reduce the peak at response curve of optical gain. Recently, a flat-gain amplifier was also demonstrated using new types of gain medium such as bismuthate based EDF and Zirconia co-doped EDF (Zr-EDF) with very high erbium concentration doping (Ahmad et al., 2010; Harun et al., 2011). Bismuthate based EDF is difficult to be integrated with other optical devices while Zr-EDF shows a promising candidate to obtain the optimum average flat-gain for long distance applications.

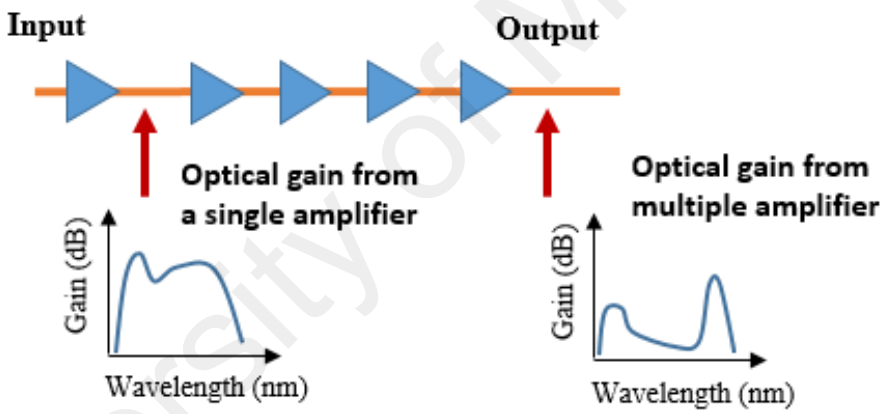

Figure 2.5: Optical gain spectrum with single and multiple amplifier in long haul signal transmission

2.5 Nonlinear Effects in Optical Fiber

A dielectric medium of optical fiber will respond to the nonlinearities when exposed to strong electromagnetic fields. The basic principle of nonlinear effects is related to a harmonic motion of bound electrons under the influence of an applied field. Consequently, the total polarization activated by electric dipoles is changed from linear to nonlinear by following equation (Agrawal, 2006):

$$\boldsymbol{P} = \varepsilon_0 \chi^{(1)}.E + \varepsilon_0 \chi^{(2)}.E^2 + \varepsilon_0 \chi^{(3)}.E^3 \quad (2.3)$$

where ε_0 is the vacuum permittivity whereas $\chi^{(1)}, \chi^{(2)}$ and $\chi^{(3)}$ are the linear susceptibilities. As the field intensity increases, these nonlinear polarization of $\boldsymbol{P}$ become more and more important, and this will lead to a large variety of nonlinear optical effects. The first order of $\chi^{(1)}$ represents the linear optical and is the dominant contribution to **P**. The second order of $\chi^{(2)}$ is responsible to second harmonic and total frequency generation while the third order of $\chi^{(3)}$ is subjected to the third harmonic generation, nonlinear refraction and four wave mixing.

Optical fiber nonlinearities can be classified into two categories. The first group of nonlinearities arises from the changes refractive index of optical fiber which is known as Kerr effect. These effects include self-phase modulation (SPM), cross-phase modulation (XPM), four-wave mixing (FWM) and saturable absorption. The second group encompasses nonlinear inelastic scattering processes which are stimulated Brillouin scattering and stimulated Raman scattering. For the following section, only the applicable nonlinear effects such as SPM, XPM, FWM, saturable absorption and NPR are presented.

2.5.1 Self-Phase Modulation (SPM)

SPM attributes to self-induced nonlinear phase shift of pulsed laser due to the changes of refractive index in response to optical intensity. The refractive index n of fiber is depended on optical intensity and thus it is expressed by (Keiser, 2003):

$$n = n_0 + n_2 I \quad (2.4)$$

where n_0 is the linear refractive index, n_2 is the nonlinear refractive index and I is the light intensity. Thus, the higher intensity of light will response to the high refractive index of fiber compared to the lower light intensity when the pulse propagates through the fiber. The fluctuating refractive index $\emptyset_{NL}$ over the fiber length L will induce nonlinear phase change of an optical pulse by (Agrawal, 2000):

$$\emptyset_{NL} = \frac{2\pi}{\lambda} n_2 LI \tag{2.5}$$

where λ is the operating wavelength. To observe the effect of SPM, consider an optical pulse propagates in a fiber as illustrates in Figure 2.6. The edge of the pulse represent a time-varying intensity, which will generate a time-varying refractive index. Thus, the rising edge will see a positive $\frac{dn}{dt}$ whereas the trailing edge will see a negative $\frac{dn}{dt}$.

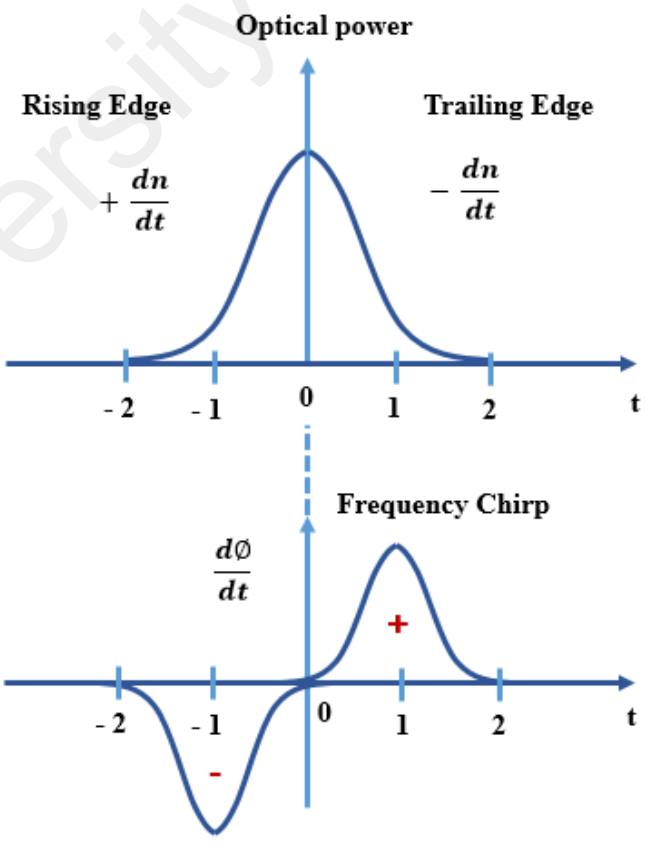

Figure 2.6: Phenomenological description of a pulse broadening due to SPM

Then, the phase fluctuations will result different phase shift due to intensity dependent. SPM effects more on higher intensity pulses due to degree of chirping is dependent on optical power. The frequency change is given by (Tai & Wilkinson, 2003):

$$\delta\omega(T) = -\frac{\partial \emptyset_{NL}}{\partial T} \tag{2.6}$$

The time dependence of $\delta\omega$ is referred as frequency chirping. The rising edge of a pulse experiences a red shift in frequency (toward downshift frequencies), while the trailing edge of a pulse experiences a blue shift in frequency (toward upshift frequencies). This chirp will increase with propagated distance. As pulse propagates through a fiber, new frequencies are generated. The SPM induced chirps and effect to dispersion, thus it leads to the spectral broadening.

2.5.2 Cross-Phase Modulation (XPM)

XPM is similar to SPM, except it happens when two or more pulses with different frequencies overlap. These frequencies co-propagate simultaneously in a nonlinear medium. The reason is each nonlinear refractive index of signal changes not only be influenced by light intensity, but also depends on the intensity of the co-propagating light. The refractive index that change due to XPM can be expressed as (Agrawal, 2000):

$$n = n_0 + n_2 |I_1 + I_2|^2 \tag{2.7}$$

The equation above illustrates that refractive index change is influenced by intensity and the co-propagating pulses. The sum of nonlinear phase shift is expressed by (Singh & Singh, 2007):

$$\emptyset_{NL}(t) = \frac{2\pi}{\lambda} n_2 L [I_1(t) + 2 I_2(t)] \tag{2.8}$$

The expression shows that the strength of the effect is increased by a factor of 2 and effectively doubled the nonlinear refractive index n_2 in XPM. In fact, XPM always presents together with SPM in an optical fiber.

2.5.3 Four-Wave Mixing (FWM)

FWM is a kind of optical Kerr effect and it occurs when at least two or more frequencies are involved, and generate a new wave at new frequency. FWM is a third-order nonlinearity susceptibility of $\chi^{(3)}$ in silica fibers. The combination of SPM and XPM are significantly mainly for high bit rate systems, however the FWM effect is independent of the bit rate and critically depends on the channel spacing and fiber dispersion. Figure 2.7 shows the FWM phenomena between two and three signal frequencies in optical fiber. A simple example for two interaction signal frequencies between ω_1 and ω_2 generate another two new frequency components at frequency ω_3 ($\omega_3 = 2\omega_1 - \omega_2$) and ω_4 ($\omega_4 = 2\omega_2 - \omega_1$) as shown in Figure 2.7 (a). Similarly, Figure 2.7 (b) describes nine sidebands frequencies are generated when three optical signals at frequencies ω_1, ω_2, and ω_3 interact each other. Thus, for N-wavelengths launched in a fiber, the number of generated sidebands frequencies M is (Keiser, 2003):

$$M = \frac{N^2}{2}(N-1) \tag{2.9}$$

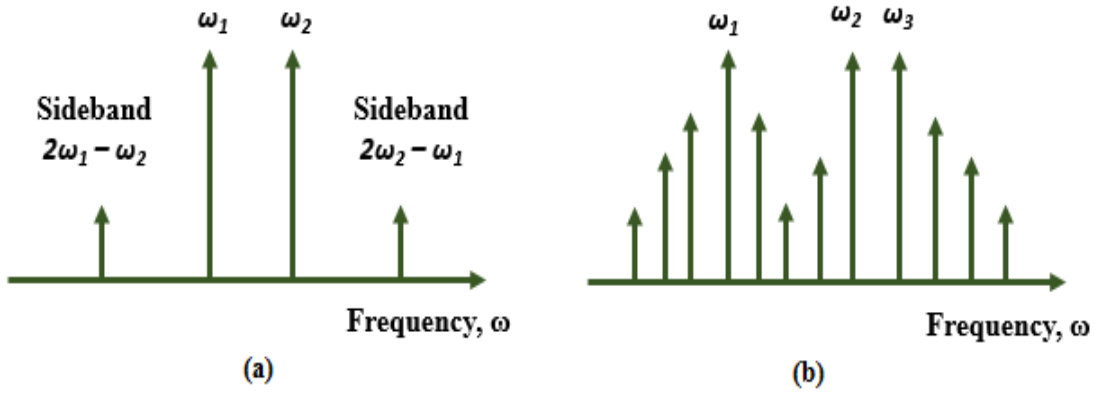

Figure 2.7: FWM phenomena: (a) two and (b) three optical signals co-propagating in optical fiber

In general, FWM effect can be either damaging or beneficial in optical fiber depends on the applications. FWM decreases WDM systems performance due to inter-channel crosstalk and creates additional noise in the system. However, this effect still can be useful in other application such as for the formation of anti-Stokes lines in multiwavelength fiber laser. It can stabilize and flatten multiwavelength emission due to the capabilities to suppress the mode competition caused by EDF when energy is transferred from high to low power signal.

2.5.4 Saturable Absorption

Saturable absorption is related to a situation where any low intensity light will be absorbed whereas high intensity light is delivered with less attenuation. In other word, the absorption finally saturates and disappears at high intensity light. The absorption coefficient is explained by (Nisoli et al., 1997):

$$a = \frac{a_0}{1+I/Is} + a_{\text{us}} \qquad (2.10)$$

where $\frac{\alpha_0}{1+I/Is}$ is the saturable absorption, α_{us} is the un-saturable absorption, α_0 is the linear absorption coefficient while I and Is are the optical and saturation intensity, respectively. Saturation intensity of a saturable absorber is defined as the required optical signal intensity in a steady state to decrease the absorption into half of its small-signal value. For the generation of ultrafast pulsed laser, saturation intensity is a crucial parameter for the initialization pulse formation process. The saturation intensity is described as the following equation (Nisoli et al., 1997; MacDonald, 2010):

$$Is = \frac{hv}{\sigma\tau} \tag{2.11}$$

where hv is the photon energy, σ is the absorption cross section from ground state to upper state and τ is the recovery time. Recovery time is the return of the atom population to the ground state. Therefore, for ultrashort pulses, the high saturation intensity potentially to produce a slower recovery time and allows self-starting mode-locked from normal noise fluctuations in fiber laser cavity.

Table 2.1 illustrates the two categories for saturable absorption effect that uses in fiber laser. The first category of saturable absorber is named as real saturable absorber (SA) such as semiconductor SA mirrors (also known as SESAMs) (Moghaddam et al., 2011; Li et al., 2012), GaAs, thin layers of CNT (Ismail et al., 2012; Harun et al., 2013), graphene (Haris et al., 2015; Zen et al., 2013) and in rare cases, the SA materials are used from optical fiber. The common fiber that acts as SA are chromium (Laroche et al., 2006), holmium (Kurkov et al., 2009), or bismuth (Dvoyrin et al., 2007; Bufetov & Dianov, 2009) that show an ability to generate Q-switching pulses. The second category is the artificial SA, which is normally realized by using certain optical components to mimic the real SA for pulse generation. The components are Kerr lensing combined with an aperture, nonlinear polarization rotation (NPR) in a birefringence fiber with polarizing

element, nonlinear loop mirror (NOLM) and nonlinear waveguide arrays. A laser with SA tends to operate with minimum cavity loss per round trip and the longitudinal modes of laser become phase locked.

Table 2.1: Saturable absorption effect categories

Real Saturable Absorber	Artificial Saturable Absorber
SESAM, GaAs, CNT, Graphene, Optical fiber (Chromium, Holmium and Bismuth fiber)	Kerr lens mode-locking, NPR, NOLM, Nonlinear waveguide arrays

2.5.5 Nonlinear Polarization Rotation (NPR)

NPR or also known as nonlinear birefringence is a phenomenon that causes a rotation of light in a fiber depend on the strength of light intensity. The rotation will change the phase shift and state of polarization (SOP). It is a nonlinear intensity-dependent loss process due to the effect of polarization rotation relies on light intensity. Physically, this effect is related to SPM and XPM as well as birefringence of the fiber. Besides, NPR effect is capable to suppress the mode competition in EDF and allows dual or multi-wavelength generation for ultrashort pulses. The important components required to accomplished NPR effects are a birefringence fiber or a high nonlinearity fiber and a polarization controller (PC). The birefringence degree B_{m} is defined as (Agrawal, 2006):

$$B_{\mathrm{m}} = |n_{\mathrm{x}} - n_{\mathrm{y}}| \tag{2.12}$$

where n_{x} and n_{y} are the refractive indexes of the x and y axis in the fiber. Birefringence is also known as double refraction because it refract into two different directions when light goes into a fiber.

The basic operation of NPR is illustrated in Figure 2.8, as a light propagates in a fiber, the polarization is oriented to x and y-axis that occurs from birefringence fiber and produce an angle for the rotated light. The two orthogonal polarized light of E_x and E_y will gather nonlinear phase shift due to the SPM and XPM in the fiber. The degree of rotation is directly proportional to the light intensity where the high intensity will obtain larger phase shift compared to the lower intensity of light. PC is used to twist the polarization of light, thus only certain polarization of light that is exactly aligned to the axis of the polarizer passes through the polarizer. The transmission of light can be expressed as (Agrawal, 2006):

$$T = cos^2\alpha_1, cos^2\alpha_2 + sin^2\alpha_1, sin^2\alpha_2 + \frac{1}{2}\sin 2\alpha_1, \frac{1}{2}\sin 2\alpha_2 \cos(\Delta\emptyset_L + \Delta\emptyset_{NL}) \quad (2.13)$$

where α_1 is the angle between input signal and the fast axis of fiber, α_2 is the angle between a polarizer and the fast axis of fiber, $\emptyset_L$ is linear phase shift which is relates to SPM from birefringence fiber and $\emptyset_{NL}$ is the nonlinear phase shift that contributes from XPM effects. The blending of PC-fiber-PC-polarizer components acts as an artificial saturable absorber that contributes for the mode-locking generation. The PC is twisted to allow the high intensity of light passes whereas the low intensity of light is restrained. Subsequently, this leads to the formation train of pulses.

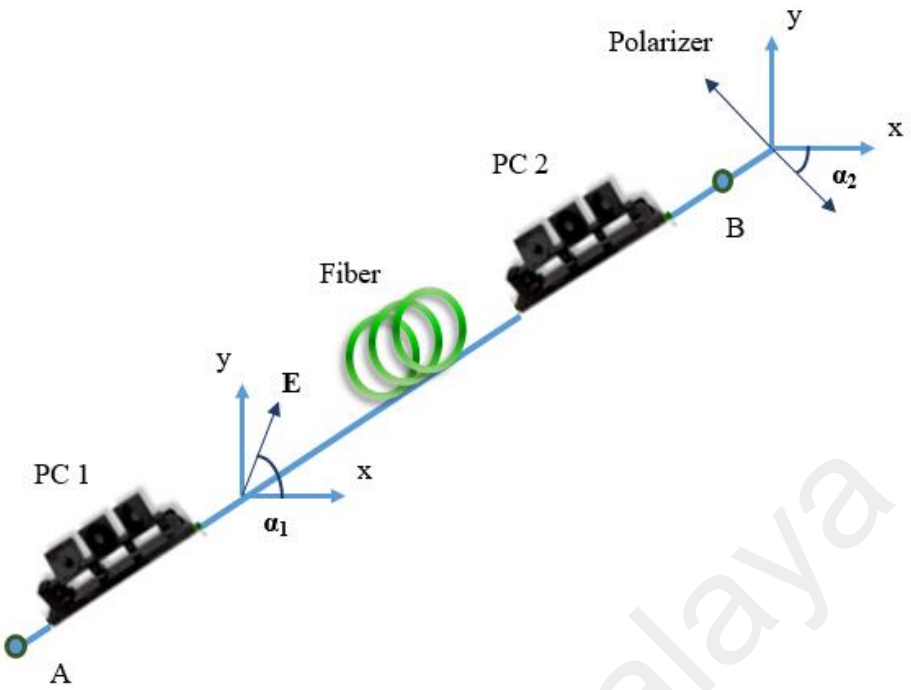

Figure 2.8: Basic operation of NPR

2.6 Pulsed Laser

A continuous wave (CW) laser means the laser runs continuously over the time while a pulsed laser produces a pulse train with a certain repetition rate of duration. The CW laser usually oscillates in random phase and amplitudes. The pulse laser can be classified into two common categories based on operating conditions in generating laser; Q-switching and mode-locking. Both categories are able to obtain pulses either by using active or passive method. An active method involves an external signal component, a type of modulator that induces a modulation of intra-cavity light and producing a long pulse duration whereas passive method, can be achieved by incorporating a SA with suitable properties into a laser cavity (Harun et al., 2015; Ismail et al., 2014). As comparison, active method generates a longer pulse since it needs an external device such as optical modulator to initiate pulse. In addition, the active laser is more complexity in design laser cavity. While passive method offers the development of much shorter pulses, that driven by a very short pulses due to employment of SA, and modulates the cavity losses swiftly

than electronic modulator. The shorter the circulating pulses, the faster the loss modulation obtained. The next sub-section further explains the Q-switching and mode-locking principles. The related techniques for the pulsed generation in this PhD work is also reviewed such as NPR and SAs.

2.6.1 Principles of Q-switching

Q-switching is a method of pulsing the laser output by insertion a time variable loss inside the laser cavity to modulate a quality factor (Q-factor) of an optical resonator. The Q-factor describes the rate of photon loss out of the cavity where a high Q value represents a low loss cavity and able to store a large amount of energy and vice versa for a low Q value. Figure 2.9 shows a schematic diagram to explain the Q-switching phenomena. In Q switching, the Q-value is first kept low in order to suppress lasing and store energy inside the laser material as shown in Figure 2.9 (a). As a gain medium is pumped, the doped fiber begin to develop population inversion and allows the fiber to store more energy in cavity as shown in Figure 2.9 (b). After a while, as illustrated in Figure 2 (c), all the electron reached at the upper level which defines as excellent population inversion, and then the gain starts to saturate Figure 2.9 (c). The loss reduces as the gain increases due to the large number of the photons generated. This activates to a high Q factor in cavity to allow a rapid onset of lasing in the cavity. The abrupt changes of number of photons causes a giant optical pulse with high peak power is generated as illustrated in Figure 2.9 (d).

Passively Q-switched pulsed laser activates without the need any external control depending on the saturable absorption process. The function of light intensity enhances by transmission of SA or Q-switched. Firstly, the SA pulse is unstable and put the cavity at low Q. The population inversion and gain increases by constantly energy feeds into the systems, proportionally over the time. Eventually the laser touches the threshold at low

Q and then, the cavity starts to generate coherent and desired light. When the SA is bleached, it swiftly shrinking the loss and boost the gain of the pulsed laser to the highest value. Before the SA starts its recovery for the next cycle, a giant pulse is released by the stored inversion. Normally, the pulse duration of Q-switched is in nano- and micro-seconds depending on the photon lifetime whereas the repetition rate is ranging between kilo- to micro-Hertz.

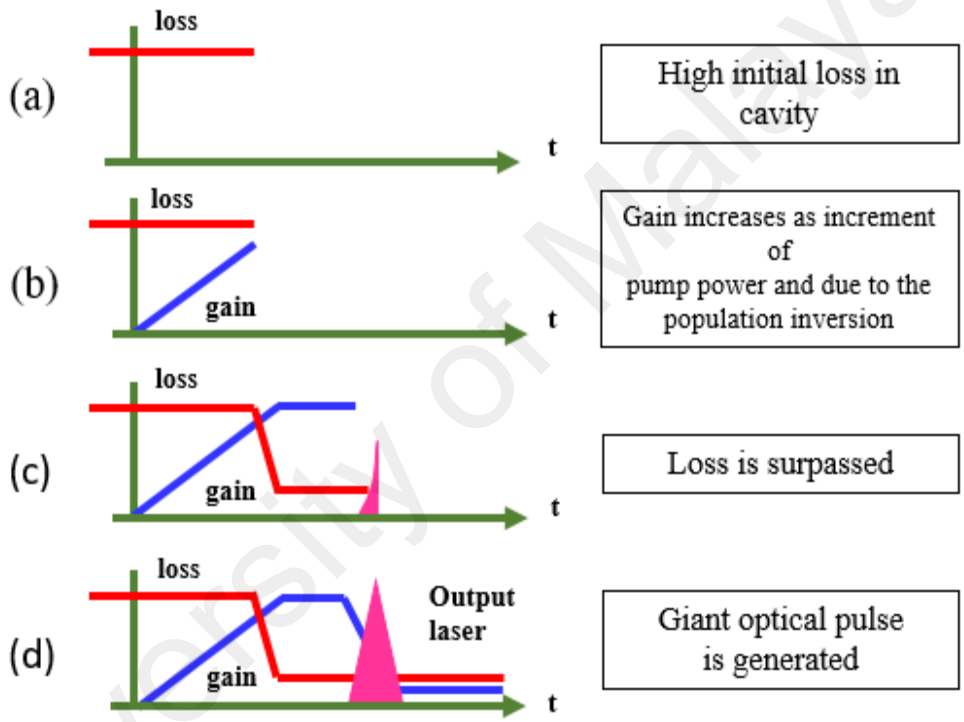

Figure 2.9: The generation of Q-switched pulse

2.6.2 Principles of Mode-locking

In laser cavity, longitudinal modes are produced when a group of frequencies circulating in laser cavity and develop more optical gain than losses. They also known as independent oscillators which allows the laser to emit continuously. Figure 2.10 illustrates three independent longitudinal modes that propagates in mode-locked laser cavity. When a fixed phase exists between these modes, the cavity starts to produce a

generation train of pulses. A narrower pulse duration is obtained when more modes are locked together where typically smaller than Q-switched pulsed laser, in the range of pico- to femto-seconds subjected to the laser cavity properties.

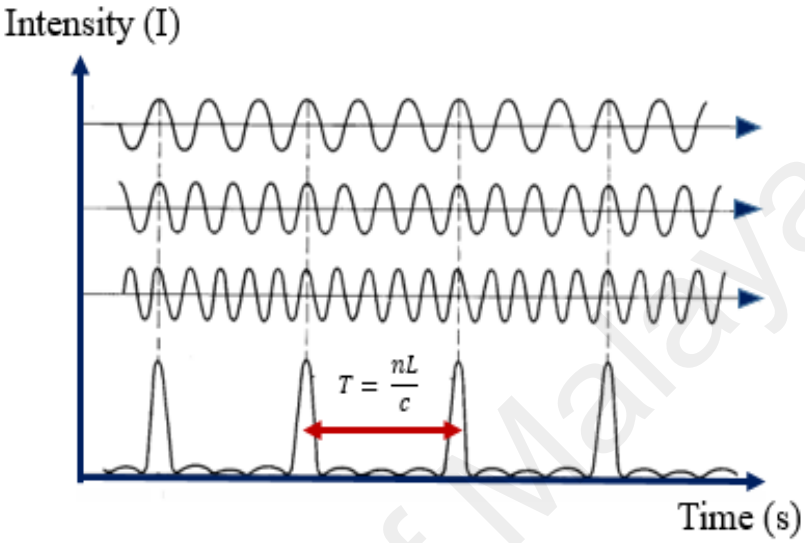

Figure 2.10: Three longitudinal modes leads the principles of mode-locking

Moreover, when a single pulse is circulating in a ring cavity, the period T is defined as (Agrawal, 2007):

$$T = \frac{nL}{c} \tag{2.14}$$

where L is the length of total cavity, n is refractive index of fiber and c is speed of light. Mode-locked pulse grows a spotlight due to its capabilities to develop very high repetition rate in the range of Mega- to Tera-Hertz with an ultrashort pulse duration.

2.6.3 Development of NPR and SAs in Pulsed Generation

As mentioned, Q-switched and mode-locked pulses can be generated by using either active or passive element in cavity. Active method uses an external modulator to induce a modulation whereas passive method is relies on some nonlinear element which

induces an intensity-dependent response and cause a self-modulation of light. Only applicable techniques are demonstrated at following sub-sections, and there are NPR and saturable absorber (SA) method. Hofer et al., was the first demonstrated the NPR method using exploitation of SPM and XPM to generate pulsed laser with pulse duration of 70 fs back in 1991 (Hofer et al., 1991). Further experiment arose with the development of bright soliton with pulse duration of 1.5 ps on 1992 whereas dark soliton with the pulse duration of 500 ps on 2009 by using this technique in anomalous and normal dispersion, respectively (Matsas et al., 1992; Zhang et al., 2009). The important components required to create NPR method are polarization sensitive element and birefringence fiber to allow an intensity dependent transmission for pulsed laser development. The advantages of NPR technique are flexibility due to capability to be applied in all-fiber configurations, as polarizing fiber isolators, polarization controller and birefringence fiber are widely existed.

Figure 2.11 shows the configuration setup of NPR based passively mode-locked Erbium-doped fiber laser (EDFL). The EDFL uses a polarization dependent isolator (PDI) and PC to control the polarization of light in the cavity and initiate NPR effect for mode-locking. However, it has a drawbacks due to temperature sensitivity that comes from the optimum polarization setting and lead to the birefringence fluctuation. This event affects the mode locking process and difficult to regenerate the experiment to achieve the same repetition rate and pulse duration. Still, NPR is relevant to generate dark pulse, ultra-short and switchable pulse with the utilization of various saturable absorption strength (Tiu et al., 2014; Song et al., 2009; Li et al., 2011).

Mode-locked with the insertion of SA initiates from fluctuation noise in cavity. The losses is decreased with the enhancement of gain in a round trip when a noise spike surpasses the threshold saturation of an absorber. The initiates spike is continuously grows and becomes narrower until a stable pulse width is formed. A pulsed laser with SA

has the capability to function in minimal loss per round trip in cavity and then, the longitudinal modes of laser develop phase locked. The SA materials such as carbon nanotubes (CNTs) and graphene has gained much attention in years within various research organization, globally. These materials have been demonstrated and offered a fast recovery time and saturable absorption including the nonlinearity of high third order which can contributes to the pulsed laser formation (Bao et al., 2009; Zhao et al., 2011; Zhang et al., 2006) To date, over hundreds investigation have been reported in employment of CNT and graphene SA for the Q-switched or mode-locked pulsed laser. The most recent, black phosphorus and Molybdenum disulfide (MoS_2) has captivates much attention due to its narrow direct band-gap compare to graphene. They also show the capabilities to generate ultrashort pulse duration in femto-seconds with performances either similar or greater than graphene families (Sotor et al., 2015; Luo et al., 2015; Ahmed et al., 2016).

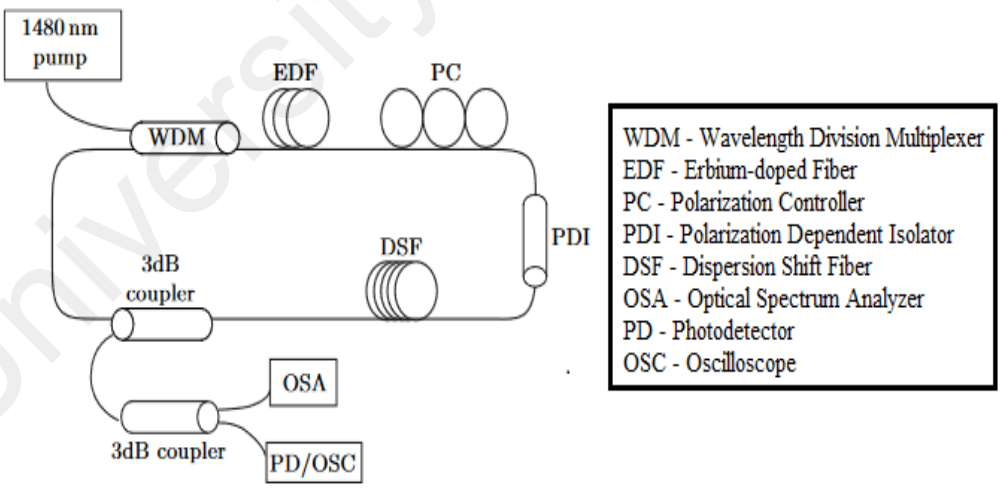

Figure 2.11: Configuration setup for passively mode-locked by using NPR technique

(Tiu et al., 2014)

2.7 Important Parameters of Pulsed Laser

Figure 2.12 illustrates various laser parameters to evaluate the performance of a pulse train. These parameters are repetition rate, pulse width, peak power, optical signal to noise ratio (OSNR) and pulse energy. Peak power of an optical pulse is defined as the maximum optical power of pulse which is measured directly with combination of oscilloscope (OSC) and photodiode. Besides, it also can be calculated especially for short pulse duration in pico- and femto-seconds by following:

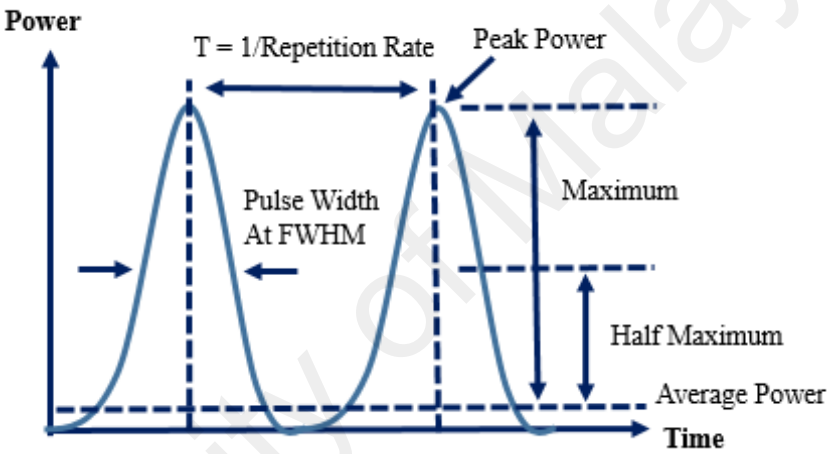

Figure 2.12: Important parameters of pulsed laser

$$P_{\mathrm{p}} = \frac{E_{\mathrm{p}}}{\tau_{\mathrm{p}}} \qquad (2.15)$$

where E_{p} is the pulse energy and τ_{p} is the pulse width.

The total amount of energy that released over the period of the cycle is determined as the average power of a pulsed fiber laser. It able to be measured straight from a power meter. Pulse width (τ_{p}) is designated as a full width at half maximum (FWHM). It also known as duration or length of time interval with the power is in the middle at power intensity. Basically, pulse duration for Q-switched laser is broad in nano- to micro-seconds and it able to be measured straight from an oscilloscope (OSC) whereas mode-

locked with narrower width from pico- to femto-seconds can be done using an autocorrelator.

Repetition rate or known as pulse repetition frequency is the number of pulses per second that emitted. Common Q-switched laser operates at lower repetition rate in the kilo-Hertz range while mode-locked laser operates at higher repetition rate from Mega- to Giga-Hertz. It can be measured directly by using OSC and able to be confirmed by using RF spectrum analyzer to make sure that fiber laser is operates in the specific repetition rate.

Pulse energy (E_p) is total energy of an optical pulse an expressed in Joule (J). Normally, Q-switched pulsed laser produces higher energy of pulse compared to the mode-locked pulsed laser. It calculated by equation:

$$Ep = \frac{Pave}{Repetition\ Rate} \tag{2.16}$$

The spectral and temporal of pulsed lasers is generally characterized or defined in the term of time bandwidth product (TBP). TBP is equal to $\Delta\tau\Delta v$, where $\Delta\tau$ is full width at half maximum (FWHM) of the intensity of pulsed whereas Δv is frequency bandwidth FWHM with $\omega = 2\pi v$. Besides, TBP is also acknowledged as minimum pulse duration of a pulse spectrum, thus the value of TBP is supposedly smaller than the real practice of pulsed laser and it can be expressed as (Marchic, 2008):

$$\Delta\tau\Delta v \geq K \tag{2.17}$$

where K is a number which depends on the type of pulse shapes in Table 2.2 (Weber & Nakazawa, 2007). Then, the minimum pulse duration can be calculated by equation (Marchic, 2008):

$$\Delta\tau \geq K \frac{\lambda 0^2}{\Delta\lambda . c} \quad (2.18)$$

where $\Delta\lambda$ (nm) is the central of wavelength, $\lambda 0$ (nm) is the 3 dB bandwidth at FHWM and c (m/s) is the speed of light. An important type of pulsed laser in nonlinear optics is the secant pulsed shape due to balance between nonlinearity and dispersion of fiber especially to a soliton pulsed. A soliton exhibits a linear frequency, or known as 'chirp'. Thus, in the absence of chirp, soliton pulses have TBP of 0.315, a slightly small than Gaussian pulse shape (Marchic, 2008; Liu et al., 2013).

Table 2.2: TBP values for various pulse shapes

Profile Shape	K
Gaussian	0.441
Secant	0.315
Lorentz	0.142

Optical signal to Noise Ratio (OSNR) is a measurement that used to differentiate between information signals to the background noise level. It is a ratio concerning the signal powers to the noise power and describes in decibel (dB) unit. The larger the OSNR, the greater desired signal is obtained compare to the noise in cavity. The stability of pulse is measured with Radio Frequency Spectrum Analyzer (RFSA) and illustrated in Figure 2.13.

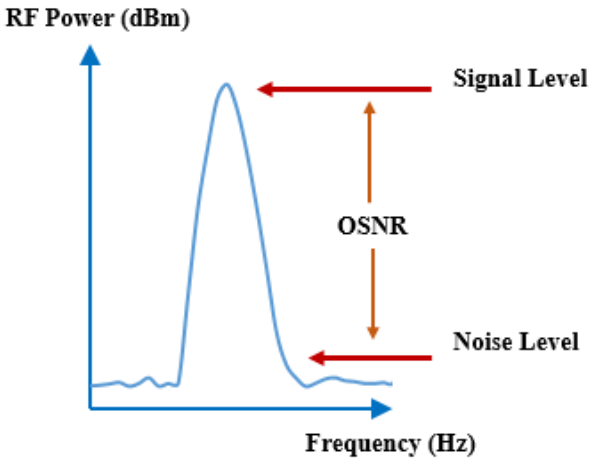

Figure 2.13: SNR measurement from radio frequency (RF) spectrum

2.8 Dark Pulse

Alternate to the bright, the propagation of dark pulse or dark soliton was first theoretical observed by Hasagewa and Tappert back in 1973. It defined as a pulse train with a dip in the intensity of CW background of laser emission. However, these idea remain a mathematical curiosity. Only after 14 years later, the first dark soliton fiber laser was experimental demonstrated by Emplit et al., (1987) with pulse duration of 5 ps in normal dispersion region. Again, it took a very long time over 15 years to realize the generation of dark pulse in fiber laser which was successfully demonstrated by Sylvestre, et al., (2002). By using self-induced modulational-instability laser technique, the repetition rate and pulse duration obtained were 0.46 MHz and 12 ps. Then, it began the development of dark pulse and dark soliton pulsed laser generation by using various type of techniques.

Dark pulse originates was directed by nonlinear Schrödinger equation (NLSE) and describes the bright solitons are formed in anomalous whereas dark solitons are formed in the normal dispersion single mode fibers (Zhang et al., 2009; Tang et al., 2013; Tang et al., 2014). However, the NLSE is lack for the important element of nonlinear gain

and spectral filtering that leads to the complex Ginzburg-Landau equation (CGLE). The stability of CGLE for dark soliton-like is expressed by (Fang & Xiao, 2006);

$$A(z) = \sqrt{-\frac{d(z)(\beta^2-2)+6\beta(z)}{2\gamma(z)}\eta^2} \qquad (2.19)$$

where $A(z)$ is the amplitude of pulse, β is the nonlinear chirp parameter, $d(z)$ is relates to dispersion, $\gamma(z)$ nonlinear coefficient based on refractive index of n_2 and η is the pulse width of the dark pulse.

Dark pulse offers high stability in the presence of noise, low interaction between neighbouring dark solitons for their bright counterparts and less sensitive on Gordon-Haus effect in a time jitter proven numerically and analytically (Hasegawa & Tappert, 1973; Kivshar et al., 1994; Zhang et al., 2009). The most common method that revealed for the formation dark pulse are using artificial SA technique such as NPR with one or two polarization components and NOLM (Ning et al., 2012; Tang et al., 2-14; Wang et al., 2014). The most recent, dark pulse was successfully generated by using high nonlinearity SA of CNT, graphene oxide (GO) and Molybdenum disulphide (MoS_2) (Liu et al., 2014; Lin et al., 2014; Ahmad et al., 2016).

The idea to form dark pulse by using these techniques is to achieve domain wall between traveling waves that agreed by CGLE. The concept is to produce either two orthogonal polarization states of light or dual- or multi-lasing with different wavelengths that induced by high nonlinearity of birefringence in cavity (Liu et al., 2014; Yin et al., 2010; Zhang et al., 2010). Besides, the other concept is by using high nonlinearity and strong birefringence fiber with a large normal or large anomalous dispersion region (Gao et al., 2013; Zhao et al., 2014). The high nonlinearity fiber is also best work together with the employment of high nonlinearity SA that leads to the four wave mixing effect of multiwavelength generation or broad spectrum of soliton (Zhao et al., 2013; Ahmad et

al., 2016). Figure 2.14 shows the pulse train of bright and dark pulse fiber laser. The dark pulse is formed by increasing pump power.

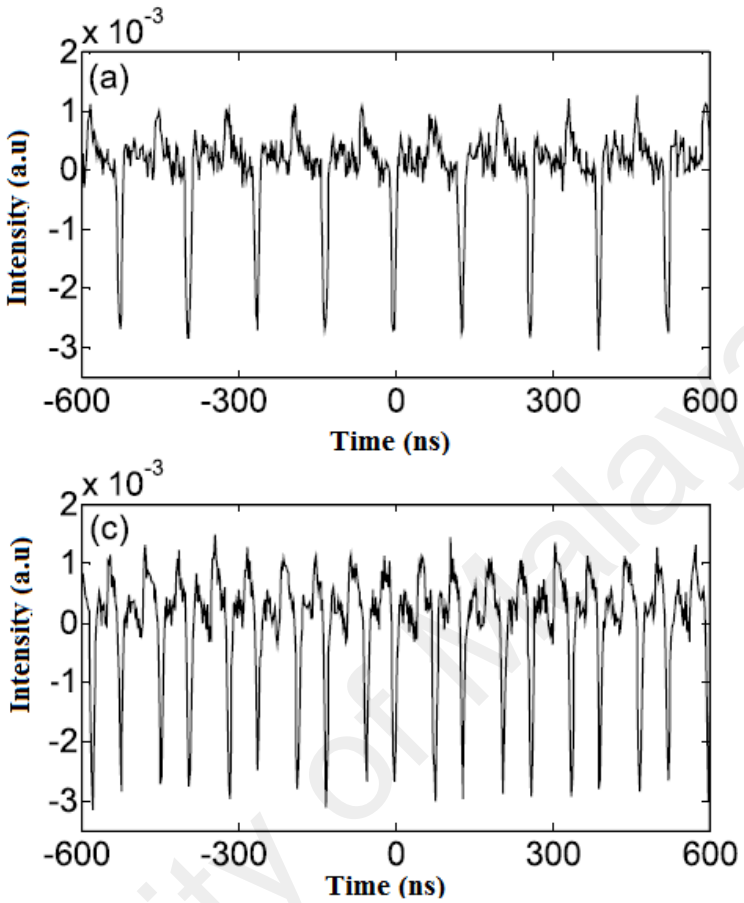

Figure 2.14: Pulse train at different pump power (a) bright pulse (b) dark pulse (Zhao et al., 2013)

2.9 Zirconia-based Erbium-doped Fiber (Zr-EDF)

A lot of effort has been put forward to manufacture the gain medium of the mode-locked pulsed laser in order to realize compact ultrafast laser with high repetition rate and narrow pulse width. The widely used erbium-doped fiber (EDF) is doped with high Erbium concentration with the aim to reduce the length of fiber used. This highly doped EDF leads to concentration quenching or cluster formation which limits the overall performance of a laser system (Digonnet, 2001; Ahmad et al., 2012). In view of this, researchers are experimenting with new host material such as telluride and bismuth as co-

dopants to enhance the performance of Erbium doped fiber laser (EDFL) (Thyagarajan & Kaur, 2000; Huang et al., 2004; Ahmad, Shahi & Harun, 2010; Harun et al., 2010). Nevertheless, these new materials are not without their drawbacks: telluride- and bismuth-based fibers cannot be easily spliced to conventional single mode fibers (SMFs), thereby increasing the complexity of the mode-locked fiber laser and making it impractical for real-world applications. Phosphosilicate fibers heavily co-doped with erbium (Er^{3+}) are most commonly used as the active medium. However, the used of phosphosilicate glass-based erbium-doped fiber is difficult due to the high splicing loss along with high background loss of the fiber, though this kind of host reduces the clustering problem of rare earth ions.

Then, an exciting potential of Zirconium ions (Zr^{4+}) co-doped silica host fiber is introduced and explored where it shows incredible results in ultrashort pulsed laser due to its optical transparency, high refractive index and photochemical stability (Lai & Su, 2000; Gengler et al., 2010). The combination of zirconia material into yttria–aluminosilicate glass host effectively avoids the detrimental effects and allows the generation of efficient flat-gain amplifier and ultrashort pulsed laser. The first EDFA based on Zr-EDF was reported by Paul et al., (2010) by using single pass configuration using a fiber with Erbium ion concentration of 4320 ppm. The highest gain was 21.8 dB at 1560 nm with variation of 4.4 dB from 1535 nm to 1605 nm. The noise figure (NF) was maintained below 9 dB for the specific wavelength region.

Further investigation was the carried out using a double pass configuration. The highest gain reported was as high as 40.8 dB. A flat-gain was also obtained at 16 dB with gain variation of 2.5 dB within a wavelength region from 1530 nm to 1590 nm (Harun et al., 2011). The work aims to achieve an efficient and compact flat-gain wideband optical amplifier with acceptable noise figure level to improve overall performance of long distance transmission. In this work, an enhanced Zr-EDF with higher Erbium

concentration is developed for this purpose. The Zr-EDF will also use to generate Q-switched and mode-locked fiber lasers in conjunction with new passive SAs. These SAs will be developed using new nanomaterials.

CHAPTER 3: ENHANCED ZIRCONIA-YTTRIA-ALUMINUM-BASED ERBIUM-DOPED FIBER AMPLIFIER

3.1 Introduction of Erbium-doped Fiber Amplifier (EDFA)

The rising demand of an advanced communication systems for outstanding flexibility and large information capacities with very high speed data rates, inspire research society, globally. Among from telecommunications devices, the invention of amplifiers was remarkable due to successfully in expanding transmission distance further than thousand kilometres. The technology to amplify the signal of light without the need to the conversion of electricity has been accomplished with rare earth doped fiber, which realizes the best amplification with high gain and low noise. The most attention of rare earth material, or also known as active medium which has less attenuation in 1550 nm transmission window is Erbium (Er^{3+}). To date, researchers are concentrate more on developing Erbium-doping, mainly in silica based fibers. The reason is due to the emission of erbium ions within a set of wavelength around 1550 nm where the silica fiber reveals the less attenuation for transmit a lot of information (Naji et al., 2011; Becker et al., 1999).

Erbium-doped fiber amplifier (EDFA) is one of the important devices in wavelength multiplexing systems (WDM) based optical communication networks. It can provide an amplification in wideband wavelength region centred at 1550 nm. Yearly demands for high transmission capacity and speed have driven the development of communications to expand the transmissions to the long wavelength (L-band) region. The incapable EDFA to be highly doped with erbium ions cause the limitation to the performance of L-band amplifier. Therefore, a lot of efforts have been devoted to search a new glass host materials. The materials such as telluride, bismuthate and zirconia have

shown the ability to be highly doped erbium concentrations without any detrimental effects (Mori, 2008; Cheng et al., 2009; Harun et al., 2011). However, telluride and bismuthate based Erbium-doped fiber (EDF) had a big numerical aperture (NA) around 0.2 and lower melting temperature, thus it suffers in splicing and become incompatible with conventional silica fibers (Mendez & Morse, 2011; Ahmad et al., 2010). Then, a unique fiber of Zr-EDF gained a great attention due to its capabilities to enhance erbium ions concentration without detrimental effects, thus realizes for compact design system with a very short gain medium. It also has a standard NA to be easily integrated with conventional silica fibers which is a backbone for the most optical transmission systems. Moreover, the Zr-EDF is easily to be manufactured by using modified chemical vapor deposition (MCVD) that successfully become the cost-effective fiber and increases the potential to commercialize in wide applications.

Previously, a wideband EDFA was demonstrated using a new type of erbium-doped fiber (EDF), which is fabricated in a ternary glass host, zirconia–yttria–aluminum (Zr–Y–Al) co-doped silica fiber. With a combination of both Zr and Al, a high erbium doping concentration of 2800 ppm was achieved in the glass host without any phase separations of rare-earths (Ahmad et al., 2011). In this chapter, a new Zr-EDF with a higher erbium concentration is proposed and developed to improve the attainable gain and reduce the noise figure. An efficient Zr-EDF amplifier (Zr-EDFA) with an improved gain is then demonstrated using the newly developed gain medium. Here, at first, the fabrication and optical characteristics of the new Zr-EDF are described. Then, the performance of the Zr-EDFA are investigated and demonstrated for both single-pass and improved double-pass configurations for different active fiber lengths and pump powers in order to determine the optimize design. The performance of the enhanced Zr-EDFA is also compared with the use of the conventional Zr-EDF and other high concentration

EDFs such as Bismuth-based EDF (Bi-EDF) and commercial IsoGain^{TM} I-25 silica based EDF.

3.2 Fabrication and Characteristics of the New Zr-EDF

A new class of Zr–Y–Al co-doped EDF with a higher erbium ion concentration is developed in this study. At first, a Zr–Y–Al co-doped EDF preforms based on zirconia–yttria–alumina–phospho silica glass with a high doping level of ZrO_2 around 2 wt % is fabricated using the modified chemical vapor deposition (MCVD) process. The doping of Er_2O_3 into the zirconia–yttria–alumina–phosphor silica based glass is done via solution doping process (Dhar et al., 2006). A small amount of Y_2O_3 and P_2O_5 is added at this stage to serve as a nucleating agent. This step is necessary to increase the phase separation for the generation of Er_2O_3 doped micro crystallites in the core matrix of optical fiber preform (Paul et al., 2010). The glass formers incorporated by the MCVD process are SiO_2 and P_2O_5 along with the glass modifiers Al_2O_3, ZrO_2, Er_2O_3, and Y_2O_3, which are also incorporated by the solution doping technique using an alcoholic–water mixture of suitable strength (1:5) to form the complex molecules $ErCl_3 \cdot 6H_2O$, $AlCl_3 \cdot 6H_2O$, $YCl_3 \cdot 6H_2O$, and $ZrOCl_2\ 8H_2O$. The inclusion of the Y_2O_3 particulates into the host matrix also serves the additional purpose of slowing down or eliminating changes in the ZrO_2 crystal structure. This is a crucial factor in the fabrication process. Pure zirconium dioxide can exist in three distinct crystalline structures in a bulk glass matrix, depending on the temperature range.

At above 2350 °C, ZrO_2 behaves as a cubic structure, while at temperatures between 1170 °C and 2350 °C, it forms a tetragonal structure. Below 1170 °C, pure zirconium dioxide crystals exist as a mono-clinic structure. The problem posed by these different states is that the shift from the tetragonal to monoclinic structure is very fast and

involves an increase in volume between 3 to 5 %. This rapid increase results in a significant cracking in the developed fiber during the cooling process (observed primarily in the core region, as this is where the concentration of ZrO_2 crystallites is the highest) and destroys the mechanical properties of the fiber. Adding a minute amount of Y_2O_3, or other oxides such as MgO, CaO can slow down or stop the changes in the crystalline structure by preserving the mechanical strength and integrity of the fiber (Paul et al., 2010). It can be seen that ZrO_2 crystallites are able to sustain their crystalline structures at a temperature used to collapse the silica rod and draw the fiber from the preform. This clearly confirms the existence of some ZrO_2 crystallites within the host matrix of the preform and, subsequently, the drawn fiber.

After the fabrication of the preform by the MCVD process, it was annealed at 1100 °C for 3 hour in a closed furnace under heating and cooling rates of 20 °C/min to generate Er_2O_3-doped ZrO_2 rich nano-crystalline particles. The fiber was drawn at around 2000 °C from the annealed preform and simultaneously coated with resin using fiber drawing tower. The nano-crystalline host of ZrO_2 was preserved in the silica glass matrix as confirmed by the transmission electron microscopy (TEM) analyses with energy dispersive X-ray analysis (EDX) spectra and electron diffraction patterns (Pal et al., 2011). The average particle sizes were around 10–20 nm. The core and cladding geometry of the fiber was inspected by an optical microscope (Olympus BX51). The core was homogeneous and had no observable defects at the interface between the core and the silica cladding.

The fiber cross-section view is given in Figure 3.1 (a), which shows the core and cladding diameters of the fiber at 10.04 µm and 126.83 µm, respectively. The average dopant distribution along the diameter of the core is shown in Figure 3.1 (b). The preform RI profile is shown in Figure 3.2 (a) as measured by a preform analyzer. The spectral attenuation curve of the fiber is given in Figure 3.2, and it shows 80.0 dB/m absorption

loss at 980 nm wavelength and 220 dB/m at 1550 nm. The fiber core contains SiO_2, Al_2O_3, Y_2O_3, ZrO_2, P_2O_5, and Er_2O_3 doping host. The fiber has a numerical aperture of 0.17.

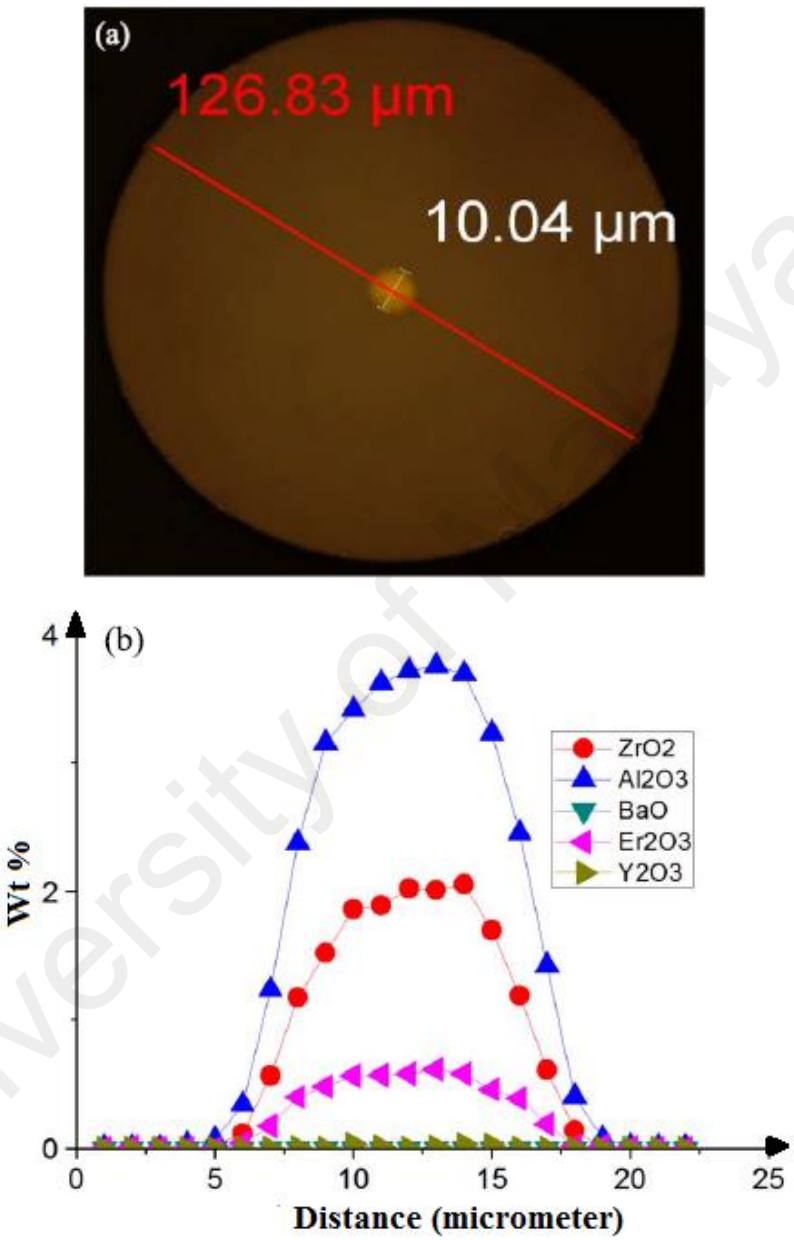

Figure 3.1: (a) Cross-sectional view of the high ZrO_2 co-doped EDF. (b) Dopant distribution profile of the fiber

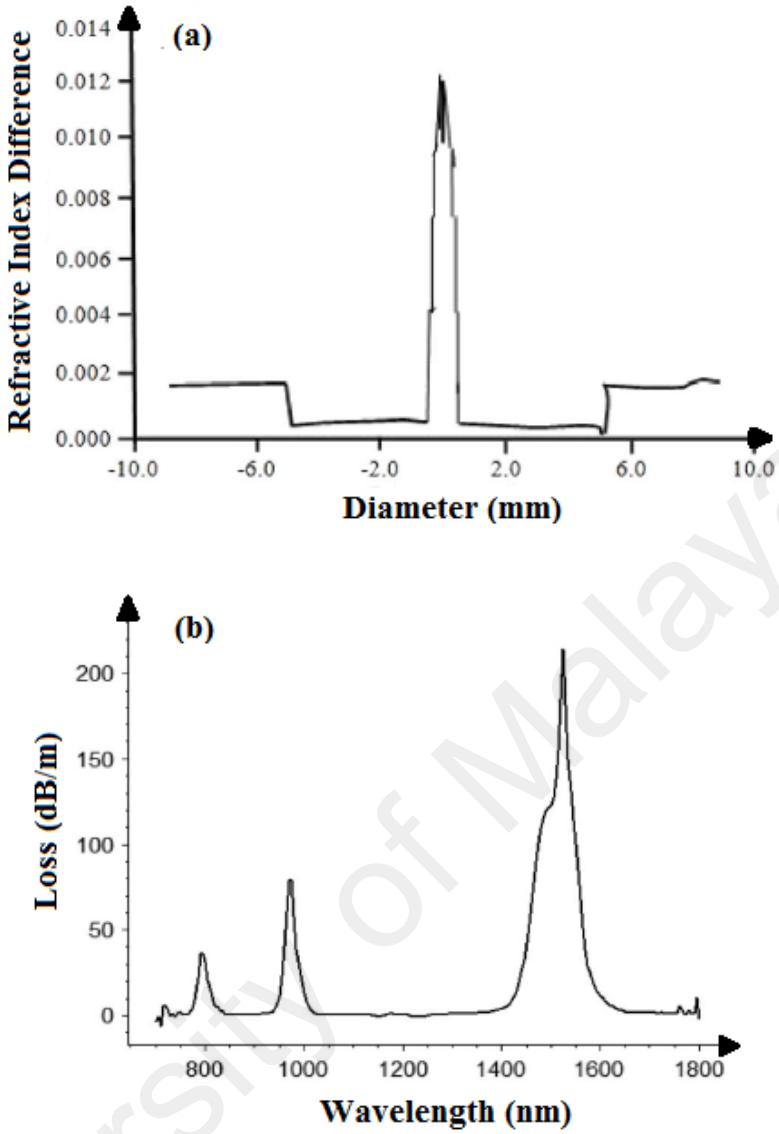

Figure 3.2: (a) Refractive index profile of the fiber preform (b) Absorption loss curve of the enhanced Zr-EDF with high ZrO_2 co-doping

3.3 Amplified Spontaneous Emission (ASE)

Figure 3.3 shows the ASE spectra from the Erbium Zirconia Yttria Aluminum Co-doped Fiber (Zr-EDF) at three different lengths ranging from 0.5 m to 2 m. In the experiment, the EDF is forward pumped by a 980 nm laser diode. The pump power is fixed at 130 mW. As observed in Figure 3.3, the spectrum is shifting to the right side, from C-band to the closer of L-band region as the Zr-EDF length increases. The ASE power also increases as a longer fiber is used in cavity. The highest peak intensities of -

37.4 dBm, -40.0 dBm and -41.0 dBm are obtained at 1560 nm, 1555 nm and 1545 nm when the EDF lengths are fixed at 2.0, 1.0 and 0.5 m, respectively. It is also observed that the use of 2 m long EDF produces an interesting ASE characteristic with the broadest bandwidth of 85 nm. The ASE bandwidth are obtained at 80 nm and 45 nm with the use of 1.0 and 0.5 m long EDF, respectively. This result indicates that the 2 m long EDF produces a better ASE in term of its total intensity, bandwidth and operation in L-band region as compared to other lengths. This is attributed to the use of longer fiber allows the higher population inversion which responsible for more efficient ASE generation. However, a further experiment is still required to determine the optimum length for amplifier's applications.

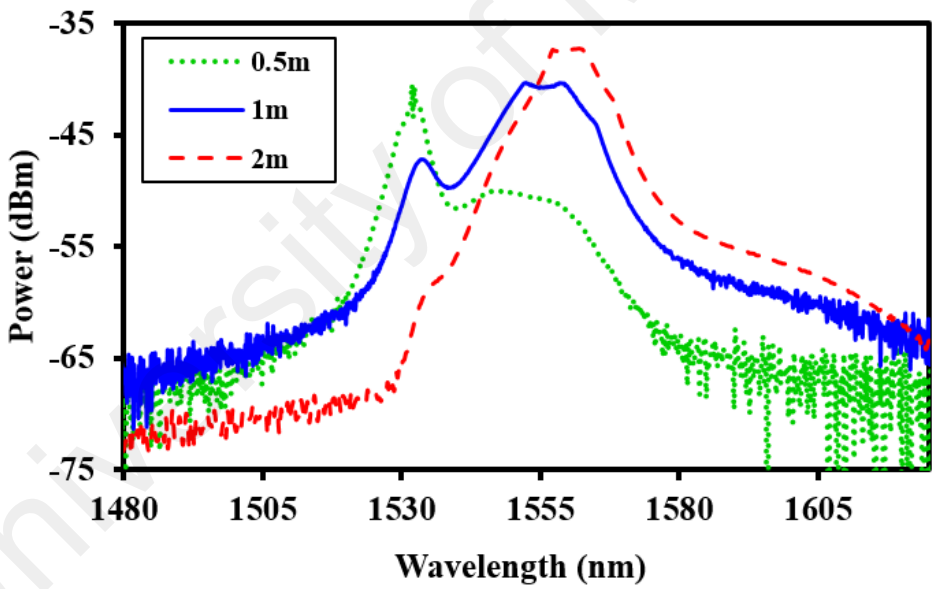

Figure 3.3: ASE spectrum for different lengths of Zr-EDF when pumped with 980 nm laser diode at 130 mW

3.4 Flat-gain Optical Amplifier with Zr-EDF

Figure 3.4 shows the experimental setup to investigate the gain and noise figure characteristics of the fabricated Zr-EDF. In the experiment, tunable laser source (TLS) as

an input signal was varied from 1520 nm to 1620 nm wavelength. The variable optical attenuator (VOA) was used to obtain the specific and accurate input power to the cavity. An isolator is placed after the VOA to ensure unidirectional operation of the amplifier and to prevent any backward ASE noise from damaging the TLS.

A short piece of the newly developed Zr-Y-Al based EDF is used as a gain medium. The EDF is forward pumped by a 980 nm laser diode via a 980/1550 nm wavelength division multiplexing (WDM) coupler. The results were analyzed and measured by optical spectrum analyzer (OSA), which was located at the end of the configuration setup of the amplifier. The performance of the proposed amplifier is also compared with the conventional amplifier, which was obtained using the previous Zr-EDF with a lower Erbium concentration (Harun et al., 2011). Table 3.1 compares the specification of the new Zr-EDF with the conventional Zr-EDF.

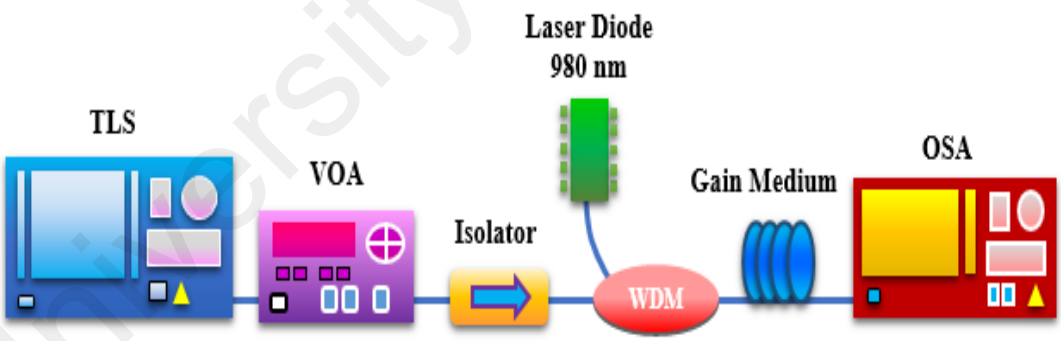

Figure 3.4: Experimental setup for the flat-gain optical amplifier

Table 3.1: Specification comparison between the new and conventional Zr-EDF

Types	Conventional Zr-EDF	New Zr-EDF
Erbium-doped Concentration	2800 ppm	4000 ppm
Absorption Rate	14.5 dB/m at 980 nm 58.0 dB/m at 1550 nm	80.0 dB/m at 980 nm 220.0 dB/m at 1550 nm
Refractive Index Difference	0.010	0.012
Core Diameter	Less 10 µm	10.04 µm
Fiber Diameter	125 µm	126.83 µm
Core Composition	$SiO_2 + Al_2O_3 + ZrO_2 + P_2O_5 + Er_2O_3 + Y_2O_3$	$SiO_2 + Al_2O_3 + ZrO_2 + P_2O_5 + Er_2O_3 + Y_2O_3$
Numerical Aperture (NA)	0.17	0.17

At first, the gain and noise figure of the new EDF based optical amplifier were investigated for three different lengths and the results are shown in Figures 3.5 and 3.6 for input signal power of -30 dBm and -10 dBm, respectively. In the experiment the pump power was fixed at 130 mW, while the fiber length was varied from 0.5 to 2 m. At input signal of -30 dBm, the gain improves especially at around 1560 nm region as the EDF fiber length is increased from 0.5 to 1 m. However, the gain reduces especially at shorter wavelength region as the EDF is further increased to 2 m. Among the 3 different lengths of the fiber tested, it is found that 1 m gives the best amplification performance. At 1 m length, the EDFA operates in the C-band region with a flat gain of around 27 dB within a wavelength region between 1530 to 1565 nm with a gain fluctuation of less than 3 dB. The highest gain of 28.6 dB is obtained at 1555 nm wavelength. The noise figures within the flat-gain region are maintained less than 6.9 dB. The noise figure reduces as the

operating wavelength increases due to the fiber loss, which is smaller at the longer wavelength.

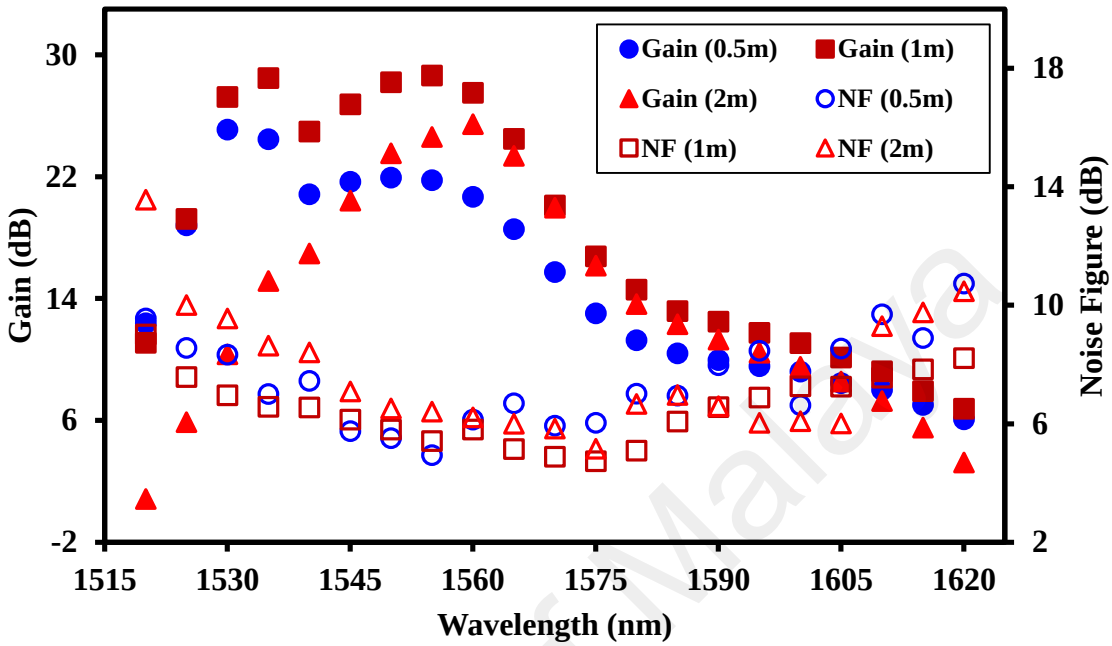

Figure 3.5: Optical gain and noise figure spectra at -30 dBm input signal and 130 mW pump power for three different EDF lengths

At the input signal power of -10 dBm and pump power of 130 mW, the flat-gain operations are obtained at EDF lengths of 0.5 m and 1.0 m as shown in Figure 3.6. The flat gains of 17.6 dB and 19.6 dB are observed within 30 nm wavelength bandwidth with the use of 0.5 m and 1.0 m long EDF respectively, as the gain medium. As shown in Figure 3.6, the highest gain spectrum of 19.6 is obtained at EDF length of 1 m where a wide flattening optical gain was obtained with very small variation gain of 0.27 dB within 1530 nm to 1570 nm wavelengths. The noise figure is maintained below 11.0 dB within the flat-gain region operation. Therefore, we consider the optimum length for the EDF is around 1 m for operation with the maximum pump power of 130 mW. At 0.5 m long

EDF, the amplifier operates at a slightly lower flat-gain value with a gain variation of 0.23 dB from 1530 nm to 1565 nm wavelengths but with a slightly better noise figure.

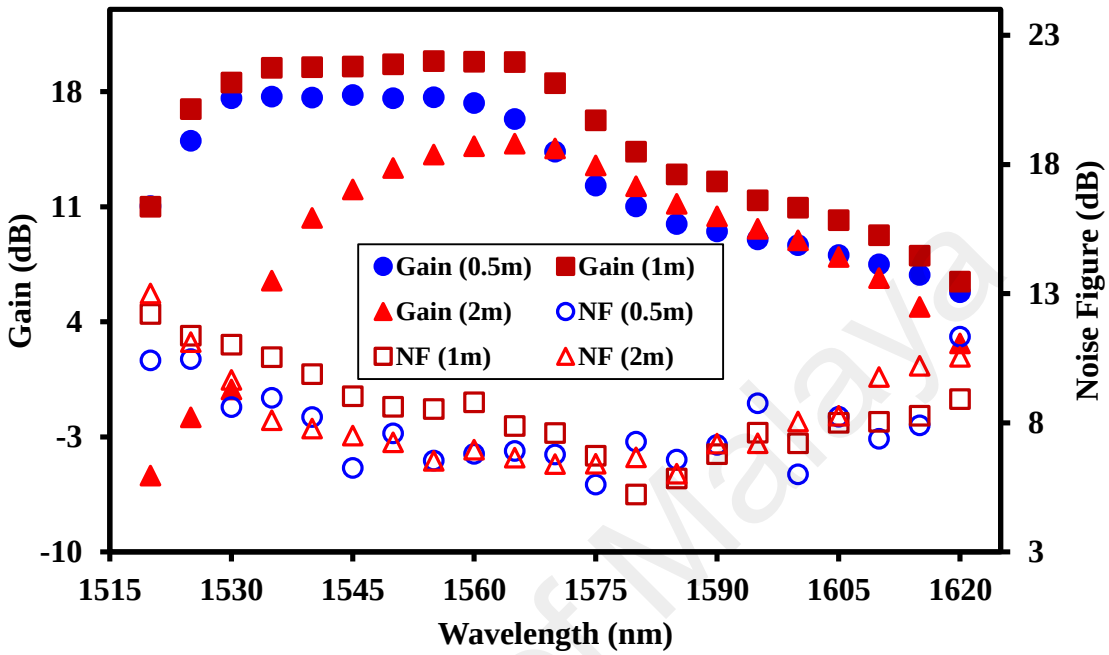

Figure 3.6: Optical gain and noise figure spectra at -10 dBm input signal and 130 mW pump power for three different EDF lengths

The gain and noise figure spectra of the amplifier are also investigated for different pump powers at the optimum EDF length of 1m. In the experiment, the input signal power is fixed at -10 dBm. Figure 3.7 shows the experimental result, which indicates that the C-band gain increases especially at shorter wavelength region as the pump power increases from 61 mW to 130 mW. This is attributed to the population inversion, which increases with the pump power. For instance, 1530 nm gain improves by 5.4 dB as the power is varied from 61 mW to 87 mW. This gain is further improved by 6.9 dB as the pump power is further increased to 130 mW. Both gain improvements are however reduced at 1565 nm, which resulted in a flatter gain spectrum due to

saturation effect. At C-band region, the lowest noise figure spectrum are obtained at 87 mW pump power due to the efficient population inversion at this pump power, which reduces the ASE noise.

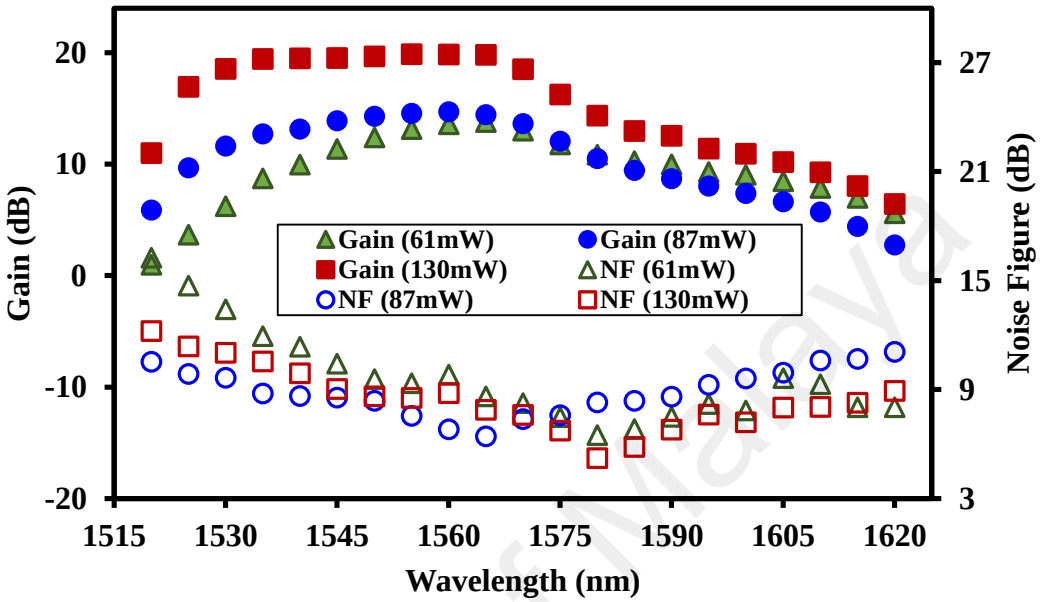

Figure 3.7: Optical gain and noise figure at different pump powers when the input signal and EDF lengths are fixed at -10 dBm and 1m, respectively

The performance of the proposed amplifier with new high erbium doped modified silica glass based zirconia yttria aluminum co-doped fiber is also compared with the lower erbium doped modified silica glass based zirconia yttria aluminum co-doped fiber based EDFA having an absorption characteristic of 14.5 dB/m at 980 nm as the gain medium (Harun et al., 2011). Figure 3.8 shows the measured gain and noise figure spectra of both amplifiers with the doped fiber length of 1 m, respectively, as the input signal and 980 nm pump power is set at -10 dBm and 130 mW, respectively.

As shown in the figure, the gain of the proposed EDFA improves especially at a longer wavelength as compared to that of low erbium doped EDFA. For instance, the gain enhancement of about 2.7 dB is obtained at wavelength of 1565 nm. This is attributed

to the higher concentration of erbium ion doping in the new fiber and thus enhances the numbers of excited ions to be stimulated. Additionally, the higher Erbium ion concentration increases the gain bandwidth of the amplifier to cover L-band region. Moreover, the proposed amplifier shows a reasonably low noise figures especially at L-band region. This is attributed to the majority of upper level ions that have been used for amplification and thus decreases the ASE, which in turn reduces the noise figure.

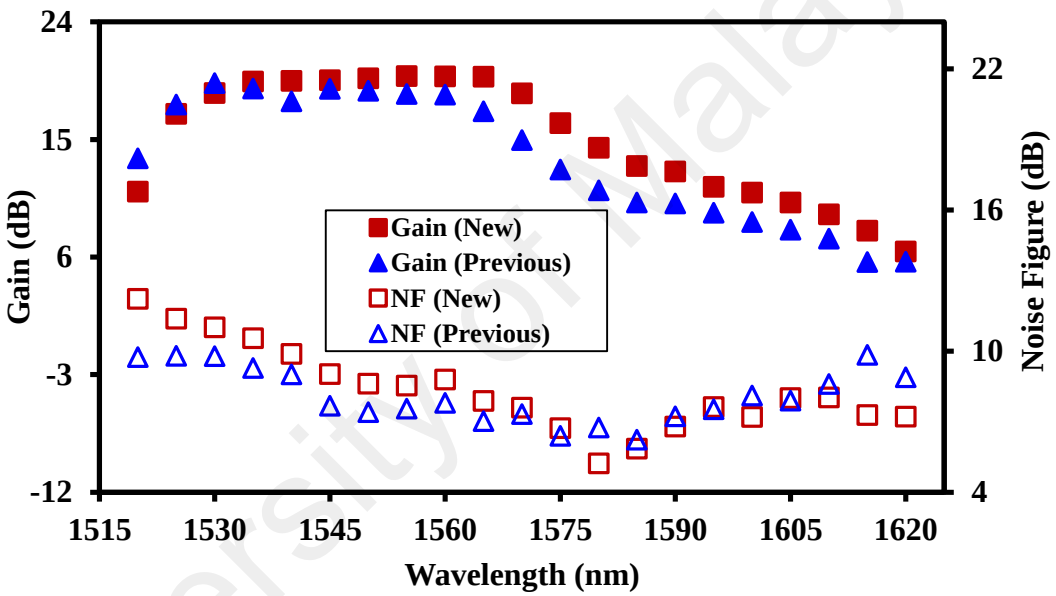

Figure 3.8: Comparison of the gain and noise figure spectra between the high erbium doped EDFA and low erbium-doped Zirconia based EDFA when the input signal and pump powers are fixed at -10 dBm and 130 mW, respectively

3.5 Enhanced Zr-EDFA with a Double-Pass Configuration

In this section, an efficient Zr-EDFA with an improved gain is demonstrated using the newly developed gain medium in conjunction with a double-pass configuration. Figure 3.9 shows the configuration of the proposed double-pass EDFA using a short piece

of the newly developed Zr-Y-Al based EDF as a gain medium with a broadband reflector. The EDF is forward pumped by a 980 nm laser diode via a 980/1550 nm WDM coupler. A broadband fiber mirror is used to route the forward ASE and the input signal back into the amplifier's system. An optical circulator is used to launch the input signal into the gain medium and route the amplified signal into the OSA. The circulator prevents any reverse direction of ASE from entering the input fiber to cause detrimental effects. The performance of the proposed double-pass Zr-EDFA is characterized using a TLS in conjunction with an OSA. A VOA is used to control the input signal power into the optical amplifier.

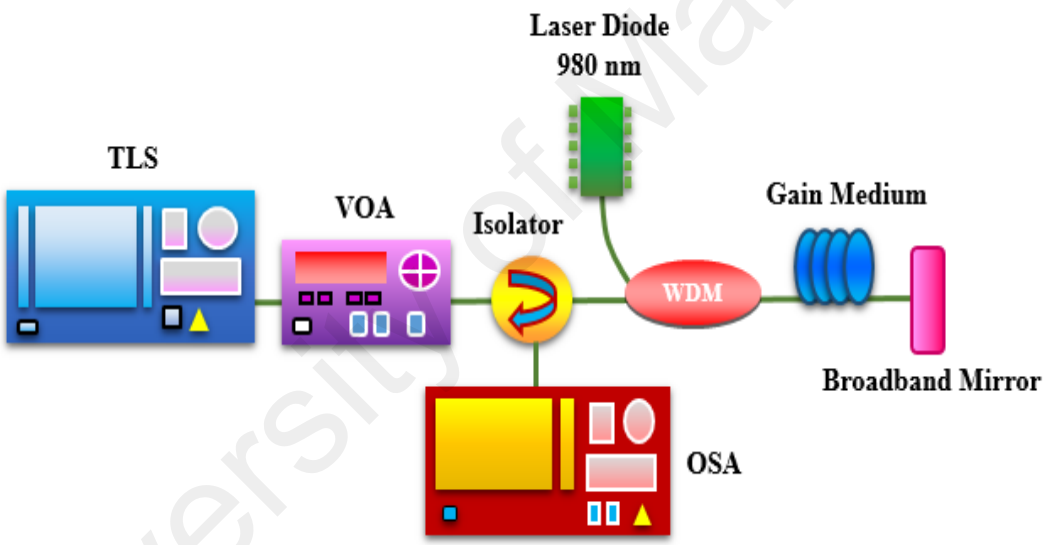

Figure 3.9: Configuration experiment setup of double pass Zr-EDFA by using a broadband fiber mirror

At first, the gain and noise figures of the Zr-EDFA configured with the new EDF were investigated at different lengths of EDF. In the experiment the pump power was fixed at 130 mW whereas the length of Zr-EDF was varied from 0.5 to 2 m. The results are shown in Figures 3.10 and 3.11 for input signal powers of -30 and -10 dBm, respectively. At input signal of -30 dBm, the gain improves and its spectrum moves toward a longer wavelength region as the EDF fiber length is increased from 0.5 to 1 m.

However, the gain reduces as the EDF is further increased to 2 m. Among the 3 different lengths of the fiber tested, it is found that 1 m gives the best amplification performance. At 1 m length, the EDFA operates in the C-band region with a flat gain of 38.0 ±1.5 dB within a wavelength region between 1530 to 1565 nm. The highest gain of 40.3 dB is obtained at 1560 nm wavelength. The noise figure within the flat-gain region is lowest at 1 m at less than 6 dB. The noise starts to increase as the operating wavelength increases above 1570 nm. This is attributed to the amplifier's gain, which reduces at a longer wavelength.

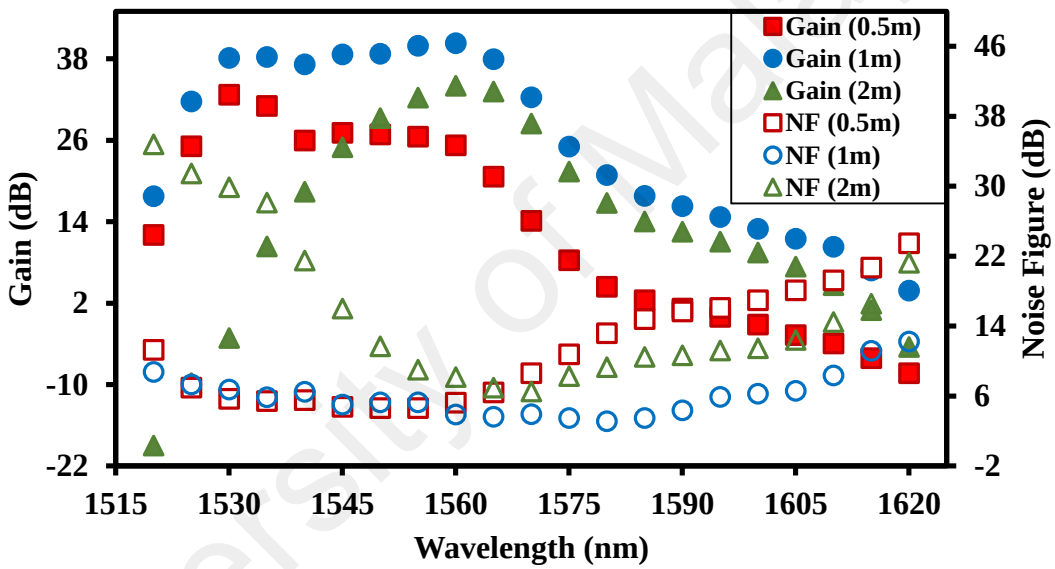

Figure 3.10: Gain and noise figure spectrum with different lengths of the new Zr-EDFs when the input signal and pump powers are fixed at -30 dBm and 130 mW, respectively

At the input signal power of -10 dBm, the highest gain spectrum is also obtained at Zr-EDF length of 1 m. As shown in Figure 3.11, the measured gain varies from 12.5 to 21.1 dB within the wavelength region from 1520 nm to 1580 nm, where the noise figure is maintained at below 9 dB. The highest gain of 21.1 dB is obtained at the input signal wavelength of 1560 nm. Besides that, the flat-gain operation at 13.5 dB is obtained at a

shorter EDF length of 0.5 m with gain variation of less than 2 dB. When using a length of 2 m, the gain spectrum shifts to a longer wavelength but with a lower value compared to a shorter length. The gain reduction with a longer fiber is due to pump attenuation along the gain medium. Close to the end of the fiber there is loss instead of gain for the signal due to insufficient pump power to support population inversion. The reduced gain also increases the noise figure at a longer wavelength. The noise figure spectrum is relatively higher with 2 m long EDF. The red-shift in the operating wavelength of the EDFA with a longer EDF is attributed to a quasi-two level system effect in the gain medium which absorbs the shorter wavelength photons and emits at longer wavelengths.

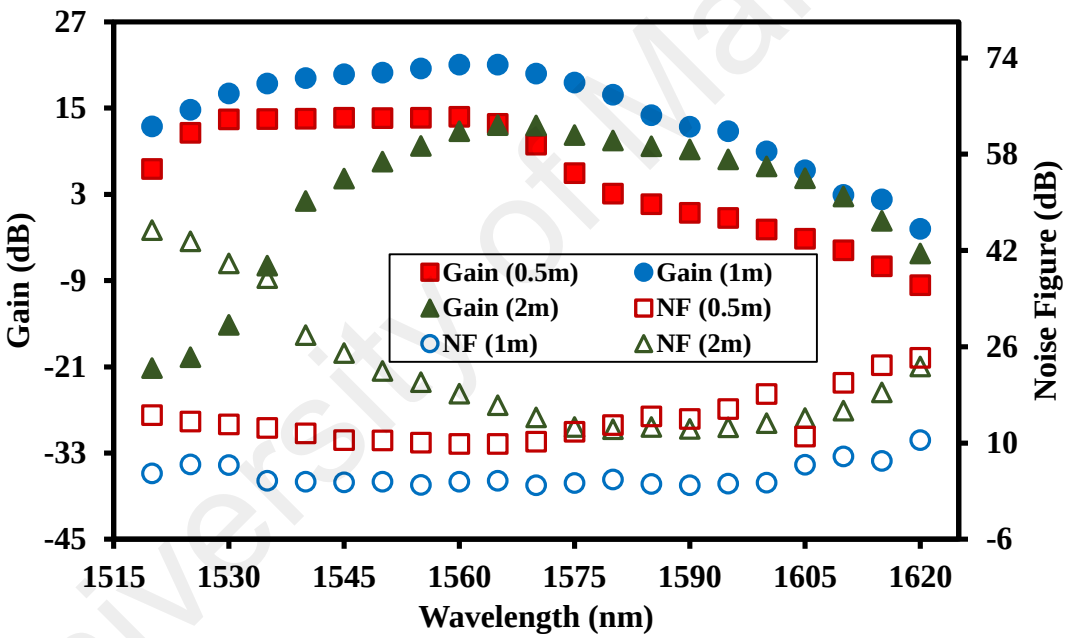

Figure 3.11: Gain and noise figure spectra with different lengths of Zr-EDFs when the input signal and pump powers are fixed at -10 dBm and 130 mW, respectively

The performance of the new Zr-EDFA is also compared with the conventional Zr-EDFA, which was obtained using a previous Zr-EDF with an absorption characteristic of 14.5 dB/m at 980 nm as the gain medium. Figure 3.12 shows the measured gain and noise figure spectra of both amplifiers with the doped fiber length of 1 m, respectively, as the input signal and 980 nm pump power is set at -30 dBm and 130 mW, respectively. As

shown in the figure, the gain of the proposed Zr-EDFA improves especially at a longer wavelength as compared to that of the previous Zr-EDFA. For instance, the gain enhancement of about 15.8 dB is obtained at wavelength of 1560 nm. This is attributed to the higher concentration of erbium ion doping in the new fiber and thus enhances the numbers of excited ions to be stimulated. Additionally, the higher Erbium ion concentration increases the gain bandwidth of the amplifier to cover L-band region. Moreover, the proposed amplifier shows a reasonably low noise figures especially at L-band region. This is attributed to the majority of upper level ions that have been used for amplification and thus decreases the ASE, which in turn reduces the noise figure.

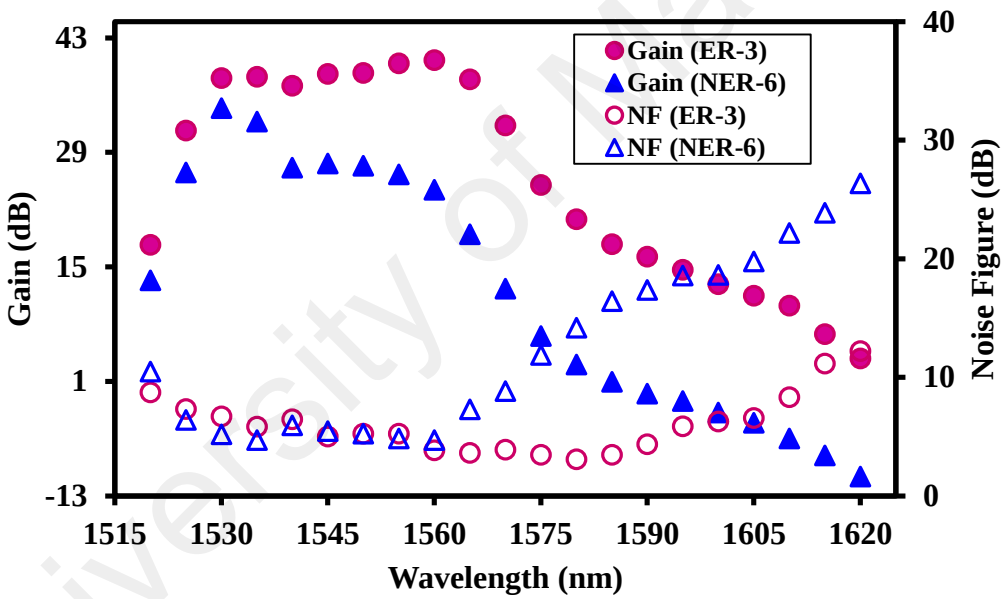

Figure 3.12: Comparison of the gain and noise figure spectra between the new Zr-EDFA (with ER-3 fiber) and the previous Zr-EDFA (with NER-6 fiber) when the input signal and pump powers are fixed at -30 dBm and 130 mW, respectively

The gain and noise figure comparison between both fibers is also carried out at input signal power of -10 dBm, which shows a similar trend as depicted in Figure 3.13. In the experiment, the pump power is fixed at 130 mW. The new Zr-EDFA shows a higher measured gain at all wavelength tested compared to the previous Zr-EDFA. For the new

Zr-EDFA, the gain is maintained at above 12.5 dB within a wavelength region of 1520 nm to 1590 nm. The maximum gain of 21.1 dB is obtained at 1560 nm wavelength. For the previous Zr-EDFA with NER-6 fiber, a flat-gain of 14.1 dB is obtained within the wavelength region from 1530 nm to 1565 nm with a gain variation of less than 1 dB. On the other hand, the noise figure is significantly improved in the new Zr-EDFA compared to the previous amplifier. This is attributed to the population inversion, which is higher in the new fiber. The noise figure is maintained at a level below 6.5 dB within the wavelength region from 1520 nm to 1590 nm.

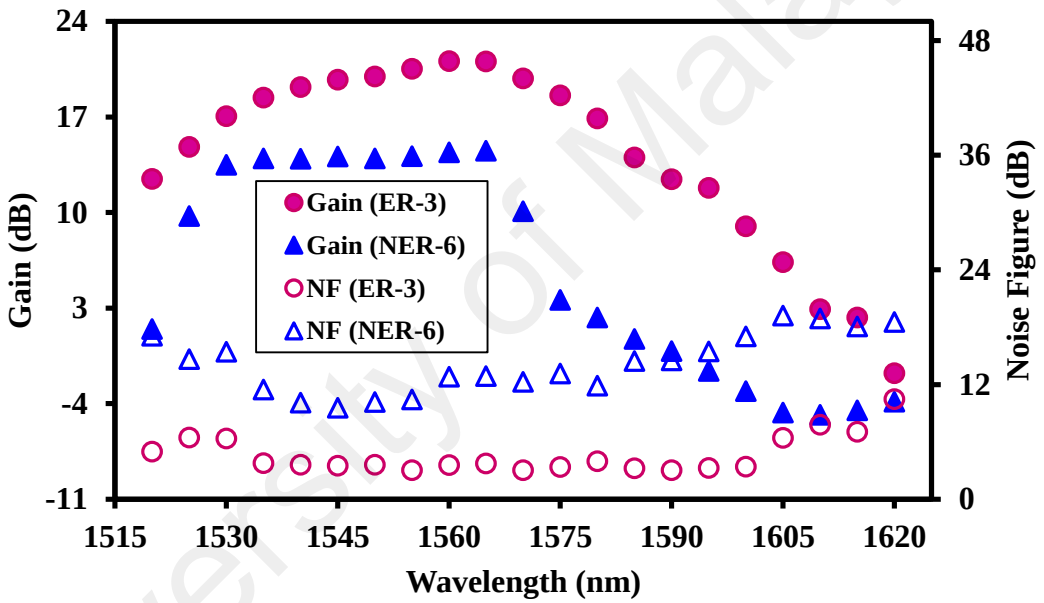

Figure 3.13: Comparison of the gain and noise figure spectra between the new Zr-EDFA (with ER-3 fiber) and the previous Zr-EDFA (with NER-6 fiber) when the input signal and pump powers are fixed at -10 dBm and 130 mW, respectively

A wideband operation within 1520 to 1615 nm is observed as zirconium oxide has a stretching vibration at about 470 cm^{-1}, which is very low compared with that of Al_2O_3 (870 cm^{-1}) and SiO_2 (1100 cm^{-1}) (Paul et al., 2010; Ahmad et al., 2012; Pal et al., 2011). In the proposed fiber, the particles possess lower phonon energy and thus reduce

non-radiative decay, which in turn increase the emission cross section (Myslinski, Nguyen & Chrostowski, 1997; Miniscalco, 1991). The introduction of Zr^{4+} in the fiber avoids the formation of Er^{3+} clusters in silica host and consequently increases the Er^{3+} ion density to make more intense luminescence. By replacing the intermediate Al_2O_3 with the modifier ZrO_2, the number of non-bridging oxygen is expected to increase, which makes the silica network structure more open. As the result, Zr-EDF has wider emission spectra as compared to silica-EDF, especially at longer wavelengths around 1620 nm because of its larger emission cross-section (Ahmad et al., 2010; Paul et al., 2010). The widening of the ASE spectra towards a longer wavelength is believed to be the result of the Stark level of the Er^{3+} ions in the Zr-EDF, which has a larger separation due to the intense ligand field. This is due to the inhomogeneous energy level splitting that the ligand field of the Zirconia host glass induces as a result of site-to-site variations, also known as the Stark effect, causing the widened optical transitions.

3.6 Performance Comparison with the Conventional Bi-EDFA

The EDFA has gained wide interest due to high power transmission efficiency from pump to signal power, wide spectral amplification with flatter gain, low noise figure and suitable for long-haul applications. To upgrade as ultrafast devices, a compact fiber laser with minimizes both of total gain medium length and dispersion is compulsory. In order to avoid pair-induced quenching effect which is the main degradation performance of EDFA, a strong interest in heavily doped erbium ion concentration by using various type of glass-host materials has been identified as a solution (Myslinski, Nguyen & Chrostowski, 1997). At first, Fujimoto and Nakatsuka (2001) were discovered that bismuthate-based optical fiber had a strong broadband near-IR luminescence. This fiber was also found to have the ability to be highly doped with erbium ions without decreasing the transmission performance (Ahmad et al., 2010). Then, many works have been

reported on Bi-EDF applications in amplifiers and pulsed fiber lasers developments (Cheng et al., 2009; Ahmad, Shahi & Harun, 2010).

In this section, the amplification performance of the enhanced Zr-EDF is compared with the Lanthanum/erbium co-doped Bi_2O_3 - based fiber (Bi-EDF). This is attributed to the fact that Bi-EDF was widely known as a choice for high flatness gain, wideband transmission, and the most interesting reason is due to its capabilities to accomplish by using very short gain medium, rewards for compact design system (Cheng et al., 2009; Cheng et al, 2011; Dianov, 2012). The improved Zr-EDF can be an alternative fiber to replace Bi-EDF due to the characteristic of Zr-EDF, which is more compatible to integrate with other transmission link and easily splice with other fibers using a commercial splicer. Furthermore, Bi-EDF suffers from large NA and cause the complication to integrate with other standard fiber and demands a special splicer. To realize the compact design system, both lengths of Zr-EDF and Bi-EDF are fixed at 0.5 m in this study.

3.6.1 Comparison of Optical Characteristics

Bi-EDF was fabricated from a preform that prepared by a melting technique and it was a commercial fiber from Asahi Glass Co. Ltd. The erbium ion concentration is 6300 wt. ppm with 4.4 wt. % La concentration. The La is used to decrease the quenching of concentration of the erbium ions. The Bi-EDF was fusion-spliced to high-NA fibers (Corning HI980) using a commercial fusion splicer, and the average splice loss was estimated to be less than 0.5 dB/point. Angled-cleaving and splicing were applied to suppress the reflection owing to the large refractive-index difference between the Bi-EDF and silica fiber. Table 3.2 compares the optical characteristics between Zr-EDF and Bi-EDF. Bi-EDF has a higher erbium ions concentration of 6300 ppm compare to 4000 ppm for Zr-EDF. The higher erbium ions concentration in gain medium, the higher optical

gain is predicted to be achieved. Once again, Bi-EDF shows high absorption rate of 141 dB/m at 1480 nm pump power, corresponds to the high concentration of erbium ions. The refractive index difference is almost similar, which determines both of fiber has a minimum waveguide loss. For core diameter, Zr-EDF has a larger diameter with 10.04 µm compare to Bi-EDF with only 4.5 µm. Core diameter is important parameter in fiber fabrication to determine fiber efficiency due to efficient light is traveling through the core instead of incoherent light in cladding. Therefore, the larger core diameter, the more efficient and coherent light capable to travel inside the gain medium. The most disadvantage of Bi-EDF is the large NA of 0.20, cause more difficulties to be integrated with other transmission link. It increases the total loss in cavity and thus, decrease the overall performance of amplifier.

Table 3.2 Optical characteristics between Zr-EDF with Bi-EDF

Types	New Zr-EDF	Bi-EDF
Erbium-doped Concentration	4000 ppm	6300 ppm
Absorption Rate	80.0 dB/m at 980 nm	141 dB/m at 1480 nm
Refractive Index Difference	0.012	0.010
Core Diameter	10.04 µm	4.5 µm
Numerical Aperture (NA)	0.17	0.20

3.6.2 Single-pass Performances

The performance comparison between Zr-EDF and Bi-EDF as gain medium by using single pass configuration is illustrated in Figures 3.14 and 3.15. The input powers are fixed at -30 dBm and -10 dBm, respectively. In the experiment, the length for both fibers is fixed at 0.5 m while the pump power is fixed at 130 mW. At input power -30 dBm, the gain performance of the Zr-EDF was successfully overcome Bi-EDF with

improvement of 5.3 % from 1520 nm to 1575 nm. The highest gain of 27.45 dB is obtained for Zr-EDFA at 1535 nm, which showing that the amplifier operates in C-band region with the short length of 0.5 m. The L-band gains are low since the length used is insufficient to create an efficient population inversion in L-band region. However, the Bi-EDFA gain grows higher in L-band region ranging from 1580 nm to 1620 nm. This is most probably due to the Erbium ion concentrations which is higher in the Bi-EDF. The highest gain for Bi-EDFA is 26.51 dB, which is obtained at 1535 nm. On the other hand, the noise figure performance for the Zr-EDFA is better than that of Bi-EDFA especially at C-band region. It is maintained below than 10 dB from 1520 nm to 1620 nm with total average of 7.46 dB. Bi-EDFA suffers to a slightly higher noise figure with total average of 8.01 dB due to the slightly higher splicing loss in the amplifier's system.

Figure 3.15 shows the comparison result at input signal power of -10 dBm. Similarly, the gain performance of the Zr-EDFA had surpassed Bi-EDFA with improvement of 8.3 % from 1520 nm to 1580 nm. The average gain for Zr-EDFA and Bi-EDFA for the mentioned region were 16.51 dB and 13.97 dB, respectively. It is also observed that the Zr-EDFA managed to provide a flat-gain at around 16.5 dB with small fluctuation of less than 1 dB from 1530 nm to 1575 nm. On the other hand, the noise figures for both amplifiers are maintained below 12 dB from 1525 nm to 1620 nm.

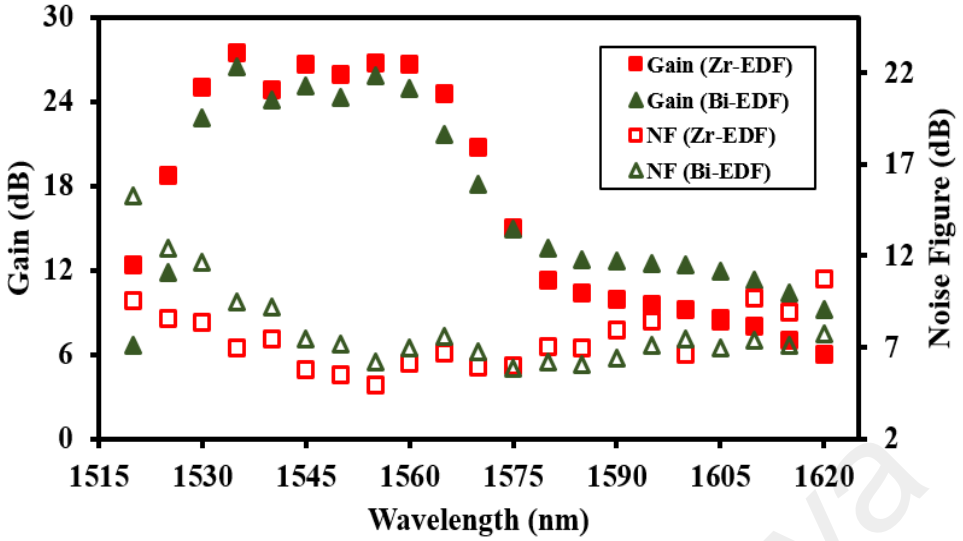

Figure 3.14: Comparison of the gain and noise figure spectra between the single-pass Zr-EDFA and the Bi-EDFA when the input signal and pump powers are fixed at -30 dBm and 130 mW, respectively

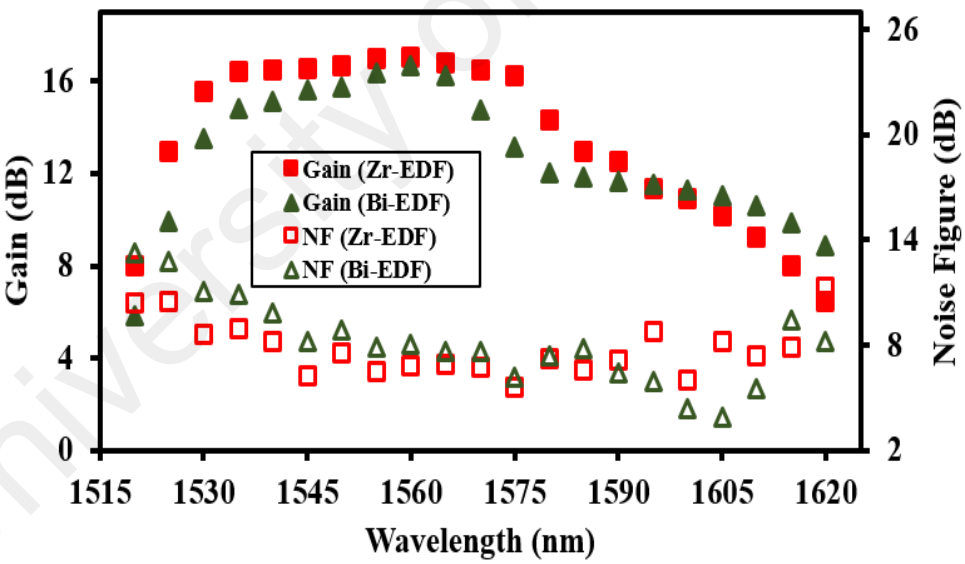

Figure 3.15: Comparison of the gain and noise figure spectra between the single-pass Zr-EDFA and the Bi-EDFA when the input signal and pump powers are fixed at -10 dBm and 130 mW, respectively

3.6.3 Double-pass Performances

In this sub-section, the performance of the double-pass Zr-EDFA of Figure 3.9 is investigated and compared with the conventional double-pass Bi-EDFA. The double-pass Bi-EDFA is obtained by replacing the Zr-EDF with Bi-EDF in configuration of Figure 3.9. Meanwhile Figure 3.16 shows the measured gain and noise figure of both Zr-EDFA and Bi-EDFA with the doped fiber length of 0.5 m as the input signal and 980 nm pump power is set at -30 dBm and 130 mW, respectively. Both EDFAs operate in C-band region with a relatively flat gain characteristic. The highest gain of 33.7 dB was obtained at 1530 nm for the Zr-EDFA. Within the wavelength region from 1530 to 1560 nm, overall gain for Zr-EDFA obtained was more than 29.8 dB with gain variation of less than 3 dB. The measured noise figure was less than 5.3 dB within this wavelength region. However, the maximum gain achieved for Bi-EDFA was 27.1 dB at 1555 nm with the corresponding noise figure of 6.7 dB. Overall, the gains for Zr-EDFA are higher by more than 3.4 dB compared to that of the Bi-EDFA, at a flat-gain wavelength region. The strong increment of noise figure for EDFAs at longer wavelength was due to the output signal was reflected back to the cavity, thus it enhanced the ASE noise and suppressed the achievable gain.

Figure 3.17 shows the measured gain and noise figure of both Zr-EDFA and Bi-EDFA when the input signal and pump power is set at -10 dBm and 130 mW, respectively. As seen in the figure, the gain varies from 18.8 to 21 dB within the wavelength region from 1525 to 1565 nm for the Zr-EDFA. The gain is about 2-3 dB higher compared to the Bi-EDFA at the flat gain region, which is due to the lower splicing loss in the amplifier's system. On the other hand, the noise figure is maintained below 14.7 and 20.6 dB within the flat gain region for Zr-EDFA and Bi-EDFA, respectively. At the wavelength region above 1575 nm, however, the gain of Bi-EDFA is relatively higher due to the suppression of excited-state absorption at this wavelength region.

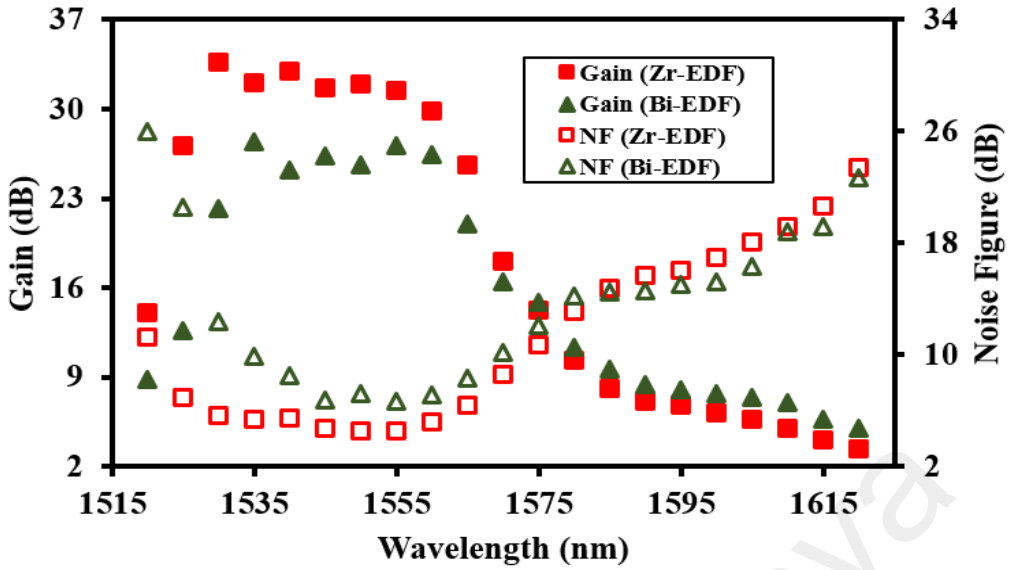

Figure 3.16: Comparison of the gain and noise figure spectra between the double-pass Zr-EDFA and the Bi-EDFA when the input signal and pump powers are fixed at -30 dBm and 130 mW, respectively

It is observed that a flat gain bandwidth is also broader with the Zr- EDFA compared with the Bi-EDFA at C-band region. This is probably due to the smaller energy transfer from shorter wavelength to a longer wavelength at the 1565 nm region. This is due to the up-conversion process that suppresses the amplification at an extended L-band region. This effect is less in the Bi-EDFA owing to incorporation of lanthanum ions. The noise-figure characteristic is strongly dependant on the cavity loss as well as the gain of the EDFA. Therefore, the noise figure reduces as the operating wavelength increases because of cavity loss that is lower at the longer wavelength. The noise figure is also lower with the Zr-EDFA, which exhibits a higher gain.

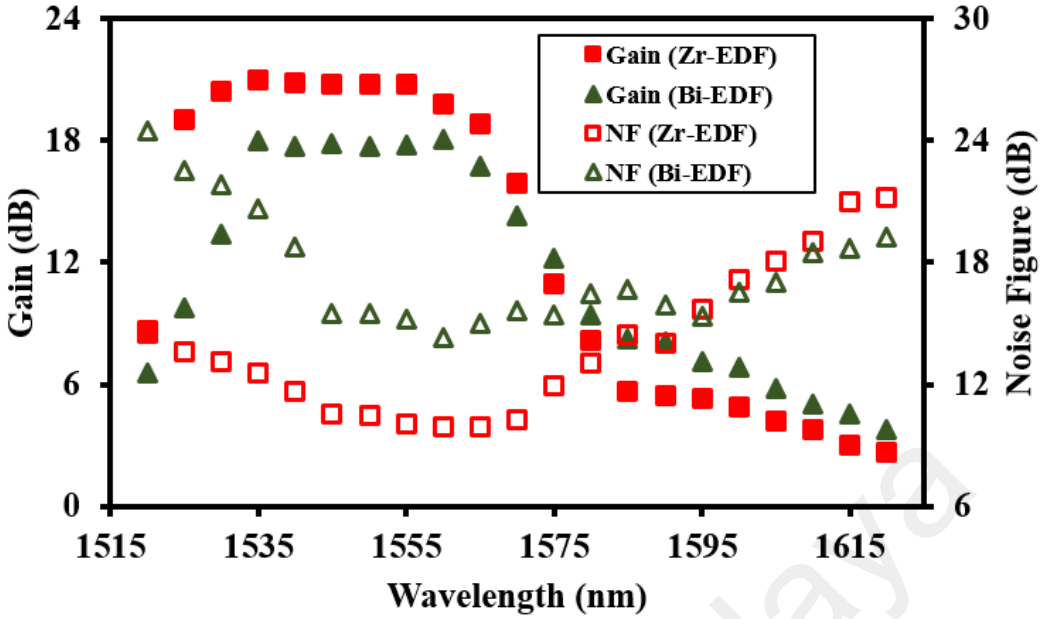

Figure 3.17: Comparison of the gain and noise figure spectra between the double-pass Zr-EDFA and the Bi-EDFA when the input signal and pump powers are fixed at -10 dBm and 130 mW, respectively

These results show that the enhanced Zr-EDFA can achieve better gain and noise figure characteristics to the conventional Bi-EDFA for C-band operation. The large core diameter of Zr-EDF contributes to the improvement due to more useful light was traveling through the core, lowering the loss inside the fiber and thus it enhances the population inversion in the active fiber. There the Zr-EDF is expected to be preferable than Bi-EDF to provide high flatness gain in wideband transmission distance with very short length of gain medium, and realizes the future miniature and compact device systems. Compared to the Bi-EDF, the Zr-EDF is compatible and easier to be spliced with the standard SMF.

3.7 Performance Comparison with the Conventional Si-EDFA

In the choice of glass host, many researchers have focused on only high silica glass owing to its proven reliability and compatibility with conventional fiber-optic components. In this section, a comparison of the performance of a Zr-EDFA and a silica

based Erbium-doped fiber amplifier (Si-EDFA) is presented. Table 3.3 illustrates the optical characteristics comparison between the enhanced Zr-EDF and commercial Silica based Erbium-doped fiber (Si-EDF). This fiber is known as IsoGain^{TM} I-25 and is commonly used for both C- to L-band optical amplifiers. It has an absorption rate of 23 dB/m at 980 nm, which can be translated to Erbium ions concentration doping of 2200 wt. ppm. EDF without any co-doped material suffers from incapable to be highly doped with erbium ions due to damaging effects such as pair-induced quenching (PIQ) effect. This kind of effect reduces the efficiency of pump power conversion, and thus it increase the noise figure of EDFA (Harun, Saat & Ahmad, 2005). There are no much differences in other parameters such as refractive index difference between core and cladding, fiber diameter and NA. Both fibers has NA of 0.17, and thus they are expected to have a high flexibility in transmission network.

Table 3.3: Specification comparison between Zr-EDF with EDF

Types	New Zr-EDF	Si-EDF
Erbium-doped Concentration	4000 ppm	2200 ppm
Absorption Rate	80.0 dB/m at 980 nm 220.0 dB/m at 1550 nm	23.0 dB/m at 980 nm 40.0 dB/m at 1531 nm
Refractive Index Difference	0.012	0.010
Fiber Diameter	126.83 µm	125 µm
Numerical Aperture (NA)	0.17	0.17

At first, the performance comparison is investigated based on a basic single-pass configuration of Figure 3.4. In the experiment, the fiber length is fixed at 1 m for both EDFs. Figure 3.18 shows the measured gain and noise figure of both amplifiers at an input signal power of -30 dBm. In the experiment, the pump power is fixed at 130 mW.

The maximum gain of 28.5 dB and 30.5 dB are obtained for the Zr-EDFA and Si-EDFA, at 1535 nm and 1530 nm respectively. The Zr-EDFA illustrates a more efficient and flatter gain compared to Si-EDFA at C-band region. For instance, at 1555 nm, a gain improvement of 5.1 dB is obtained with the use of Zr-EDF. The gains at L-band region is also higher with the Zr-EDFA as compared to the Si-EDFA. This is attributed to the optimized doped fiber length, which is longer for the Si-EDFA. The Zr-EDF has a higher erbium ion concentration doping of 4000 ppm that enhances the attainable optical gain for a wider bandwidth up to 1620 nm. The Zr-EDFA illustrates a lower noise figure compared to Si-EDFA at wavelength region above 1550 nm. This is due to a higher gain at this region, which can be translated to an efficient population inversion, which reduces the ASE noise. The noise figures are maintained below 11 dB within a wavelength range from 1530 to 1620 nm for the Zr-EDFA.

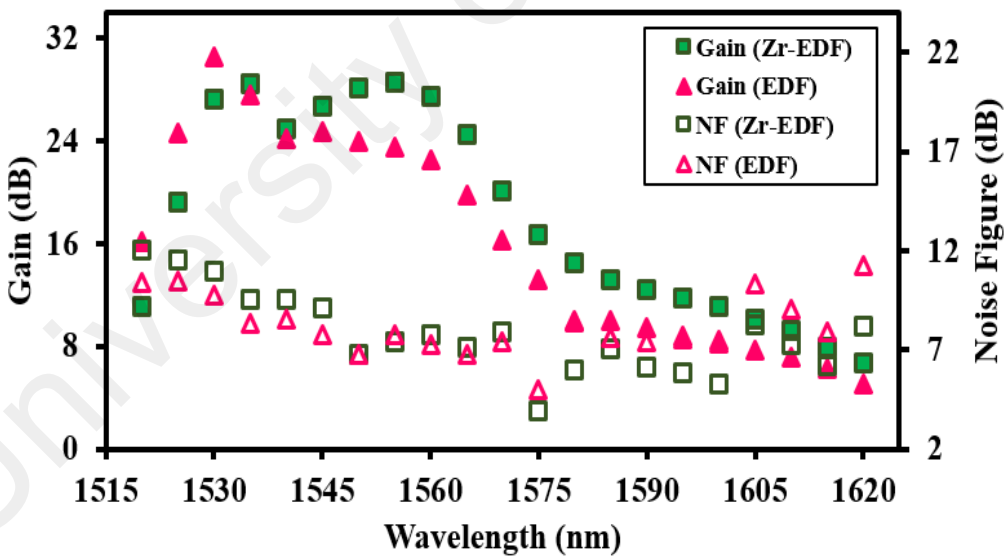

Figure 3.18: Comparison of the gain and noise figure spectra between the single-pass Zr-EDFA and the Si-EDFA when the input signal and pump powers are fixed at -30 dBm and 130 mW, respectively

Figure 3.19 illustrates the comparison of the gain and noise figure spectra between the single-pass Zr-EDFA and the Si-EDFA when the input signal and pump powers are fixed at -10 dBm and 130 mW, respectively. Compared to the conventional Si-EDFA, the gain is more efficient especially at wavelength above 1530 nm in the Zr-EDFA. The maximum gain improvement of 3.6 dB is observed at 1565 nm. A flat-gain of 19.5 dB is also obtained for the Zr-EDFA with gain variation of less than 1 dB within a wavelength region from 1530 to 1570 nm. The noise figures for both amplifiers are maintained below 12 dB for all wavelengths tested.

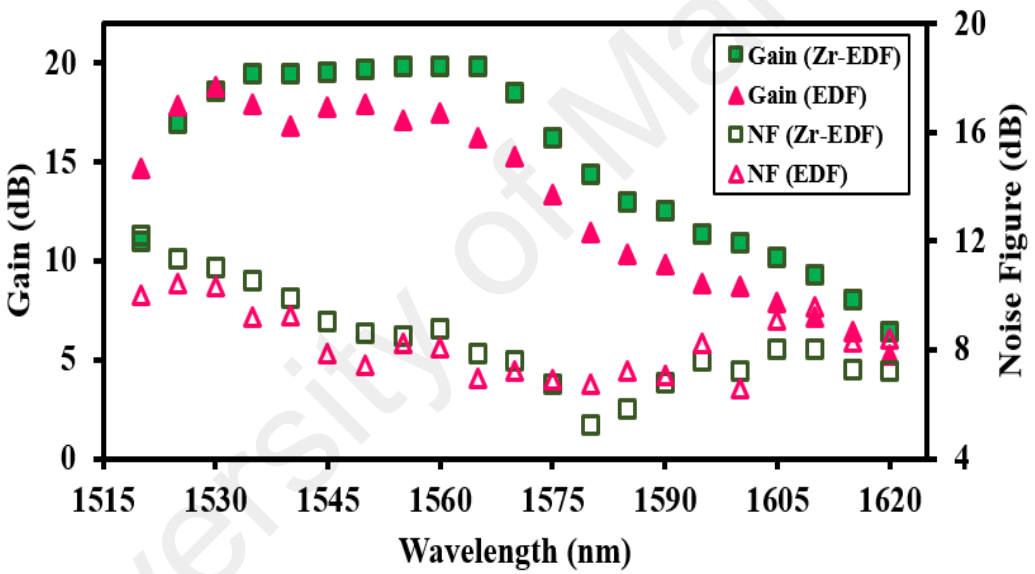

Figure 3.19: Comparison of the gain and noise figure spectra between the single-pass Zr-EDFA and the Si-EDFA when the input signal and pump powers are fixed at -10 dBm and 130 mW, respectively

Finally, performance comparison between double pass Zr-EDFA and Si-EDFA is investigated. The result is presented in Figures 3.20 and 3.21 for input signal powers of -30 dBm and -10 dBm, respectively. In the experiment, the gain length is fixed at 1.0 m for both amplifiers. The double-pass Zr-EDFA shows a more efficient gain and noise

figure compared to the double-pass Si-EDFA especially at longer wavelength region. The gain peaks at around 40 dB at 1530 nm and 1560 nm for double-pass Si-EDFA and Zr-EDFA, respectively at input signal of -30 dBm. As shown in Figure 3.20, the gain for Si-EDFA exponentially reduces as the operating wavelength is increased above 1530 nm while the noise figure also degrades exponentially as the operating wavelength is increased above 1545 nm. This is attributed to the optimum gain medium length for double-pass operation of Si-EDFA should be significantly longer. It was reported that about 10 to 50 m long of EDF (I-25) was required to achieve a wide-band operation with double-pass configuration for the Si-EDF (Harun & Ahmad, 2003; Hamida et al., 2015). This is attributed to the significantly lower Erbium ion concentration in the Si-EDF. When the signal is amplified twice in the double-pass system, the strong growth ASE noise causes the gain reduction and noise figure increment at longer wavelength region. This prevents the formation of flat-gain spectrum for the Si-EDFA especially at small input signal. On the other hand, at the input signal power of -30 dBm, the double-pass Zr-EDFA produces a flat-gain spectrum within a wavelength region from 1530 to 1565 nm with an average gain of 38.5 dB and gain variation of less than 3 dB. The corresponding noise figure is maintained below 6.5 dB at the flat-gain region.

At the input signal of -10 dBm, the higher and wider flat gain spectrum is also obtained by the double-pass Zr-EDFA compared to that of Si-EDFA. As shown in Figure 3.21, the measured gain varies from 17.5 dB to 21.3 dB within the wavelength region from 1525 to 1565 nm, where the noise figure is maintained at below 10 dB. The highest gain is obtained at 1565 nm. These results indicate that a Zr-EDFA can achieve even better flat-gain value and bandwidth as well as lower noise figure than the conventional Si-EDFA.

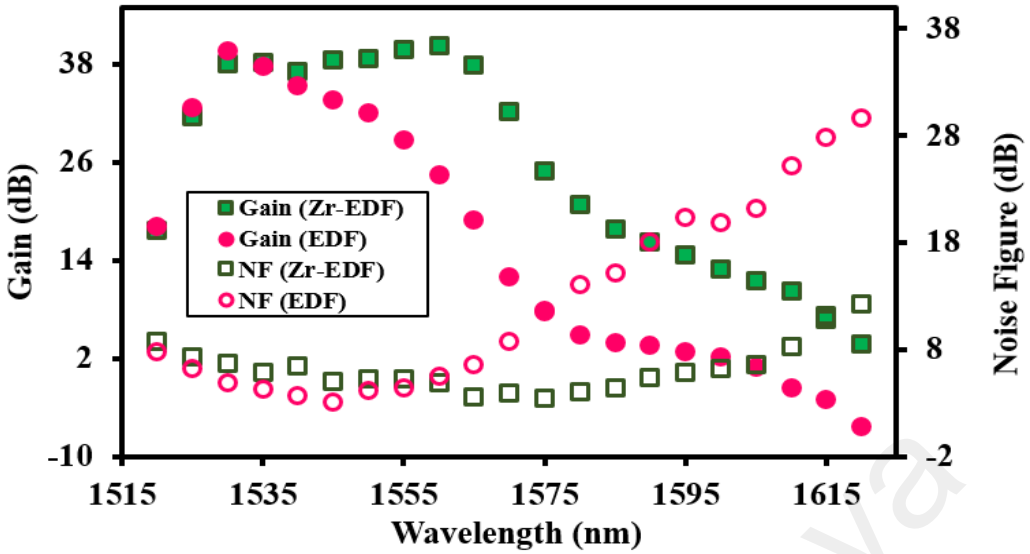

Figure 3.20: Comparison of the gain and noise figure spectra between the double-pass Zr-EDFA and the Si-EDFA when the input signal and pump powers are fixed at -30 dBm and 130 mW, respectively

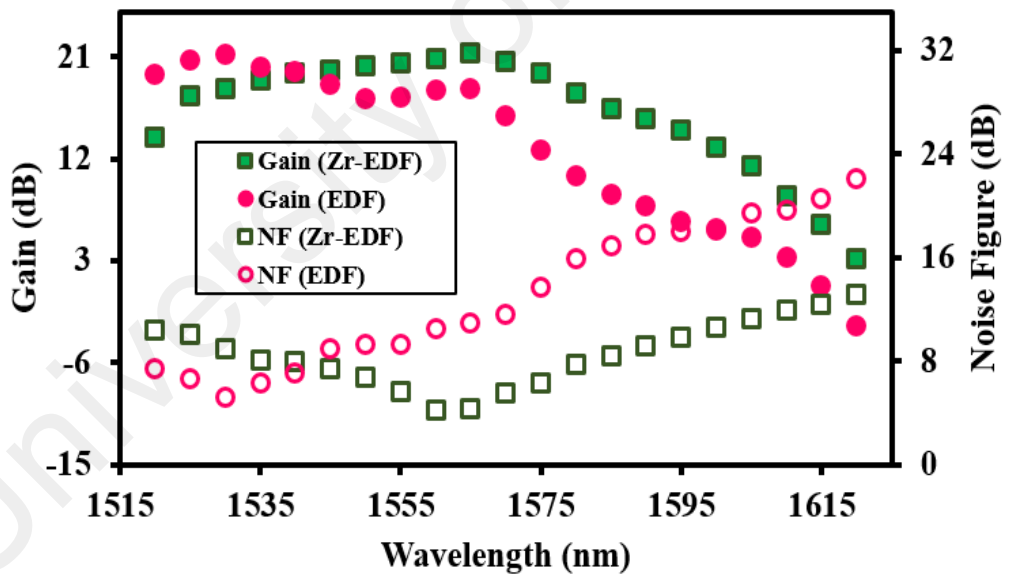

Figure 3.21: Comparison of the gain and noise figure spectra between the double-pass Zr-EDFA and the Si-EDFA when the input signal and pump powers are fixed at -10 dBm and 130 mW, respectively

3.8 Summary

A new Zr-EDFA with improved gain and noise figure characteristics are successfully demonstrated by using a newly developed Zr-EDF as the gain medium. The Zr-EDF is obtained from a fiber preform, which is fabricated in a ternary glass host, zirconia-yttria-aluminium co-doped silica fiber using a MCVD in conjunction with solution doping process. The fiber consists of Er_2O_3-doped ZrO^2 rich nano-crystalline particles and thus it has a high erbium doping concentration with absorption pump power around 80.0 dB/m at 980 nm. At the optimum length of 1 m with a standard single-pass configuration, the Zr-EDFA produces a flat-gain of 27 dB within a wavelength region between 1530 to 1565 nm with gain fluctuation of less than 3 dB and noise figure less than 6.9 dB when input signal power and 980 nm pump power are fixed at -30 dBm and 130 mW, respectively. At input signal of -10 dBm, pump power of 130 mW and fiber length of 1 m, a flat-gain of 19.6 dB is obtained within a wavelength region between 1530 to 1570 nm with a gain variation of 0.27 dB and noise figure below 11 dB. With a double-pass configuration, the Zr-EDFA produces a flat-gain of 38 dB within a wavelength region between 1530 to 1565 nm with gain fluctuation less than 3 dB. In the experiment, the fiber length is fixed at 1.0 m while the input signal power and 980 nm pump power are fixed at -30 dBm and 130 mW, respectively. Compared with the previous Zr-EDFA with a lower Erbium ion concentration, the gain of the proposed Zr-EDFA improves, especially at a longer wavelength region. The gain enhancement of about 15.8 dB is obtained at wavelength of 1560 nm for -30 dBm input signal. The performance of the Zr-EDFA are also better than the conventional Bi-EDFA and Si-EDFA.

CHAPTER 4: PULSED ZIRCONIA-BASED ERBIUM DOPED FIBER LASERS

4.1 Introduction of Pulsed Laser Applications

The development of fiber lasers has gained an increasing interest in recent years as a possible replacement to high-cost, bulk solid state lasers. These lasers have a great potential applications in various fields such as remote sensing, laser range finding, communication, marking, micro-machining, biomedical imaging and medical surgery (Fermann, Galvanauskas & Sucha, 2002; Fermann & Hartl, 2009; Lee, 2003). Fiber lasers could also operate in Q-switched or mode locked regimes to emit short pulses and ultrashort pulses at repetition rates of kHz and MHz, respectively. For instance, Q-switching fiber laser is widely used for tattoos removal and 3D optical data storage due to high peak power in nanoseconds pulse duration (Leuenberger, et al., 1999; Zhu et al., 2006). Meanwhile mode-locking ultrashort pulse with higher repetition rate have more advantages such as enabling cleaner ablation of materials in micro-machining and medical surgeries, higher efficiencies in laser communication, and precise measurement in remote sensing and laser range finding (Cheng et al., 2003; Arai et al., 1996). In this chapter, Zirconia based Erbium-doped fiber lasers (Zr-EDFLs) operating in Q-switched or mode-locked regimes are demonstrated using three different passive techniques.

4.2 An L-band Mode-Locked Fiber Laser Delivering Bright and Dark Pulses with Zr-EDF based on Nonlinear Polarization Rotation (NPR)

Dark pulse operation of lasers has attracted considerable attention in recent years with respect to bright pulses because of their potential applications (Kivshar et al., 1998). Dark pulses are defined as a train of intensity dips in the intensity of a continuous wave

(CW) background of the laser emission. Numerical simulations have found that dark pulses are less sensitive to fiber loss and more stable in the presence of noise compared with bright pulses, which have potential applications in fiber based communication system (Gredeskul & Kivshar, 1989; Zhao et al., 2013; Hasegawa & Tappert, 1973; Kivshar et al., 1994). To date, there have been many approaches for the generation of dark pulse trains. Most of these methods are based on external manipulation of laser light using pulse shaping techniques, such as direct modulation of CW light by means of a phase modulated fiber loop mirror or a phase modulated Mach–Zehnder interferometer, and passive filtering of a mode locked bright pulse train with a fiber Bragg grating or a spatial mask (Nakazawa & Suzuki, 1995; Emplit et al., 1997; Feng et al., 2010).

Dark pulse was first numerical predicted by Hasegawa & Tappert (1973), and experimental demonstrated by Emplit et al., (1987) by using optical fiber which is exposed the chances to be realized in the future fiber laser applications. Dark pulse or dark soliton originates was directed by nonlinear Schrödinger equation (NLSE) and then it was described by the complex Ginzburg-Landau equation (CGLE) (Zhang et al., 2009; Krokel et al., 1988). Sylvestre, et al., were the first demonstrated experimentally the generation of dark pulse train in mode-locked fiber laser back on 2002 (Zhang et al., 2010). However, it starts to gain attraction when it was experimental realized by Zhang et al., on 2009 by using nonlinear polarization rotation (NPR) technique in normal dispersion region and explained clearly by numerical simulations the formation of dark pulse due to dark soliton shaping (Zhang et al., 2011). By using the same technique of NPR, the generation of dark pulse were further experimental demonstrated in multiwavelength and even dark soliton in anomalous dispersion region (Yin et al., 2010; Hui-Yi et al., 2011). The concept that agreed by CGLE is to accomplished domain wall between traveling waves. It can be generated by managing either two orthogonal polarization states of light or dual- or multiwavelength that induced by high nonlinearity

of birefringence in cavity (Liu et al., 2014; Yin et al., 2010; Zhang et al., 2010). A high nonlinear medium is essential to increase the cross coupling effect between multi lasing beams and to make easier way for the dark pulse formation.

In this section, we report the experimental observation of bright and dark pulse generations in a dispersion managed Zr-EDFL cavity with net anomalous cavity GVD. The passively mode-locked operation of the fiber laser is achieved by employing the nonlinear polarization rotation technique. Together with the support from large Kerr nonlinearity in the Zr-EDF, mode-locking pulses are generated from the dispersion managed fiber laser at a relatively low pump threshold of 70 mW. The bright and dark pulses repeated at the fundamental cavity frequency can be obtained by adjusting the polarization state of laser cavity. It is also experimentally found that the bright and dark pulses are generated primarily due to the cross coupling between two-Eigen operation states of fiber laser through the nonlinear effects of optical fibers.

4.2.1 Configuration of the NPR-based Zr-EDFL

Figure 4.1 shows the configuration of the proposed dispersion managed fiber laser. The fiber laser has a ring cavity of about 14.5 m long consisting of a 980/1550 nm wavelength division multiplexer (WDM), Zr-EDF, polarization controller (PC), 10 dB coupler and a polarization dependent isolator (PDI). The laser cavity consists of three types of fibers: 3.0 m long Zr-EDF with a GVD parameter of about -56 ps^2/km, 3.0 m long WDM fiber with a GVD of -38 ps^2/km and 8.5 m long standard single-mode fiber (SMF) with a GVD of -21 ps^2/km. The net cavity dispersion and group delay dispersion (GDD) were estimated to be 0.338 ps/nm and -0.46 ps^2. Apart from assuring unidirectional operation, the polarization-dependent isolator (PDI) also provides spectral filtering effect by combining with the intra-cavity birefringence. PC was used to adjust

the polarization of light in the cavity and switched the operation of the mode-locked laser from bright to dark pulse regime. The gain medium, Zr-EDF was pumped by a 980 nm laser diode (LD) through a WDM. Since all of the fibers are fastened to an optical table to prevent any movement, the fiber laser operates in a stable passive mode-locking regime. The laser output is taken out via a 5 dB fiber coupler while allowing 95 % of the light to oscillate in the ring cavity. The pump power and average output power were measured by a photodiode power meter. The monitoring of the output spectra and pulse trains was performed using an optical spectrum analyzer (OSA) with a minimum resolution of 0.02 nm and a 500 MHz digital phosphor oscilloscope.

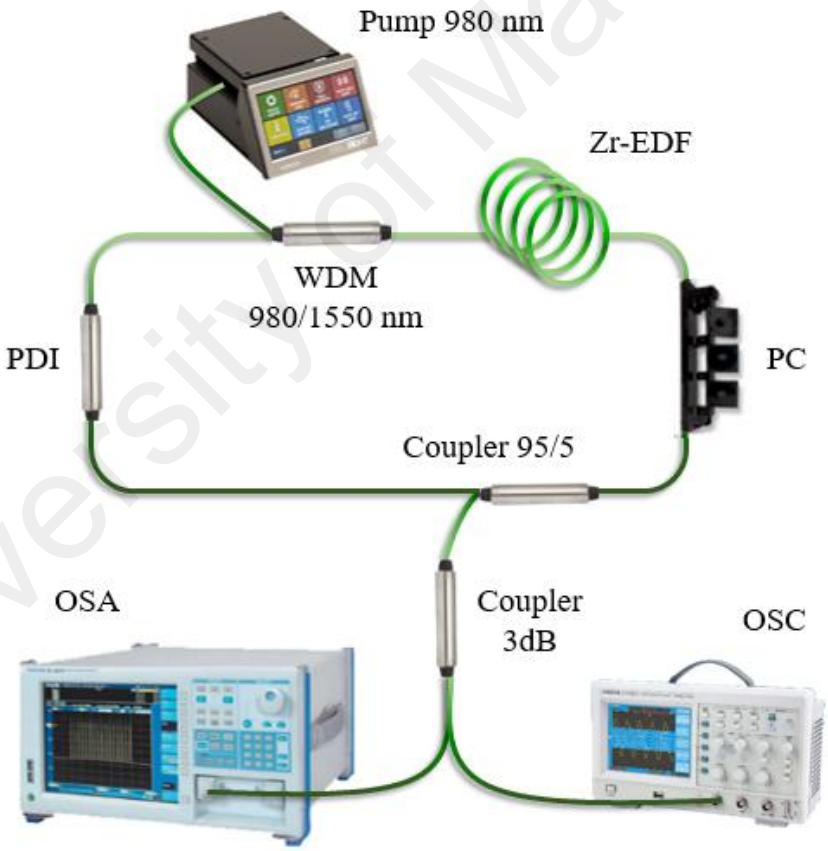

Figure 4.1: Experimental setup for the NPR based Zr-EDFL

4.2.2 Mode-Locked Zr-EDFL Performance

Generally, the Zr-EDF utilized has a very large doping concentration, which caused lasing at near 1600 nm. From this cavity, continuous wave lasing started at ~55 mW of pump power. This pump threshold is higher than that in a typical C-band fiber laser; this was associated with the much lower gain in the L-band. When the pump power continuously increased up to 70 mW, self-starting single pulse mode locking could be observed with an average output power of ~0.2 mW. The performance of the laser is maintained up to the pump power of 105 mW. The oscilloscope trace of the output pulse train is plotted in Figure 4.2 (a). It shows that bright pulses are circulating in the cavity with a round-trip time of 70.9 ns which is corresponding to the cavity fundamental frequency of 14.1 MHz. The pulse repetition rate frequency was approximately defined by the cavity length of ~14.5 m.

By adjusting the polarization state of the oscillating light with a PC, dark pulses are found to circulate in the cavity repeated at the same frequency as shown in Figure 4.2 (b), indicating that the laser operating is shifted from the bright to the dark regime. Figure 4.3 compares the typical measured output spectrum for both bright and dark pulse train. It shows a central wavelength at ~1601 nm and 3 dB bandwidth of 0.1 nm, falling in the L-band of the third telecommunication window. The output power improved and an additional wavelength component also appears in the output optical spectrum of the dark pulse as shown in Figure 4.3. Therefore, we expect that the generation of dark pulse in the proposed cavity is based on dual wavelength DW, which was achieved under the optimum polarization orientation.

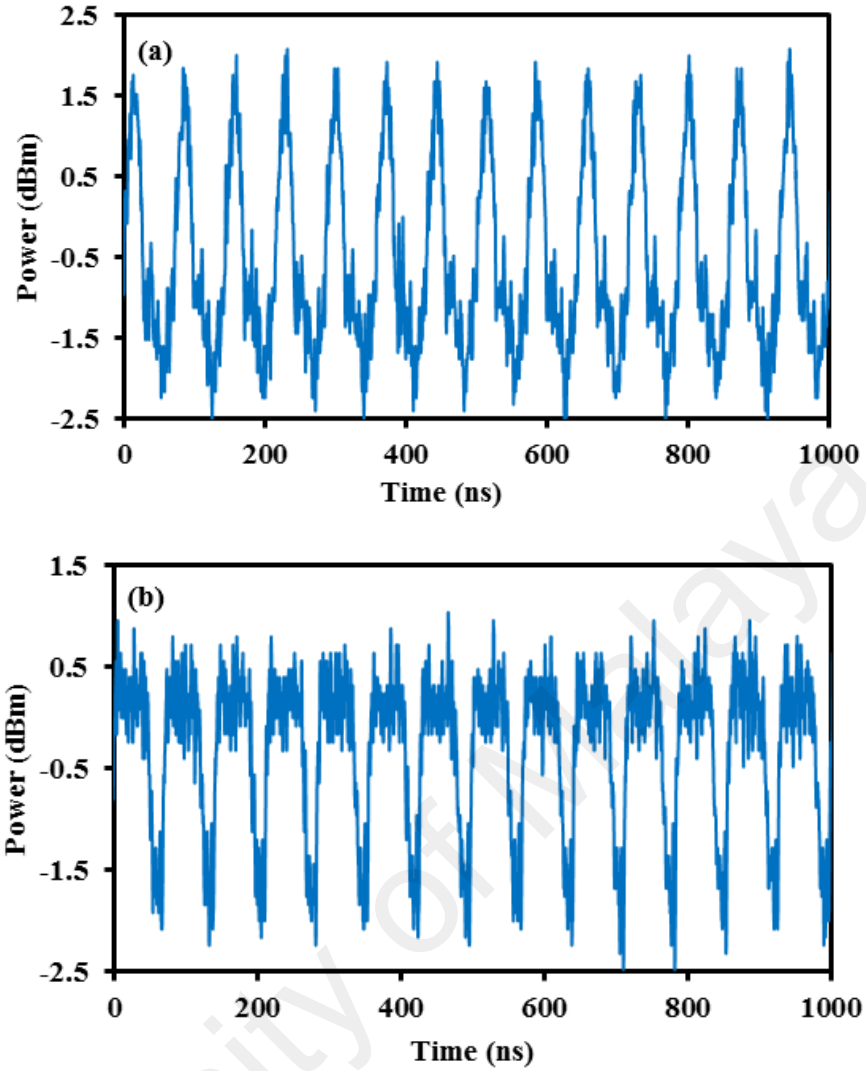

Figure 4.2: Typical oscilloscope trace of the mode-locked Zr-EDFL when emitting (a) bright (b) dark pulse train at pump power of 70 mW

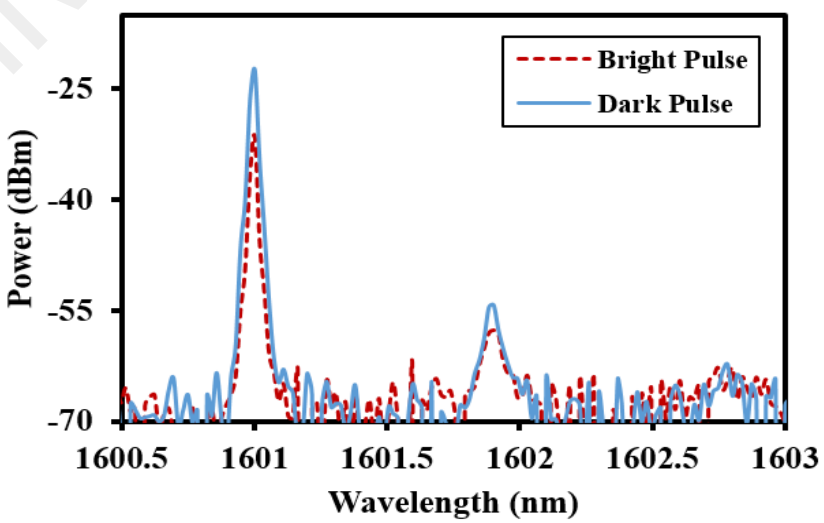

Figure 4.3: Output spectra obtained during the bright and dark pulse generation

The incorporation of a PDI and the slightly residual polarization asymmetry of the used components in the cavity and the artificial birefringent filter is produced. This artificial birefringence filter has the capability to develop multiwavelength with the help of effective optical gain of fiber. At the optimized polarization rotation and sufficient pump power, consequently, the cross coupling between the dual wavelength emission is improved. Then, a narrow with a dip intensity in the strong background of CW emission is formed and demonstrated in Figure 4.2 (b). The pulse width is measured to be around 27.8 and 27.1 ns for the bright and dark pulse, respectively. The pulse energy of the dark pulse is estimated to be around 14.2 pJ at pump power of 70 mW. Figure 4.4 shows the Radio Frequency (RF) spectrum of the dark pulse at the pump power of 70 mW. The optical signal to noise ratio (OSNR) of the laser is around 33 dB, which indicates that the laser is operating in a stable condition. Even though there are two operating wavelengths in the cavity, only a single frequency component is observed, which confirms a typical DW operation whereby the mutual coupling of two wavelengths generates a single frequency component. In the experiment, the transformation of bright pulse into dark pulse can be reversed by adjusting the PC.

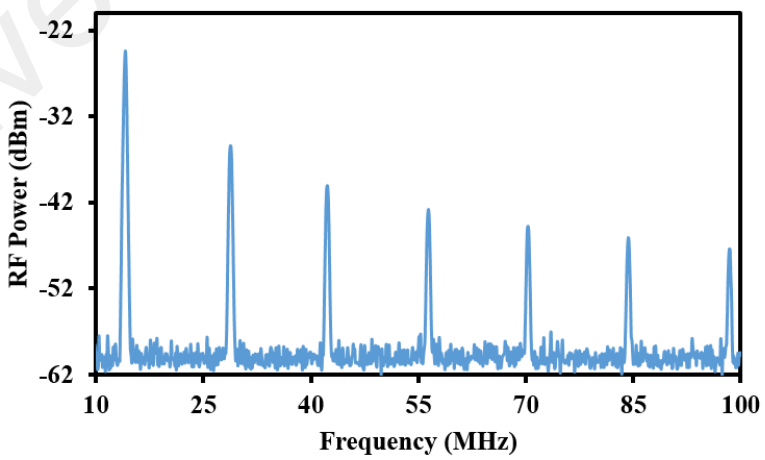

Figure 4.4: RF spectrum of the proposed dark pulse Zr-EDFL at pump power of 70 mW

4.3 Q-switched Zr-EDFL based on Thulium-doped Fiber (TDF) SA

Q-switched fiber lasers have great potential applications in many fields including spectroscopy, biomedical diagnoses, fiber communication and others. Q-switching in all-fiber lasers has been achieved by using active techniques such as piezoelectric actuators, acoustic-optics modulators or magnetostrictive transducers to modulate the Q-factor of the cavity (Li et al., 2011; Camargo et al., 1995). Q-switched fiber lasers can also be realized using passive approaches where saturable absorber (SA) is a key component. Several types of materials and construction techniques have been proposed to develop SA for passive Q-switching such as semiconductor SA mirror (SESAM), graphene and carbon nanotubes (CNTs) (Spühler et al., 2001; Popa et al., 2010; Zhou et al., 2010). SESAM is the type that widely used. Yet, it has some drawbacks such as low damage threshold, fabrication and packaging complexity and limited operational wavelength. As a favourable SAs candidate, graphene and CNTs have advantages of easy fabrication, wideband operation and low cost. However, both SAs also have a low threshold damage and thus it limits the attainable energy of pulses.

Rarely, a solid state SA optical fibers are also able to modulate the Q-factor. The benefits of this type of SA optical fiber are their high threshold damage and the capability to hold a large excited gain in fiber from lasing for high power Q-switching pulsed fiber laser. Still, only a few SA optical fibers have been realized, and Ytterbium-doped fiber lasers are the most common used experimentally (Dvoyrin et al., 2007; Kurkov et al., 2009). The energy transition $^3H_6$ - $^3F_4$ of Tm^{3+} has a very broad emission wavelength range, from 1.6 to 2.1 μm, and an absorption band from 1.5 to 1.9 μm. It is reported that the absorption cross section of Tm^{3+} doped fibers (TDFs) are larger than the emission cross sections of Erbium-doped fiber (EDF) at 1.6 μm region, suggesting a possible realization of a passively Q-switched EDFL using a TDF as a passive SA. In this paper, a Q-switched fiber laser operating at 1556 nm is demonstrated using a solid state SA fiber

based on ring laser cavity. In this work, a 2 m long newly developed Zr-EDF and 1 m long a commercial TDF are used as a gain medium and a Q-switcher, respectively.

4.3.1 Configuration of the TDF-based Zr-EDFL

Figure 4.5 shows the schematic diagram of a passively Q-switched all-fiber Zr-EDFL using a solid state SA fiber. The laser cavity consists of a 2 m long Zr-EDF as the gain medium, a wavelength division multiplexer (WDM), a polarisation controller (PC), a 10 dB coupler and 1 m long TDF as a SA and an optical isolator. The Zr-EDF is pumped by a commercial 980 nm laser diode via a 980/1550 WDM. The TDF was a 1.0 meter long with an initial absorption loss of 6 dB at 1570 nm, numerical aperture of 0.16 and core diameter of 2.9 μm. An isolator is employed to prevent the backward reflection and ensure unidirectional operation. The PC is used to control the polarization of the oscillating light and optimize the Q-switching and laser operations. The laser light is extracted from the cavity by a 10 dB fiber coupler which retains 90 % of the light in the cavity for further oscillation. An OSA is used to capture the output laser spectrum while a 350 MHz oscilloscope in conjunction with 1.2 GHz bandwidth photo-detector is used to detect the pulse train. The total length of the cavity is around 6 m.

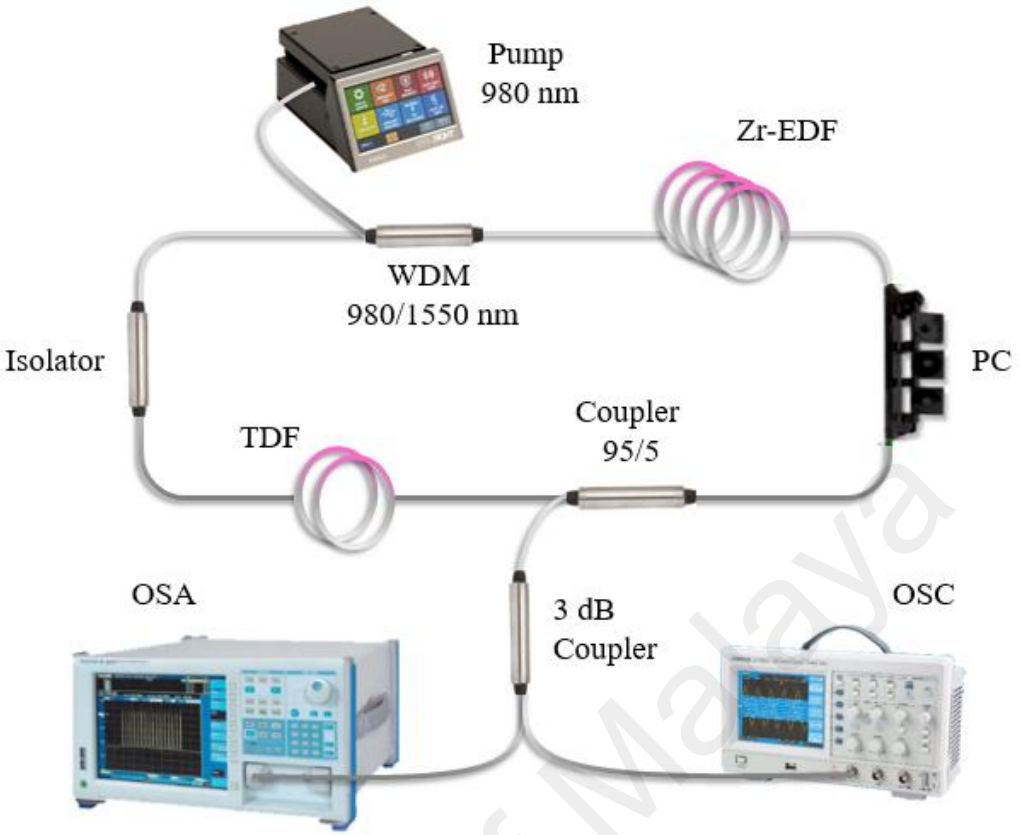

Figure 4.5: Schematic configuration of the proposed Q-switched EDFL

4.3.2 Q-switched Zr-EDFL Performance

Figure 4.6 shows the output spectra of the EDFL with and without the TDF SA when the 980 nm pump is fixed at 92.4 mW. Without Tm-doped fiber absorber we observed the stable CW operation of EDFL at 1571.2 nm. After installation of 1 m long TDF inside the cavity, a Q-switching pulse train is generated as the pump power is increased above 77.2 mW. The operating wavelength of the Q-switched laser shifts to a shorter wavelength (1556.0 nm) due to the cavity loss which increases with the incorporation of TDF. To compensate for the loss, the laser operates at a shorter wavelength which has a higher gain. Figure 4.7 shows the typical observed pulse train at pump power of 92.4 mW. As shown in the figure, the peak to peak pulse separation is measured to be around 80.9 μs, which translated to repetition rate of 12.36 kHz. The pulse width was 15.3 μs from the oscilloscope. The Q-switching pulse generation is due to gain-

switching action provided by the Thulium ions interaction with the oscillating Erbium laser.

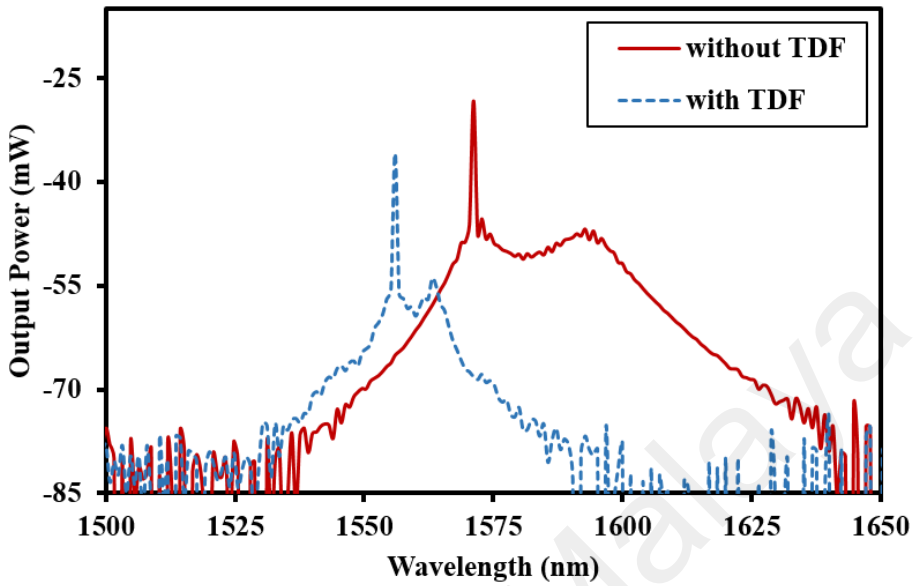

Figure 4.6: Output spectra from the EDFL with and without the solid state TDF SA

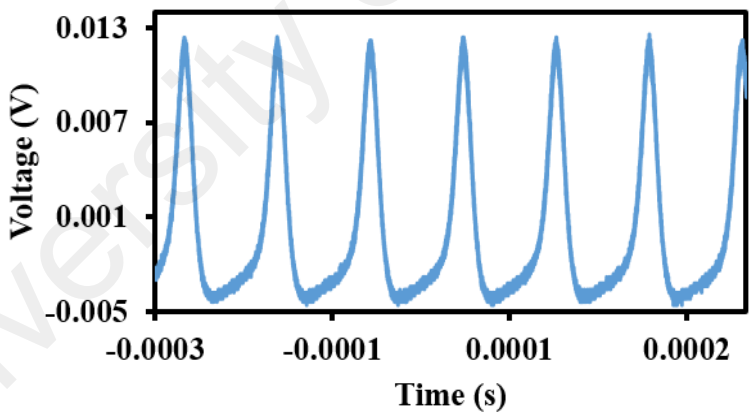

Figure 4.7: Typical pulse train of the Q-switched EDFL at pump power of 92.4 mW

Figure 4.8 shows the pulse repetition rate and pulse width as a function of the pump power. As the pump power increases from 77.2 to 97.5 mW, the repetition rate of the Q-switched pulses monotonically grows from 7.7 to 15.4 kHz. At the same time, the pulse duration reduces from 21.4 to 14.1 μs as expected. We also measured the average output power and calculated the corresponding single-pulse energy. Figure 4.9 shows the

output power and pulse energy against the 980 nm pump power. As shown in the figure, the average output power almost linearly increases with the input pump power from 77.2 to 97.5 mW. On the other hand, the pulse energy shows the similar trend as the pump power is increased within 77.2 to 92.4 mW. As the pump power further increases to 97.5 mW, pulse energy becomes saturated, which is most probably due to the timing jitter noise in the laser cavity. It is worth noting that the Q-switching pulse train becomes unstable and disappears as the pump power is increased above 97.5 mW. The reason is due to insufficient recovery time of TDF SA after generate a pulse and causes the fewer attainable gain for the following pulsing generation. It specifies that thulium-doped fiber relaxation lifetime ($^3F_4$) is less than 0.065 μs that was the inversion of the largest repetition rate before the disappearing. At the pump power of 97.5 W, the maximum output power of 0.18 mW is obtained which corresponds to the maximum pulse energy of 11.7 nJ.

It is expected that the pulse duration could be further narrowed by optimizing the parameters, including shortening the cavity length and optimizing the solid-state TDF Q-switcher. The achievable energy of pulse is confirmed as expected to generate higher than conventional SWCNTs and graphene SAs due to its higher thermal stability. The optical fiber SA is also robust and has a high damage threshold. Even though with the development of gain medium of Zr-EDF and various configuration of cavity designs, mode-locking pulsed laser still could not be realized.

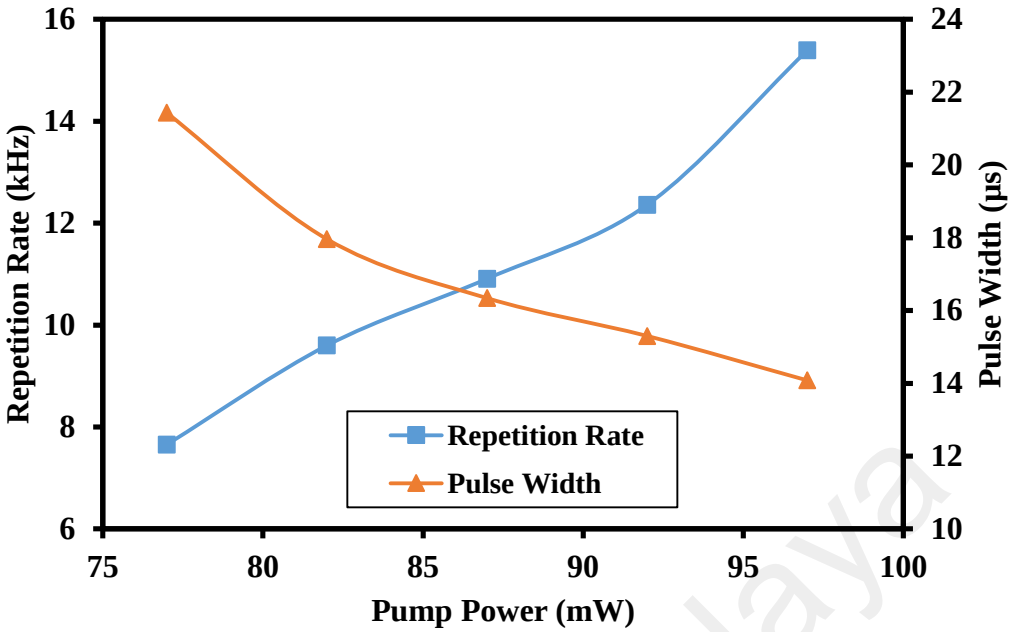

Figure 4.8: Repetition rate and pulse width of the proposed Q-switched EDFL against the pump power

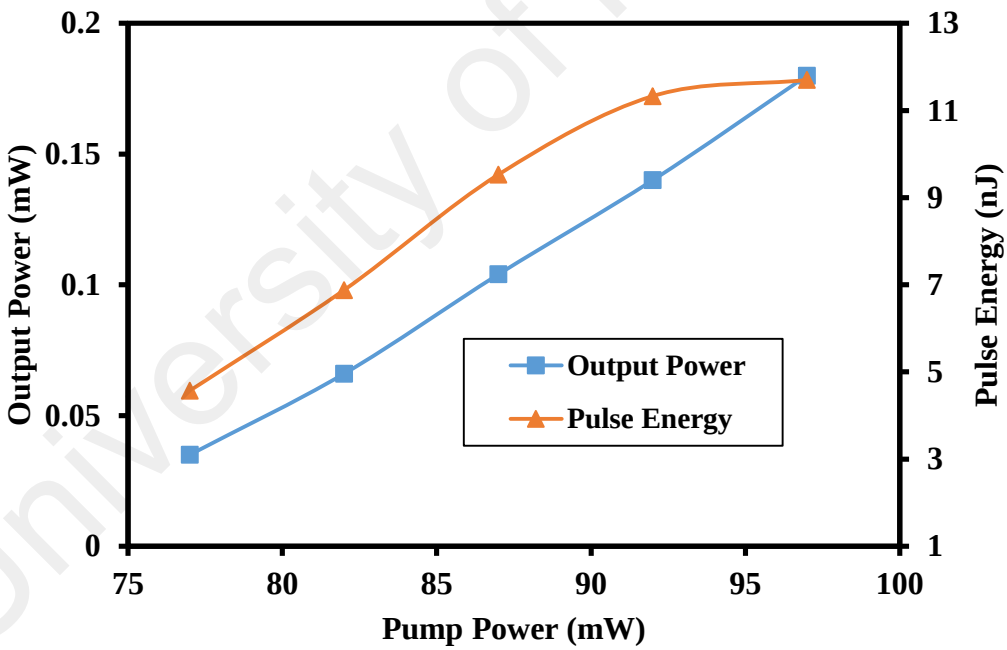

Figure 4.9: Output power and pulse energy of the proposed Q-switched EDFL against the pump power

4.4 Generation of Soliton Mode-Locking Pulse based on Single-wall Carbon Nanotubes (SWCNTs) SA

In recent years, mode-locked EDFLs are being extremely explored due to their advantages such as flexibility, compact design and cost effective. They have a wide applications in many industries such as optical communication, medical military and remote sensing. Mode locked EDFLs are most commonly accomplished by using passive modulation techniques such as nonlinear polarization rotation (NPR) and semiconductor saturable absorbers (SESAMs), but either are costly or required some delicacy to implement, thus rendering the development of a compact ultrafast fiber laser unfeasible. The use of carbon nanotubes (CNTs) and graphene material as passive saturable absorbers (SAs) have grown enormous interest of many researchers investigated on Q-switched and mode-locked fiber lasers (Ahmad et al., 2013; Ismail et al., 2012; Zen et al., 2013). The reasons are including swift recovery time, minimal intensity of saturation, broad operating transmission bandwidth and good compatibility among the fibers.

CNT-based SAs are still highly popular more than graphene, as they are easier to fabricate (Rozhin et al., 2006). Furthermore, CNT-based SAs may also have a lower non-saturable to saturable absorption ratio as compared to graphene (Martinez et al., 2010). With the outstanding quality and controllable physical parameters, CNT absorber fabrication technique is very practical for large, cost effective and high speed industrial production. A simple and cost effective fabrication technique of this SA was successfully demonstrated in a polymer matrix with implanted composite SWCNTs (Xie, Mai & Zhou, 2005). This technique easily adapted to the real application with the used of thin film formation due to outstanding homogenous dispersion of SWCNTs. To date, the fabrication of high quality SWCNT polyvinyl alcohol (PVA) composite film are less reported for the mode-locked pulsed applications (Cadek et al., 2002).

This chapter describes a proposed soliton mode locked EDFL using a simple, compact and cheap SWCNTs based SA. The SWCNTs having a large diameter precisely selected to operate at longer wavelength region of 1.5 μm and prepared using Polyvinyl alcohol (PVA) composite. The SA is designed by sandwiched together the composite film between two fiber connectors to generate mode-locked pulses with a pulse width of 770 fs as well as a repetition rate, average output power and pulse energy of 17.7 MHz, 0.91 mW and 51.4 nJ, respectively. The proposed mode locked operates from 1530 to 1565 nm is desirable for many applications, such as optical communications by using all-fiber configuration.

4.4.1 Fabrication and Characterization of SWCNT SA

The main component of the proposed mode-locked laser is the SWCNTs-based SA, which is obtained by embedding SWCNTs into a PEO polymer film. To prepare the film, SWCNTs powder synthesized by catalytic chemical vapour deposition (CCVD) process was used as raw material. The SWCNTs grains were 99 % pure with a diameter of 1-2 nm and length of 3-30 μm and thus they required no purification process. In the experiment, 250 mg SWCNTs were added to 400 ml sodium dodecyl sulphate (SDS) solution in deionized water at 1 % concentration before being sonicated for 30 min at 50 W. The dispersion of single walled CNTs in the solution was achieved ultrasonically with the aid of SDS, which induced the dispersion of the grains as separate tubes in aqueous solution. The solution was centrifuged at 1000 rpm to remove large particles of undispersed SWCNT to obtain dispersed suspension that is stable for weeks.

1.8 ml of dispersed SWCNT suspension containing 1.125 mg solid SWCNT was then added into a polymer solution, which was obtained by mixing 1 g of polyethylene oxide (PEO, average molecular weight of 1 x 106 g/mol) with deionized water. The

mixture was thoroughly mixed through a centrifuging process to form a SWCNTs-PEO composite precursor solution. Then the precursor solution was casted onto a glass petri dish and kept in a vacuum oven at 60 ^{o}C for 48 hours to form a thin film. The free standing film had a peak absorption at 1.5 µm with a thickness of around 50µm and was then used to form a fiber compatible SA device for mode-locking pulse generation in the proposed EDFL setup. The fabrication processes of the SWCNTs film is summarized in Figure 4.10. Figures 4.11 (a) and (b) show the 'real' and Field Emission Scanning Electron Microscopy (FESEM) images of the SA film, respectively. Figure 4.11 (b) indicates that the SWCNTs are randomly distributed in the polymer composite.

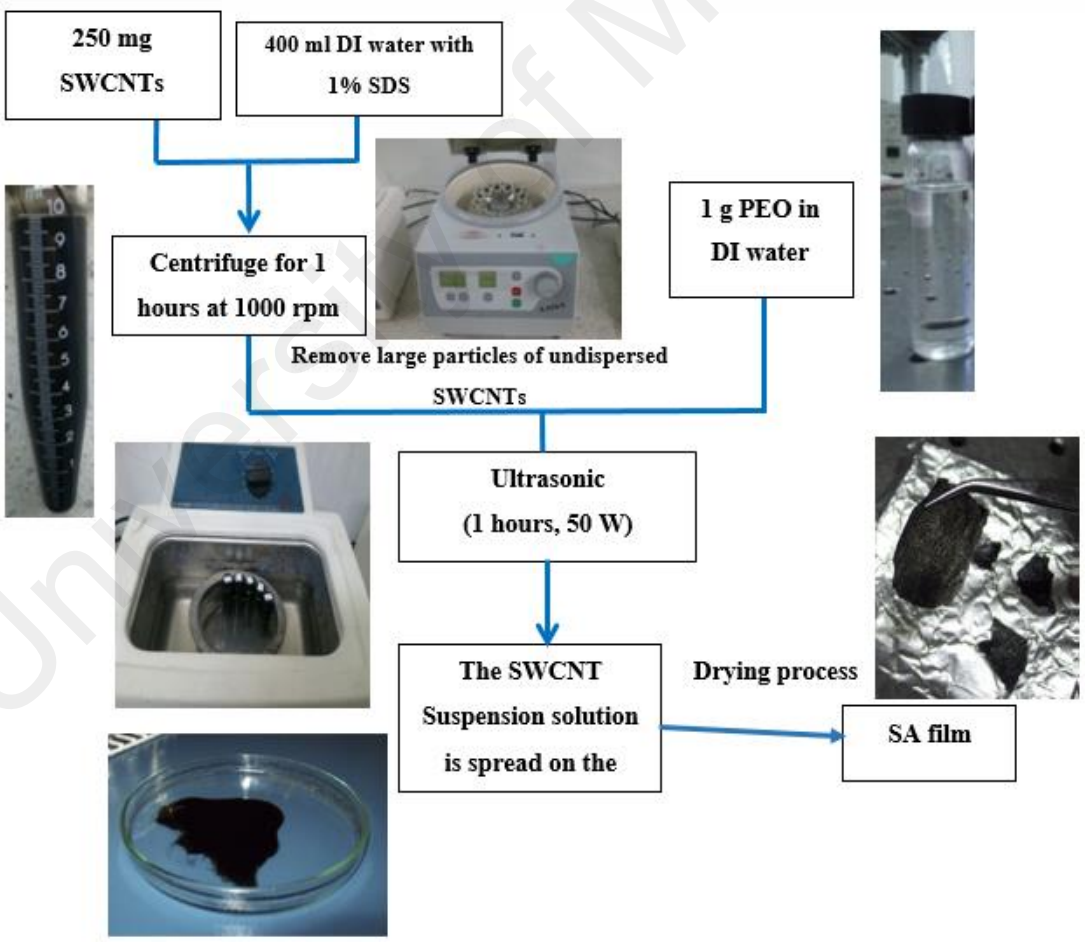

Figure 4.10: Fabrication procedures of SWCNTs-PEO

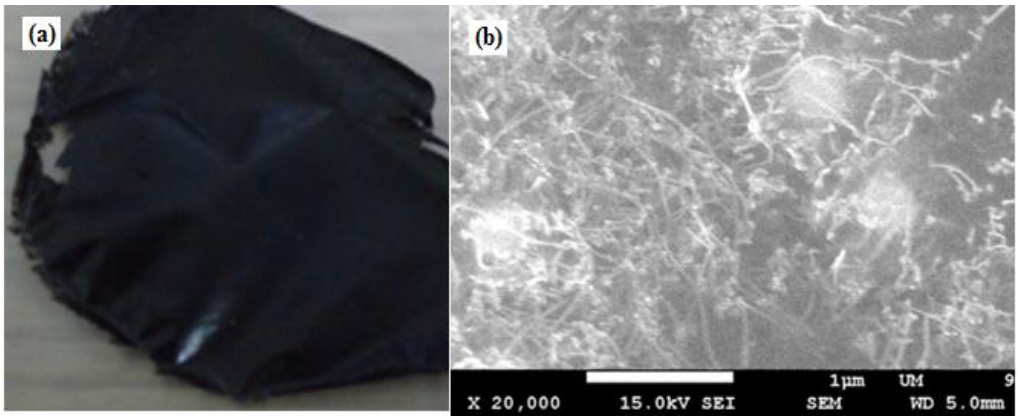

Figure 4.11: (a) actual size and (b) FESEM images of the SWCNTs-PEO composite film

Figure 4.12 shows the Raman spectrum, which can be used to confirm the presence of SWCNTs in the composite film and to determine the nanotube diameter distribution. It was obtained using a Raman spectrometer where the small piece of the SA film was excited by a 532 nm laser. As shown in the spectrum, the so-called G peak, which originates from the tangential vibrations of the carbon atoms, is prominent at 1584 cm^{-1}. In the low frequency region, the RBMs are observed, for which their energy is inversely related to SWCNT diameter. Since the distinct peaks are observed at around 214 cm^{-1}, the SWCNT diameter is estimated to be approximately 0.9 nm. This translates to the operating wavelength of around 1550 nm region. The carbon and G′peaks are also observed at 1363 cm^{-1} and 2670 cm^{-1}, respectively.

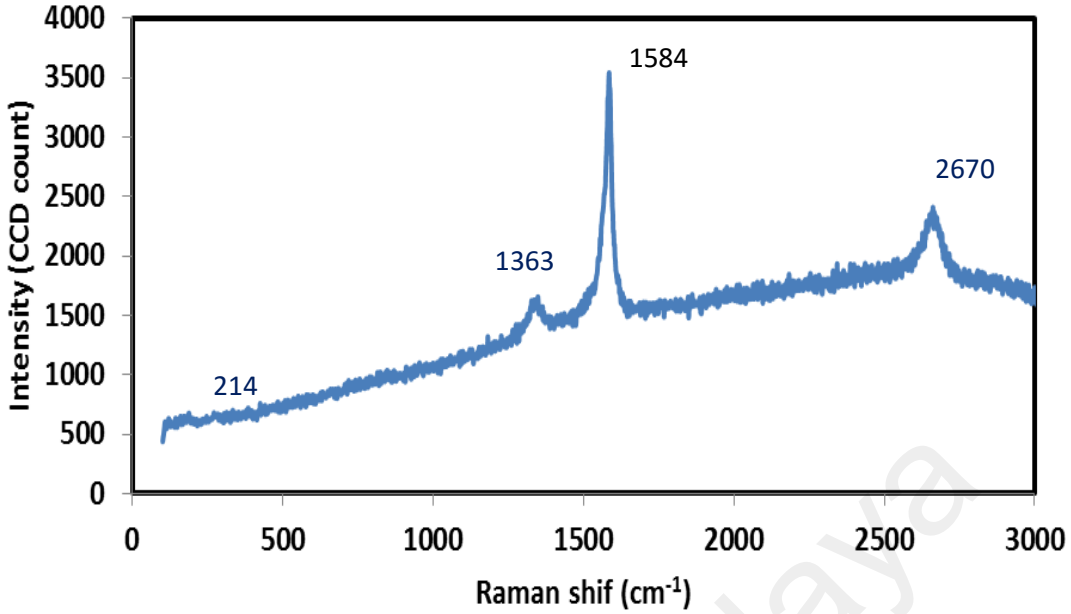

Figure 4.12: Raman spectrum of the prepared SWCNTs-PEO composite thin film

4.4.2 Configuration of the SWCNT-based Zr-EDFL

The fiber laser setup used in the experiment is schematically shown in Figure 4.13. It is in a ring configuration and is mode-locked by the SWCNTs-PEO SA. The SA was fabricated by cutting a small part of the prepared composite film and sandwiching it between two FC/PC fiber connectors, after depositing index-matching gel onto the fiber ends. The insertion loss of the SA is measured at around 2 dB at 1550 nm. The gain medium is a 2 m long Zr-EDF with the absorption coefficient of approximately 220 dB/m and group velocity dispersion (GVD) of -56 ps^2/km at 1550 nm. A 980 nm laser diode is used to pump the Zr-EDF through a WDM. The WDM comprises 3 m long pigtailed fiber with a GVD of -38 ps^2/km at 1550 nm. The single mode fiber that makes up the rest of the ring cavity is 6.5 m in length with GVD of -21 ps^2/km. The estimated net dispersion and group delay dispersion (GDD) of the cavity, ignoring the GVD of the SA are 0.279 ps/nm and -0.04 ps^2, thus the cavity operates at the anomalous dispersion region. A PC is used to adjust the state of polarization in the cavity while a polarization independent

isolator is incorporated in the laser cavity to force unidirectional propagation of light. The output of the laser is tapped from the cavity via a 95/5 output coupler, which keeps 98 % of the light oscillating in the cavity. An OSA with wavelength resolution of 0.02 nm is used to capture the output laser spectrum while a 350 MHz oscilloscope in conjunction with 1.2 GHz bandwidth photo-detector is used to detect the pulse train. The total length of the cavity is around 11.5 m.

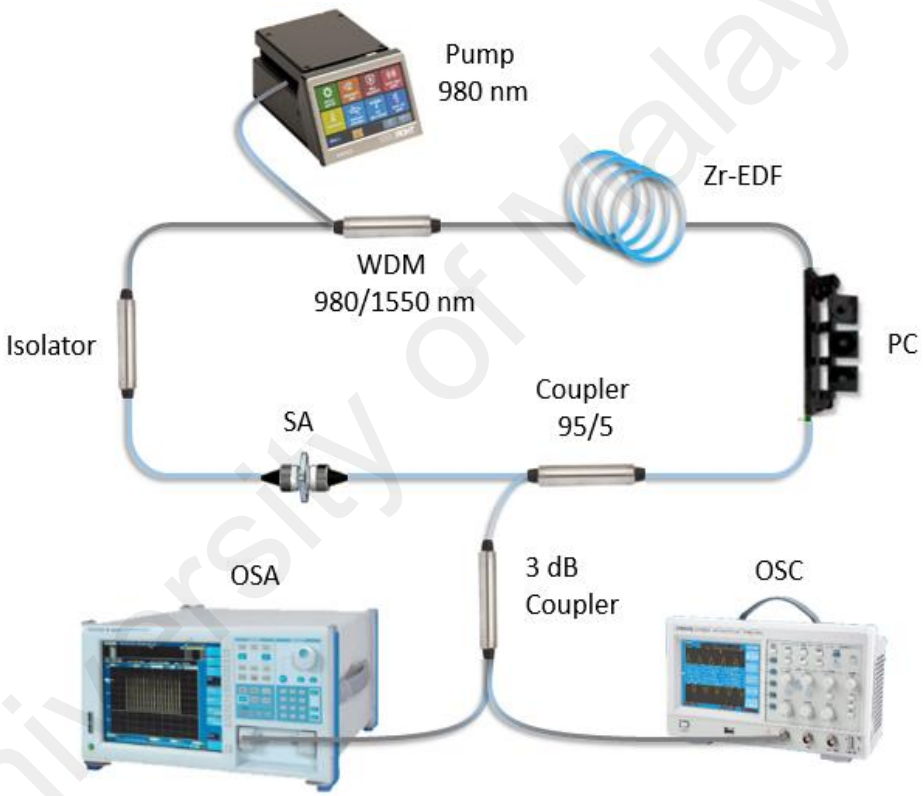

Figure 4.13: Schematic configuration of Zr-EDFL passively mode-locked by SWCNTs-PEO film-based SA

4.4.3 Mode-Locked Zr-EDFL Performance

It is observed that the laser always works in the CW operation with a threshold pump power of 45 mW in the absence of the SA in the cavity. As the SWCNT-based SA

is incorporated in the laser cavity, the mode-locked laser self-started at pump power of 67 mW with appropriate setting of PC. Figure 4.14 shows the optical spectrum of the passively mode-locked Zr-EDFL at three different pump powers, analyzed by an OSA limited by a resolution of 0.02 nm. It operates at the central wavelength of 1564.2 nm and the 3 dB bandwidth is approximately 3.8 nm with strong Kelly sidebands at the maximum pump power of 92 mW. The smooth spectrum is due to the free from parasitic lasing of continuous wave (CW). The existence of Kelly sidebands approved that the mode-locked pulsed laser is operates in anomalous dispersion regime.

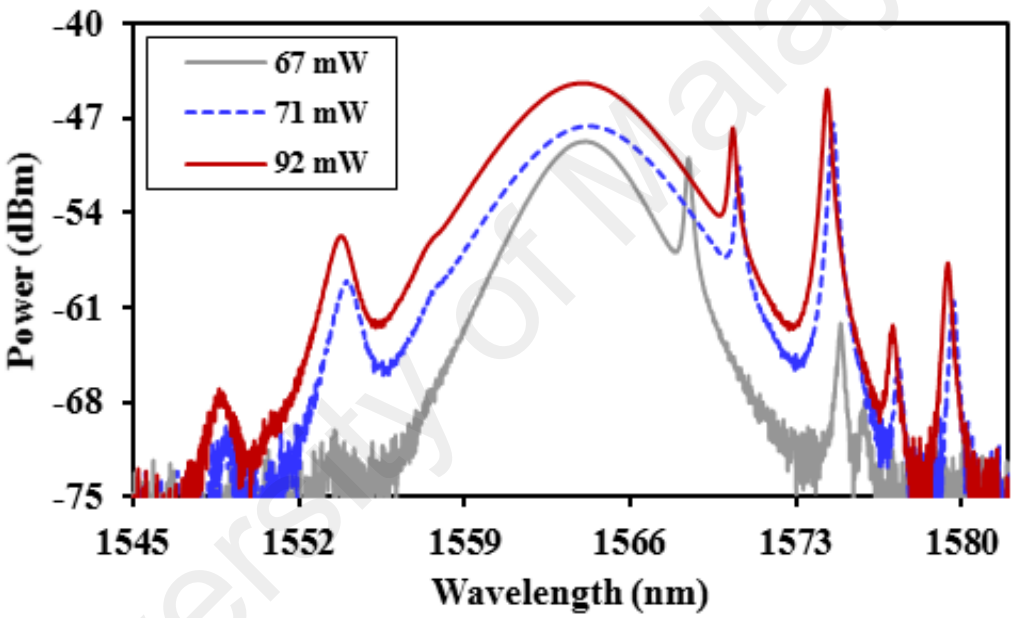

Figure 4.14: Output spectrum of the proposed mode-locked fiber laser at various pump powers

Figure 4.15 (a) shows the pulse train of the passive mode-locked fiber laser obtained at pump power of 67 mW. It has a cavity round trip time of 56 ns, corresponding to a pulse repetition rate of 17.7 MHz and a cavity length of 11.5 m. Figure 4.15 (b) shows the corresponding second harmonic generation (SHG) autocorrelation trace, with the estimated pulse duration of 770 fs at its full-width half maximum (FWHM). A time-bandwidth product (TBP) calculated from the 3 dB bandwidth of the optical spectrum

and the FWHM of the pulse is around 0.677, which indicates that the pulse is slightly chirped. The radio-frequency (RF) spectrum is shown in Figure 4.16. One can observe that the fundamental repetition rate of soliton is ~17.7 MHz. The peak-to-background ratio of the RF spectrum is 37.4 dB, implying a good mode-locking stability. At the maximum pump power of 92 mW, the output power for this fiber laser is 0.91 mW. Consequently, the resultant pulse energy is estimated to be around 51.4 nJ. We believe that the output power and pulse energy can be improved by reducing of the cavity loss and optimizing the output coupler. Based on the experiment results, we conclude that the fiber laser operates at a stable soliton mode-locking state.

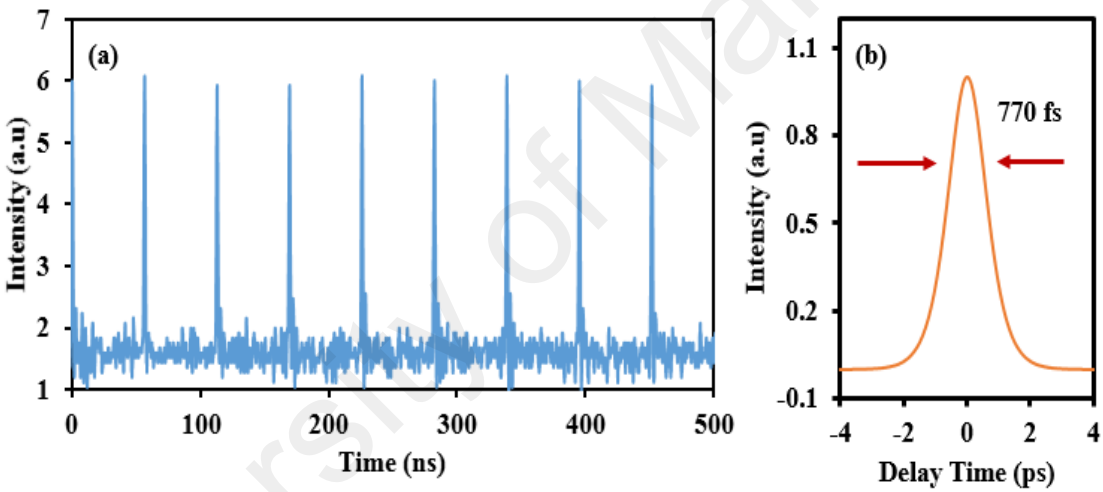

Figure 4.15: The temporal characteristics of the soliton laser (a) oscilloscope trace (b) autocorrelation trace

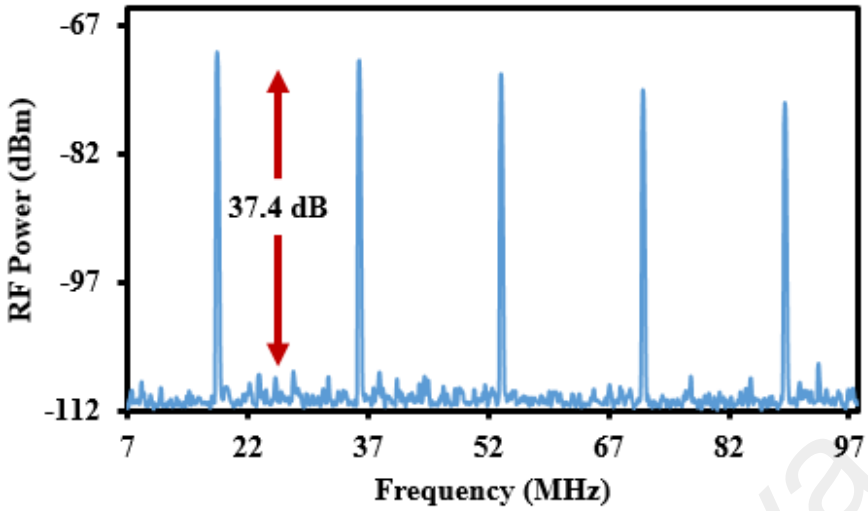

Figure 4.16: Radio-frequency spectrum of the soliton laser

4.5 Summary

Pulsed generation in Zr-EDFLs have been successfully generated using three different passive techniques. At first, bright and dark pulse generations were demonstrated using a NPR technique in a dispersion managed cavity with cavity length of 14.5 m and net cavity dispersion of –0.338 ps/nm at 1600 nm. With the help of large Kerr nonlinearity in the Zr-EDF, mode-locking pulses are generated from the dispersion managed fiber laser at a relatively low pump threshold of 70 mW. The bright and dark pulses repeated at the fundamental cavity frequency can be obtained by adjusting the polarization state of laser cavity. Both pulses operated at wavelength of 1601 nm with the fundamental repetition rate of 14.1 MHz. The generation of dark pulse in the proposed cavity is based on dual wavelength DW, which was achieved under the optimum polarization orientation. The dark pulse has a pulse width of 27.1 ns and pulse energy of 14.2 pJ at 70 mW pump power. It was found that the bright and dark pulses are formed mainly due to the cross coupling between two-Eigen operation states of fiber laser through the nonlinear effects of optical fibers. In the second experiment, a simple Q-

switched Zr-EDFL operating at 1556 nm is demonstrated based on a solid state saturable absorber fiber. The laser generates Q-switching pulse train within 980 nm pump power tuning range from 77.2 to 97.5 mW. The repetition rate of the Q-switched pulses monotonically grows from 7.7 to 15.4 kHz while the pulse duration reduces from 21.4 to 14.1 µs as the pump power increases from 77.2 to 97.5 mW. The maximum pulse energy of 11.7 nJ is obtained at pump power of 97.5 mW. Finally, a mode-locked Zr-EDFL was demonstrated using a SWCNTs based SA to generate a soliton pulse operating at fundamental frequency of 17.7 MHz. The SA is obtained by sandwiching a piece of SWCNT-PEO film between two fiber connectors for passive mode-locking. The cavity operates at the anomalous dispersion region with a length of 11.5 m with estimated net group delay dispersion of -0.04 ps^2. The pulses are characterized by a slightly chirped pulse width of 770 fs, RF signal peak to noise ratio of 37.4 and pulse energy of 51.4 nJ at pump power of 92 mW. These results shows that the newly developed Zr-EDF can be used in various fiber laser cavity for generating both Q-switched and mode-locked pulse trains.

CHAPTER 5: MODE-LOCKED FIBER LASER WITH 2D NANOMATERIALS

5.1 Introduction of Mode-locked Fiber Laser with 2D Nanomaterials

Demand for ultrafast technology is never ending due to the development of fiber laser technology which offers compact and robust source with pulse width down to the femtosecond region. Ultrafast fiber laser is desired due to its high reliability, simple fabrication and resonator, least footprint and cost effective for a large and most industrial applications. Ultrashort pulses can be generated using passive or active technique, where passive mode-locking is preferable for ultrashort pulsed laser, essentially due to the utilization of saturable absorber (SA) which modulates the resonator much swiftly than any electronic modulator that is required for an active mode-locking. Semiconductor saturable absorber mirrors (SESAMs) currently dominate passive mode-locking (Diebold et al., 2013). However, SESAMs have a narrow tuning range around ten of nanometres and complexity of the fabrication and packaging design. Recently, nanomaterials based SAs for ultrafast pulsed lasers have become the newest research topics, due to the notable advantages compared to the SESAMs. On the other hand, a new era of two-dimensional (2D) nanosystem brings the spotlight by development of novel 2D nanomaterials.

A lot of research efforts have also been put forward in recent years on developing new active fibers with high active ions concentrations in order to realize compact ultrafast laser with high repetition rate and narrow pulse width. The highly doped Erbium-doped fiber (EDF) is required to reduce the cavity length of the fiber laser. This highly doped EDF leads to concentration quenching or cluster formation which limits the overall performance of a laser system (Harun et al., 2011; Ahmad et al., 2012). In view of this, researchers are experimenting with new host materials such as telluride and bismuth as co-dopants to enhance the performance of Erbium doped fiber laser (EDFL) (Gao et al.,

2013; Ahmad et al., 2014). However, these materials have their drawbacks where they are difficult to be spliced with the conventional single mode fiber (SMF) and thus impractical to be integrated with other transmission network. In this chapter, various mode-locked fiber lasers are proposed and demonstrated using the newly developed Erbium–Zirconia–Yttria–Aluminium Co-Doped Fiber (Zr-EDF) in conjunction with new SAs based on 2D nanomaterials. The performances of the mode-locked lasers are compared for three new SAs based on graphene oxide, graphene film and black phosphorus (BP).

5.2 Soliton Mode-locked Zr-EDFL with Graphene Oxide SA (GOSA)

In the previous chapter, a mode-locked fiber laser was demonstrated using single-walled carbon nanotubes (SWCNTs), which is a simpler and cost-effective alternative to SESAMs. However, the operational wavelength of SWCNTs is defined by choosing the SWCNT diameter (i.e., band gap). Tunability of the operational wavelength is possible by using a wide diameter distribution. However, at certain operating of wavelength, the SWCNTs not in resonance and unable to be used, thus it increases insertion losses and compromises device performance. Novel nonlinear materials with broadband absorption are therefore required for wideband, tunable operation. One of the important applications of 2D nanomaterials is in ultrafast photonic where this material can be used as a SA for mode-locking. Graphene was first revealed in 2D material and its saturable absorption has been concerning the most for the generation of Q-switched and mode locked lasers (Ismail et al., 2013; Tiu et al., 2014; Harun et al., 2015). Even graphene share a certain of similar qualities with SWCNTs, it still has other fascinate properties which covering a longer wavelength from visible to infrared due to its minimal intensity of saturation, low non-saturable loss, large threshold damage, zero bandgap property and higher absorption

around ~2.3 % per single graphene sheet (Liu et al., 2013; Martinez & Sun, 2013; Li et al., 2014).

On the other hand, it has been proved that graphene-oxide (GO) is comparable to graphene as an SA (Zhao et al., 2011). GO as saturable absorber (GOSA) is more comparable than graphene due to easy and faster fabrication process, higher mechanical strength that offers high flexibility based on optoelectronic productions and has ultrafast recovery time and stronger saturable absorption which enhances the capabilities to generate ultrafast fiber laser (Eda & Chhowalla, 2010; Zhao et al., 2011; Sobon et al., 2012). Furthermore, GO can be readily dissolved in water due to its hydrophilic properties, and thus it can be flexibly processed to form versatile SAs (Sobon et al., 2011). Bonaccorso et al., (2010) was first demonstrated a GO mode-locking fiber laser, attaining ~743 fs pulse duration. Liu et al., (2011) exploited a hollow-core photonic crystal fiber filled with few-layered GO solution, attaining 4.85 ns mode-locked pulses at 1561.2 nm (Liu, He & Wang, 2011). Then, an ultrafast fiber laser was successfully accomplished as short as ~200 fs soliton pulses by using a GOSA mirror (Xu et al., 2011). Normally, all the mentioned consequences operate at C-band and less attention has been paid to the longer wavelength of L-band region. Thus, in this section, a GO mode-locked fiber laser operating in L-band region is demonstrated using the Zr-EDF as a gain medium.

5.2.1 Fabrication and Characterization of GOSA

For ease of integration and stability, we incorporate the GO flakes into a host polymer. For composite preparation, chemical exfoliation method was used where the process can be briefly described as follows. Firstly, sulfuric acid (H_2SO_4), phosphoric acid (H_3PO_4), graphite flakes, and potassium permanganate ($KMnO_4$) are mixed by using a magnetic stirrer. After adding all the materials gently, the mixture was then stirred for

about 3 days to allow the oxidation of graphite. After oxidation of graphite is achieved, H_2O_2 solution was added to stop the oxidation process. Finally, bright yellow color mixture is obtained indicating a high oxidation level of graphite. The graphite oxide formed was washed three times with 1 M of HCl aqueous solution and repeatedly with deionized (DI) water until a pH of 4–5 was achieved. The washing process was carried out using simple decantation of supernatant via a centrifugation technique. During the washing process with DI water, the graphite oxide underwent exfoliation, which leads to in the thickening of the graphene solution, forming a GO gel. The GO gel was then mixed with DI water to obtain a GO solution.

To prepare the polymer, a small amount of Poly (ethylene oxide) (PEO) (with average molecular weight of 1×10^6 g/mol) is dissolve in DI water using hot plate stirrer with the aid of magnetic stirrer. From the experiment, it is observed that about three hours was taken to fully dissolve the PEO in DI water. After that, some PEO solution was poured into the dispersed GO solution and ultrasonically agitated for one hour to produce a stable GO/PEO composite solution. The final procedure was to vertically evaporate the GO/PEO solution; this lasted for more than 40 h at room temperature. Figure 5.1(a) shows the obtained GO-PEO film, which has the thickness of 50 µm. Figure 5.1(b) shows the Field Emission Scanning Electron Microscope (FESEM) image of the GO flakes. It shows a well-defined and interconnects graphene sheets forming a porous and loose sponge like structure.

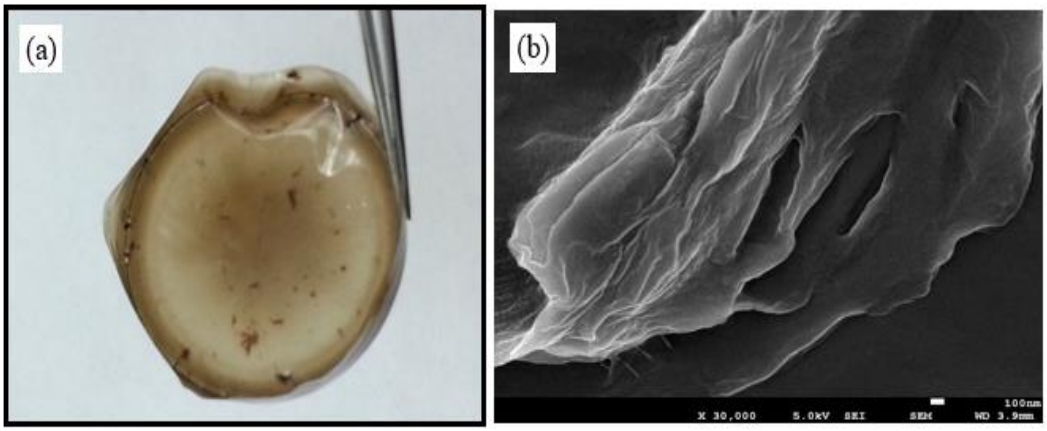

Figure 5.1: (a) GO-PEO film after let dry at room temperature (b) FESEM image of GO-PEO film

Figure 5.2 shows the Raman spectrum from the GO film. The film was excited by a 532 nm He-Ne laser. The spectrum reveals the two characteristic peaks D and G of GO (the D peak at 1375 cm^{-1} and the G peak at 1600 cm^{-1}). The D peak is from the structural imperfections created by the attachment of hydroxyl and epoxide groups on the carbon basal plane. The G peak corresponds to the first-order scattering of the E_{2g} mode. It is found that the G band is located at a higher frequency in the GO compared to that of graphite, which normally located at1580 cm^{-1} as reported in reference (Ferrari et al., 2006). The (I_D/I_G) intensity ratio for GO is 0.85 which is the measure of disorder degree and is inversely proportional to the average size of the sp^2 clusters (Kudin et al., 2008).

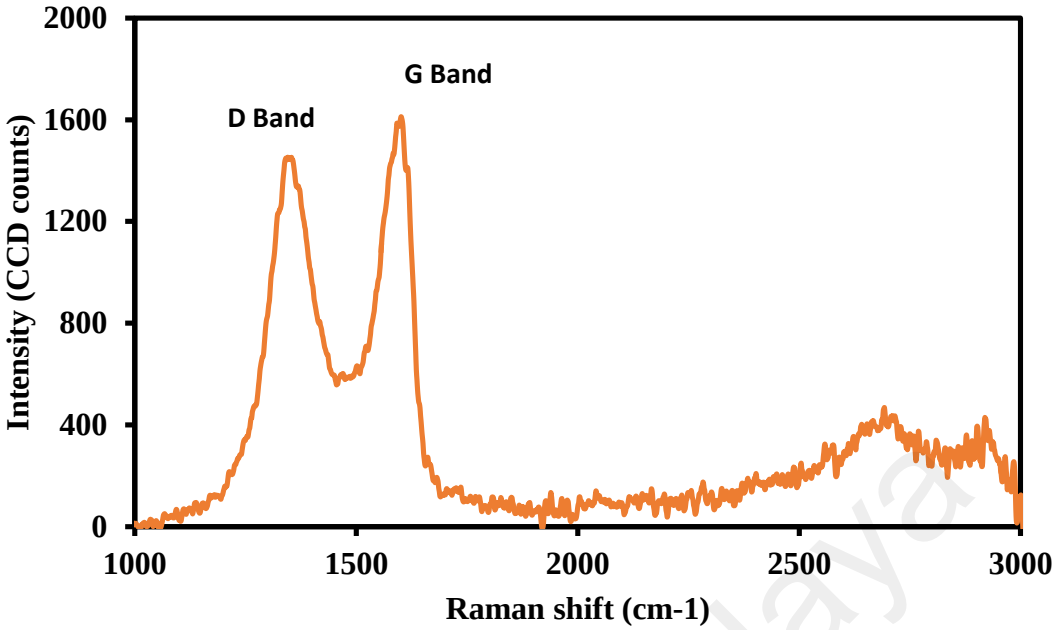

Figure 5.2: Raman spectrum of the GO film excited by a 532 nm laser

5.2.2 Configuration of the GO-based Mode-locked Zr-EDFL

We now use the fabricated GO film to build and test an ultrafast laser working at L-band region. Figure 5.3 (a) illustrates a configuration setup for the soliton mode-locked fiber laser using a 3 m long Zr-EDF as the gain medium. The mode-locker is assembled by sandwiching the GO/PEO between two fiber connectors with a fiber adapter, as schematized in Figure 5.3 (b). The Zr-EDF is pumped by a 980 nm diode laser via a wavelength division multiplexer (WDM). An isolator is placed before the WDM fiber to maintain unidirectional operation. A polarization controller (PC) is used to modify polarization state of the oscillating light and thus optimizes mode-locking. A 95/5 coupler is used to tap out the output while allowing 95% of the light to oscillate in the cavity. 10 m long SMF is also added into the cavity to optimize the mode-locking. The total cavity length is 14.7 m. The monitoring of output spectrum and pulse trains was performed using optical spectrum analyzer (OSA, AQ6317C) and a 500MHz oscilloscope (via a high

speed photodetector), respectively. The pulse width and radio frequency (RF) spectrum of the laser was measured by an autocorrelator and RF spectrum analyser, respectively.

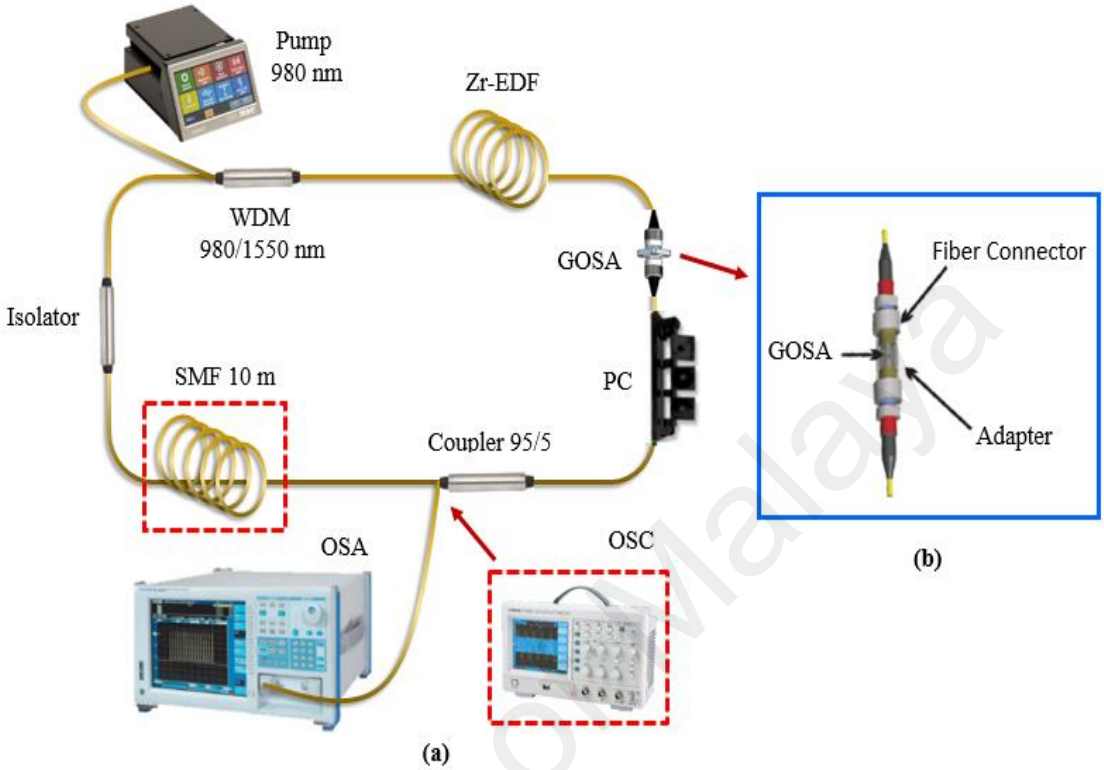

Figure 5.3: (a) Configuration of the GO mode-locked fiber laser (b) GOSA assembly

5.2.3 Performance of Soliton Mode-locked Zr-EDFL

The laser cavity consists of a 3 m long Zr-EDF (with a dispersion of 41.37 ps/km.nm and GVD coefficient -56 ps^2/km), 3 m long of WDM fiber (with dispersion of 28.07 ps/km.nm and GVD coefficient -38 ps^2/km) and accumulated single mode fiber (SMF) (with dispersion of 15.5 ps/km.nm and GVD coefficient -21 ps^2/km). Therefore, the calculated dispersion for the total length of 14.7 m ring cavity is approximately to 0.35 ps/nm. The positive value of dispersion indicates that the fiber laser of cavity is operating in anomalous dispersion regime (Agrawal, 2007). The threshold pump power for continuous wave lasing is 55 mW. When the pump power is increased to 78 mW, stable mode-locking can be initiated by introducing a disturbance to the intra-cavity fiber.

Once stable output is achieved, no further polarization controller adjustment is needed. When mode-locked, the laser produces a pulse train at a rate of 13.9 MHz. The mode-locking is maintained up to the maximum pump power of 268 mW. At this pump power, the mode-locked pulse fiber laser lases stably with consistent repetition rate. The GOSA film was found to be in a good condition at this pump power without thermal damage.

The Zr-EDF used was very long, taking into account the large doping concentration of the fiber, which caused lasing at L-band region. Figure 5.4 (a) shows a typical output spectrum at pump power of 105.5 mW. The spectrum was centered at 1577.46 nm with the 3 dB full width at half maximum (FWHM) bandwidth of 5.4 nm. The positive net cavity dispersion favors $sech^2$-profile soliton-like mode-locking. The observed side-bands in the spectrum are typical of soliton-like pulse formation, resulting from intra-cavity periodical perturbations. The soliton spectrum has two pairs of symmetrically Kelly sidebands; the left sidebands centered at 1571.89 nm and 1569.24 nm whereas the right sidebands centered at 1583.31 nm and 1585.81 nm. The first Kelly sideband appear due to resonant coupling interaction between soliton and dispersive wave, which is a signature of the solitonic behavior of the mode-locked pulse visible in the spectrum. Whereas the outer pair of the second-order Kelly sideband is generated from high peak intensity that circulating in Zr-EDFL cavity (Lin & Lin, 2013; Liu, 2011).

Figure 5.4 (b) shows the measured RF spectrum to investigate the stability behaviour of the mode locked pulse operation. It shows the pulse repetition rate of 13.9 MHz with the signal to noise ratio (SNR) of about 43 dB, which indicates the stability of the soliton generation. The oscilloscope trace of the output pulse train is plotted in Figure 5.4 (c). The pulse repetition rate was measured as 13.9 MHz, approximately defined by the cavity length of about 14.7 m. Figure 5.4 (d) shows the measured autocorrelation trace, which gives a pulse width of 0.6 ps if $sech^2$ profile is assumed. The recorded 3 dB bandwidth of 5.4 nm (or 0.65 THz), the time-bandwidth product (TBP) of the laser is

0.48, which is slightly deviates from transform limit for sech^2-shaped laser pulses of 0.315. This indicates that soliton pulse is chirped and the incident of chirping in the pulse cause by dispersion and nonlinearity balance of laser cavity (Agrawal, 2007). The calculation of pulse energy is 2.74 pJ with the output power of 38.1 µW at pump power of 84.1 mW.

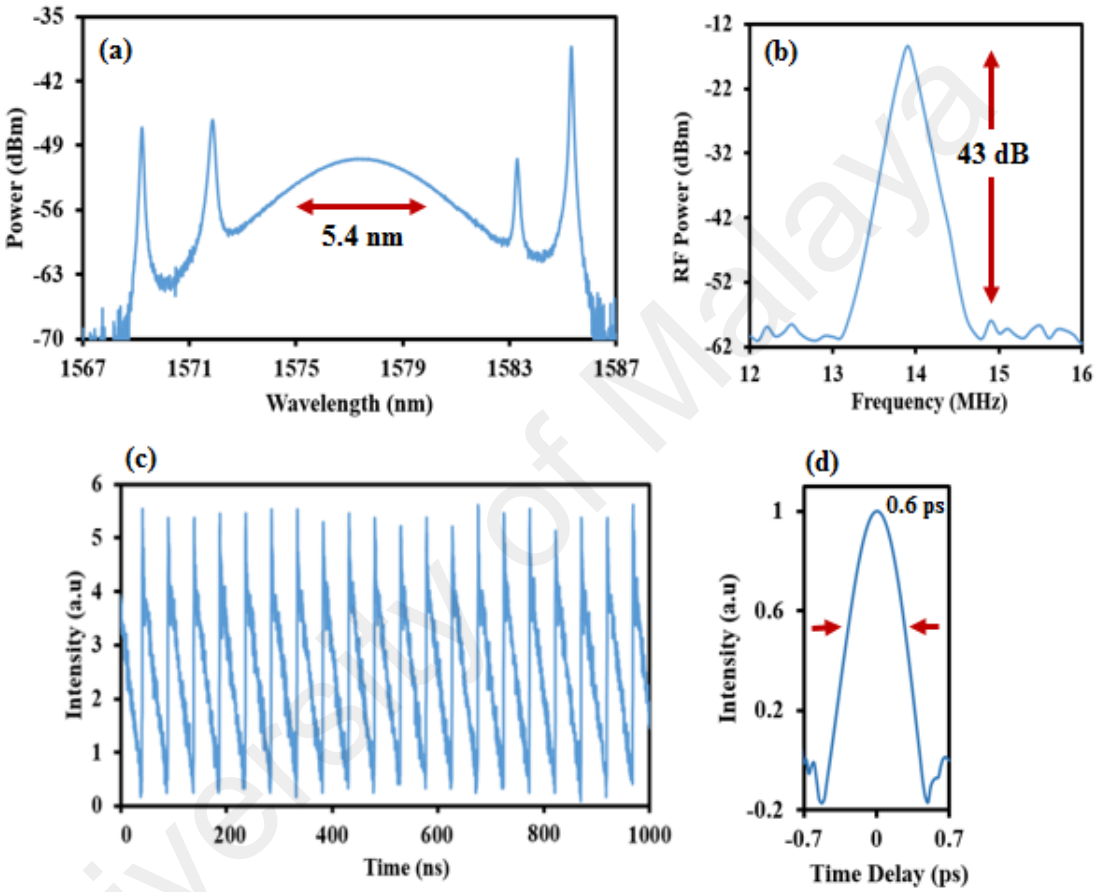

Figure 5.4: The spectral and temporal characteristics of the soliton mode-locked Zr-EDFL at pump power of 105.5 mW (a) Optical spectrum (b) Single RF pulse with SNR of 43 dB (c) Output pulse train with repetition rate of 13.9 MHz (d) Autocorrelator trace with pulse width of 0.6 ps

5.3 Multiwavelength Dark Pulse Mode-locked Zr-EDFL with GOSA

Mode-locking and ultrafast laser formation are attractive topics that have been extensively investigated in recent years due to the wide applications in optical communications, instrumentations and sensors. Up to date, most of the reported fiber lasers were focused on mode-locking operation in the bright pulse regime (Harun et al., 2015; Ahmad et al., 2014; Ahmed et al., 2016). For instance, ultrashort bright soliton pulsed laser was successfully demonstrated in the previous section with the utilization of GO film based SA with the pulse duration of 600 fs. Alternate to the bright, dark pulse offers high stability in the presence of noise, low interaction between neighbouring dark pulses for their bright counterparts and less sensitive on Gordon-Haus effect in a time jitter proven numerically and analytically (Kivshar et al., 1994). Dark pulses have the form of a density dip with a phase jump across its density minimum. And this kind of localized nonlinear waves exists on the top of a stable continuous wave background (Agrawal, 2007). The first discovery of dark pulse fiber laser was experimental demonstrated and reported by Zhang et al., (2009) by using nonlinear polarization rotation technique back in 2009.

However, only two type materials of SA were reported in producing dark pulse, namely are carbon nanotubes (CNT) and graphene oxide (GO) (Liu & Chow, 2014; Lin et al., 2014). GOSA is also the key to create multiwavelength pulsed laser due to its broadband saturable absorber and capabilities to generate four-wave-mixing (FWM) process (Luo et al., 2011). In this section, dark pulses formation in GO based mode-locked Zr-EDFL will be investigated and demonstrated for the first time to our knowledge. In order to controlling the cavity and allows the formation of the dark soliton, an additional length of SMF is added in the laser cavity. Multiwavelength lasing is also observed due to the enhanced nonlinearity in the cavity.

5.3.1 Configuration of the GO-based Dark Pulse Mode-locked Zr-EDFL

The experimental setup of the proposed mode locked Zr-EDFL with GO film as SA is shown in Figure 5.5. This configuration setup is also used for the following experiments with replacing the SA to the graphene film and black phosphorus. The performance of Zr-EDFL with different SAs are discussed on individual section. The Zr-EDF was forward pumped by a 980 nm laser diode via a 980/1550 nm WDM coupler. One port of the WDM was fusion spliced to the newly developed 3 m long Zr-EDF, and another port was attached to the 95 % port of an optical coupler. The laser output emerging from the Zr-EDF was fusion spliced to the SA device which is GO film is sandwiched between the fiber connector ferrules as shown in Figure 5.3 (b). The SA was prepared by cutting a small part about 1.5 mm × 1.5 mm and was placed between two fibre connectors with the help of index-matching gel. Then, it was connected to an optical isolator to ensure a unidirectional propagation of the laser inside the cavity. The output of the isolator was subsequently connected to a PC to optimize multiwavelength and mode-locking operations by modifies the polarization state of light and allows the birefringence within the cavity to balance the optical gain and loss for generation of pulsed laser. Then, it connected to a 180 m long SMF to increase the nonlinearity and birefringence of the cavity. The SMF was then fusion spliced to a 95/5 fused bi-conical optical coupler. By using 5 dB coupler, the laser output was tapped out from cavity via 5 % port, and recorded by OSA. The temporal characteristics was measured by using oscilloscope (OSC) and RF spectrum analyzer (RFSA) for time-domain and frequency-domain, respectively. Autocorrelator (Alnairs, HAC-200) was utilized to measure pulse duration.

The cavity consists of 3 m long Zr-EDF with GVD of -56 ps^2/km, 196 m long of SMF with GVD -21 ps^2/km and 4 m long of WDM which has GVD of -38 ps^2/km. The 196 m long of SMF consists of 180 m spool of SMF and the remaining 16 m are from the

PC, coupler and isolator. By ignoring the GVD of the SA, the estimated dispersion and group delay dispersion (GDD) of the total 203 m long cavity is approximately 3.3 ps/nm and -4.4 ps^2, respectively. Thus, the proposed pulsed laser is considered to operate in anomalous dispersion region.

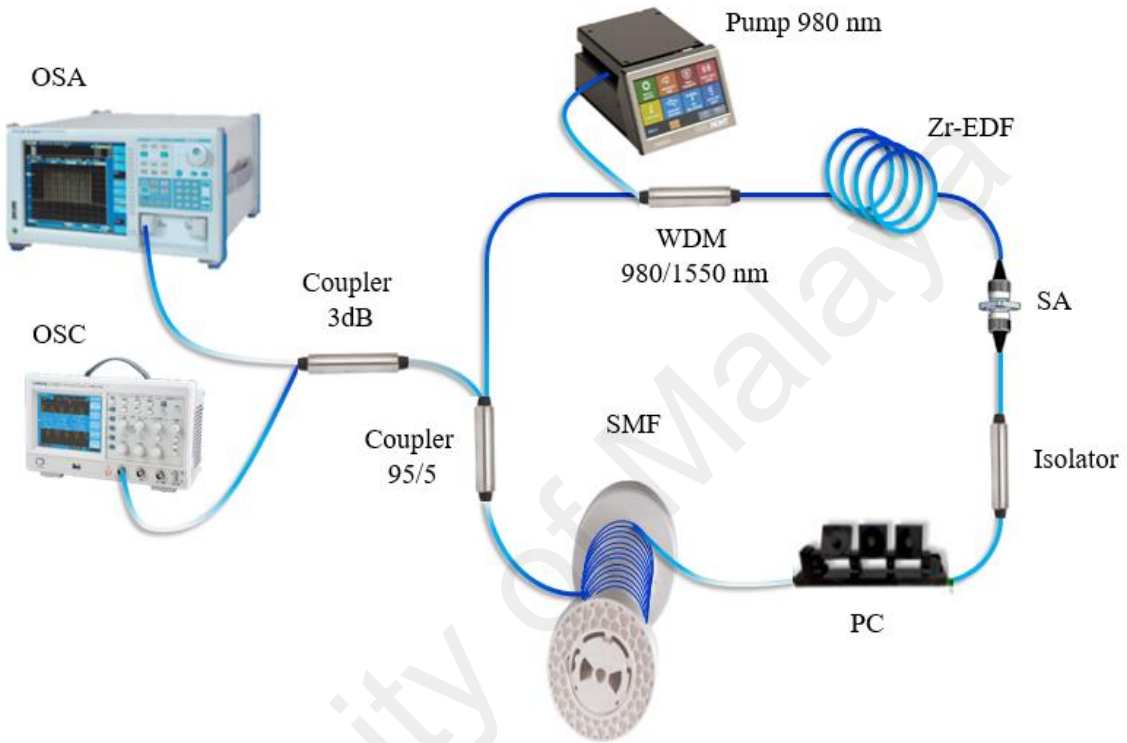

Figure 5.5: Configuration of the proposed multi-wavelength mode-locked Zr-EDFL generating dark pulse

5.3.2 Performance of Multiwavelength Dark Pulse Zr-EDFL

Dark pulse originates was directed by nonlinear Schrödinger equation (NLSE) and describes the bright solitons are formed in anomalous whereas dark solitons are formed in the normal dispersion single mode fibers (Zhang et al., 2009; Tang et al., 2013; Tang et al., 2014). However, the NLSE is lack for the important element of nonlinear gain and spectral filtering that leads to the complex Ginzburg-Landau equation (CGLE). When NLSE is dominant by Kerr nonlinearities, CGLE is affected by high order nonlinearities,

such as third order (cubic) and fifth order (quantic) nonlinearities. The most common technique that reported for development of dark pulse was using artificial SA technique such as NPR with one or two polarization components, polarization beam splitter and NOLM (Ning et al., 2012; Tang et al., 2-14; Wang et al., 2014). The most recent, dark pulse was successfully generated by using high nonlinearity SA of CNT, graphene oxide (GO) and Molybdenum disulphide (MoS_2) (Liu et al., 2014; Lin et al., 2014; Ahmad et al., 2016). The high nonlinearity SA leads to the four wave mixing effect of multiwavelength generation or broad spectrum of soliton (Zhao et al., 2013; Ahmad et al., 2016). The idea to form dark pulse by using these techniques is to achieve domain wall between traveling waves that agreed by CGLE. The concept is to produce either two orthogonal polarization states of light or dual- or multi-lasing with different wavelengths that induced by high nonlinearity of birefringence in cavity (Liu et al., 2014; Yin et al., 2010; Zhang et al., 2010). Besides, the other concept is by using high nonlinearity and strong birefringence optical fiber to generate dark pulse regime (Gao et al., 2013; Zhao et al., 2014).

The generation of dark pulse in the proposed GO based mode-locked laser cavity is based on multiwavelength DW. In the experiment, the threshold pump power for CW lasing is 47 mW. Under the optimum polarization orientation, dark pulse was achieved as pump power is increased above the pumping power threshold of 54 mW. Figure 5.6 shows the evolution of optical spectrum with its corresponding dark pulse train by increasing pump power. Figure 5.6 (a) shows an optical spectrum and its corresponding DW dark pulse train at pump power of 54 mW. The spectrum shows a single line laser centered at 1601.6 nm. By twisting the fiber in the PC and slowly increasing the pump power, a total of three lasing lines are obtained at 60 mW as shown in Figure 5.6 (b). The lasing lines are emit at wavelengths, from left, 1600.6 nm, 1601.1 nm and 1601.6 nm with a small uniform channel spacing of 0.5 nm. As the pump power is further increased up to

65 mW, a total of five lasing lines are generated as demonstrated in Figure 5 (c). As shown in the figure, the multiwavelength Zr-EDFL operates at wavelengths of 1599.6 nm, 1600.1 nm, 1600.6 nm, 1601.1 nm and 1601.6 nm. The wavelength spacing is also about 0.5 nm. The multiwavelength is formed due to the four-wave-mixing (FWM) process from high nonlinearity GOSA and birefringence in the cavity (Zhao et al., 2013).

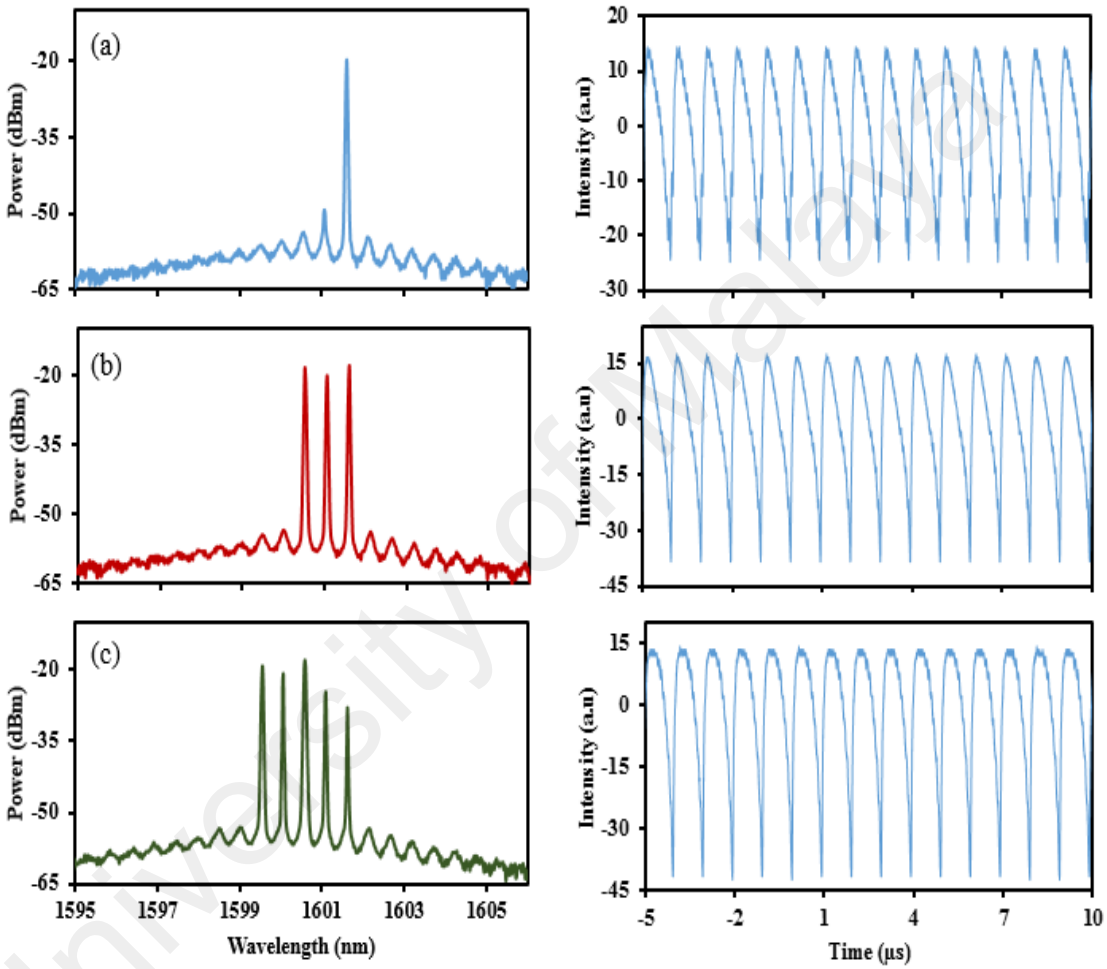

Figure 5.6: Optical spectra and its corresponding dark pulse train at three different pump powers (a) 54 mW (b) 55 mW and (c) 65 mW

The typical DW dark pulse train at pump powers of 54 mW, 60 mW and 65 mW are also shown in Figures 5.6 (a), 5.6 (b) and 5.6 (c), respectively. All the pulse trains show the repetition rate of 1.0 MHz, which corresponds to the total cavity length of 203

m. It defines that the mode-locked fiber laser functions at its fundamental repetition rate. To study the operation stability, we measure the RF spectrum within a span frequency spectrum measurements up to 20 MHz, as in Figure 5.7 (a). It shows the fundamental frequency of 1.0 MHz without any significant spectral modulations, implying no Q-switching instability. A 43 dB peak-to background ratio is observed, indicating good mode-locking stability. Figure 5.7 (b) is an auto-correlation trace of the mode-locked pulses at pump power of 65 mW. The pulse width is estimated to be around 3.43 ps.

Fig. 5.7 (c) illustrates the measured average output power against the pump power. It indicates that the output power is linearly increased from 0.25 mW to 2.01 mW as the pump power increases from 54 mW to 85 mW with regression trend line of R squared of 0.9683. The slope efficiency of the laser is estimated to be around 6 %. The single pulse energy is calculated to be 0.25 nJ and 2.01 nJ at pump powers of 54 mW and 85 mW, respectively. It is observed that the pulse train become distorted and unstable when pump power is increased above 85 mW and this limitation is most probably due to GOSA saturation.

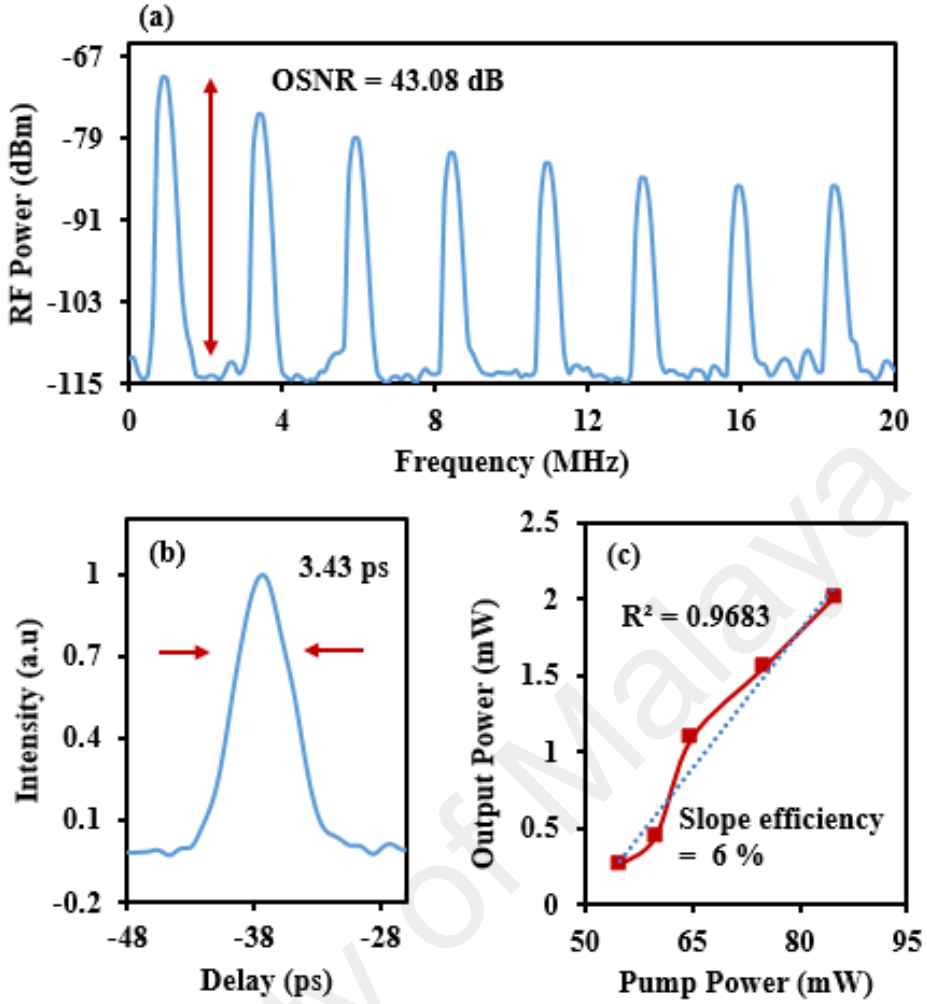

Figure 5.7: (a) RF spectrum at the fundamental repetition rate of 1 MHz (b) Auto-correlator trace with pulse duration of 3.43 ps (c) Output power against pump power

The dark pulse formation could be realized in the proposed laser cavity due to the combination of high nonlinearity Zr-EDF used and the employment of GOSA. A high nonlinearity gain medium enhances the cross-coupling effect between two or more lasing beams (Liu & Chow, 2014). When the lasing with different wavelengths oscillates simultaneously, temporal domain effectively produces topological defects, and thus a sharp dip intensity in strong CW background laser emission is formed as shown in Figure 5 and 6. The dark pulse formation is possibly due to high nonlinearity Zr-EDF, GOSA

and large anomalous dispersion in cavity. The use of a spool of 180 m SMF increases the nonlinearity and birefringence effect inside cavity and thus stabilizes the formation of dark pulse. It is also worthy to note that, the dark pulse cannot be realized inside the same cavity as the gain medium is changed to other type of fiber.

5.4 Dark Pulse Mode-locked Zr-EDFL with Graphene Film SA

Graphene grew a tremendous attention for mode-locking applications owing to its extraordinary optical properties, such as broadband wavelength tenability, fast saturable absorption and short carrier relaxation time (Xing et al., 2010; Bonaccorso et al., 2010; Li et al., 2014). To date, several methods is known to produce graphene SA applications were micro-mechanical cleavage, chemical vapour deposition (CVD) and liquid-phase exfoliation (Haris et al., 2015; Sun, Hasan & Ferrari, 2012). Nevertheless, these techniques demonstrate some disadvantages. Such a complicated process involves to build the devices when high temperature is required to mix organic solvents, the electronic assembly is high possibility to be disturbed at the end of graphene product, and the whole process is extremely exhausted and a lot of time is wasted (Yang et al., 2013; Vadukumpully, 2009; Chang et al., 2010).

Lately, electrochemically exfoliated graphene has been demonstrated using conductive electrodes (Parvez et al., 2013). In order to prepare high quality of graphene for a large scale, this technique is the most anticipated under mild situations (Wei et al., 2015). The electrochemical exfoliation technique draws some advantages such as its simple and easier fabrication process and cost effective. It leads to the possibility in optoelectronic applications with the ultrafast pulsed laser generation through the fabrication of graphene flakes (Parvez et al., 2013). In this section, an observation of dark pulse in mode-locked Zr-EDFL configured with a graphene film mode-locker is demonstrated. The graphene SA is fabricated using graphene flakes, which are obtained

from electrochemical exfoliation process. The graphene flakes is embedded in polyethylene oxide (PEO) film and is integrated in the laser cavity to produce dark pulse with a repetition rate of 1 MHz, which corresponds to the total length cavity.

5.4.1 Fabrication and Characteristic of Graphene Film SA

The base material of graphene was exfoliated through electrochemical process. In this process, two graphite rods with potential difference characteristics were immersed in sodium dodecyl sulphate (SDS) solution. After a several hours, a voltage was then applied to exfoliate the graphene flakes from the graphite rod. The following chemical reactions are involved in ions production inside the (SDS) solution:

$$H_2O \rightarrow OH^- + H^+ \quad (5.1)$$

$$CH_3(CH_2)_{11}OSO_3Na \rightarrow CH_3(CH_2)_{11}OSO_3^- + Na^+ \quad (5.2)$$

As a voltage was applied to the electrodes, the negative ions moved to the anode whereas the positive ions moved towards the cathode. Once the dodecyl sulphate ions mounted up at the anode, they reacted with the surface of the graphite rod to release graphene layers from the graphite rod (Wei et al., 2012; Lu et al., 2009). In this experiment, we applied a voltage of ~ 20 V between the graphite electrodes which were immersed in an electrolysis cell. The two electrodes were separated by about 1 cm in the electrolysis cell which contained solution of 1% SDS in deionized water as depicted in Figure 5.8.

After two hours, the solution became darker due to the accumulation of exfoliated graphene flakes. The exfoliated graphene flake suspension was then centrifuged at 3000 rpm for half an hour in order to eliminate large agglomerates. The supernatant portion of the suspension was removed and then the concentration of graphene was estimated from the weight of the suspension. Finally, the graphene suspension solution were mixed with

PEO solution, and dry at room temperature to form a graphene film. The PEO solution was dissolving by 1 g of PEO in 120 ml of distilled water. The graphene film has a thickness of ~ 50 µm and insertion loss of about 4.8 dB at 1550 nm.

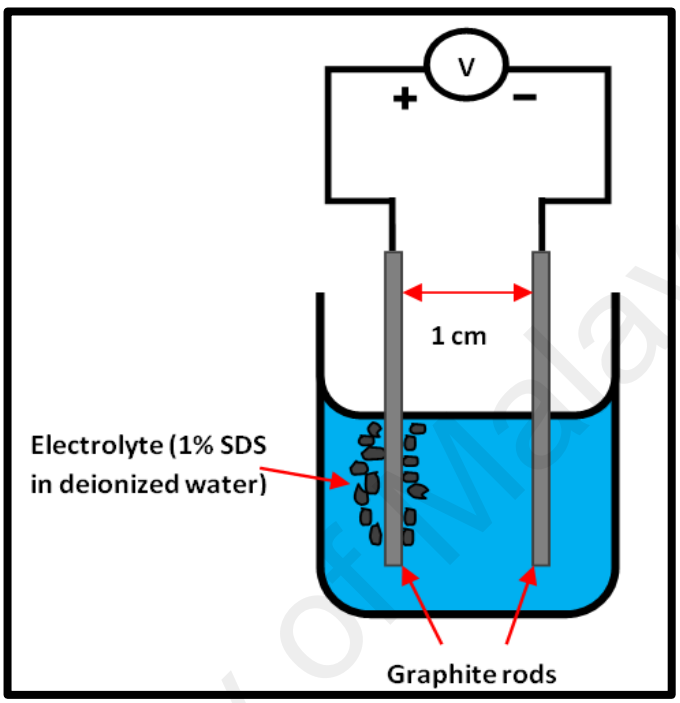

Figure 5.8: Experimental set-up of electrochemical exfoliation of graphene

Raman spectrum of the fabricated film was obtained using a probe beam of 532 nm and the result is presented in Figure 5.9. As observed in the figure, the D peak is obtained at 1351 cm^{-1}, which indicates the existence of defects in the sample while the G peak was obtained at 1617 cm^{-1}. The G peak corresponds to the Raman active E_{2g} phonon at Brillioun zone centre of graphite (Wang et al., 2011). The intensity ratio of the D to G band of the graphene sheets is about 1.2, as expected due to small size of the graphene sample. The existence of multi-layered graphene can be confirmed by considering the ratio of G to 2D peak which is higher than 0.5 (Wei et al., 2011; Lu et al., 2009). The modulation depth is measured approximately 2.48 % with non-saturable of 54.62 %

which is slightly similar to the multi-layered graphene synthesized by CVD technique designated by Huang et al. (2012).

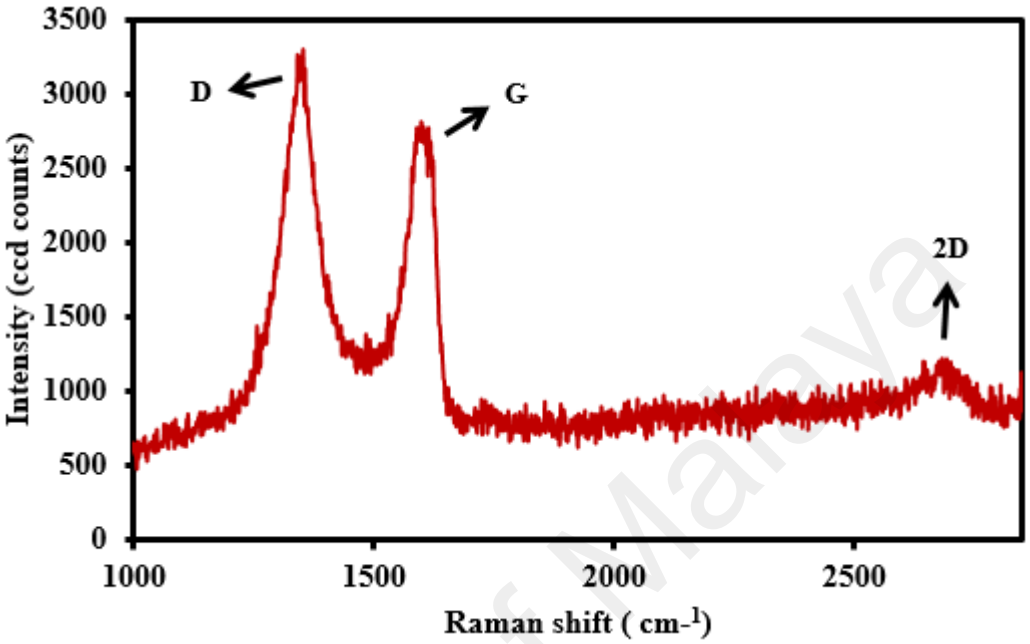

Figure 5.9: Raman spectrum from the graphene film

5.4.2 Performance of Dark Pulse Zr-EDFL

Then, the experiment is further carried out based on configuration of Figure 5.10 by replacing the saturable absorber with graphene film device. The CW lasing operation started at 55 mW pump power. As we further increase the pump power to 98 mW, the self-started mode-locking operation take over and suppress the CW operation. The optical spectrum of mode-locked Zr-EDFL graphene film is shown in Figure 5.10 (a) where the center wavelength and peak power are 1601.89 nm and -15.98 dBm, respectively. The laser operates at L-band region, with laser bandwidth spanning from 1600 nm to 1603.8 nm. Figure 5.10 (b) shows a highly stable Zr-EDFL that was observed from RF spectrum analyzer in frequency domain with frequency span and resolution bandwidth of 100 kHz and 300 Hz, respectively. The signal-to-noise (SNR) as high as 66.1 dB, indicates that the large desired signal is obtained compare to noise in cavity. The RF repetition rate of

the mode-locked pulse is about 1 MHz, matches well with the repetition rate measurement from oscilloscope. This specifies that the mode-locked laser output operates at its fundamental repetition rate.

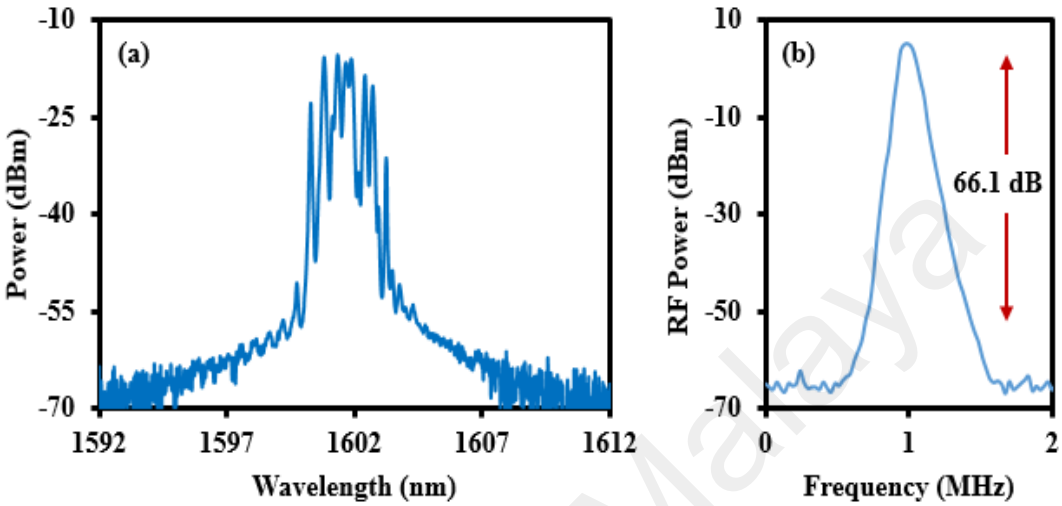

Figure 5.10: (a) Optical spectrum of Zr-EDFL by using graphene film as saturable absorber (b) RF spectrum at 1 MHz

The characteristics of the dark pulse mode-locked by using graphene film is shown in Figure 5.11. Figure 5.11 (a) shows an oscilloscope output of dark pulse train at threshold pump power of 98 mW. The measured repetition rate is 1 MHz, which corresponds to the total cavity of 203 m. Subsequently, the pulse width is measured by commercial auto-correlator. Figure 5.11 (b) indicates the corresponding measurement pulse duration at full-width half maximum (FWHM) of 3.48 ps. The span and filter resolution of the autocorrelator are fixed at 100 ps and 1 ps, respectively. As the pump power is further increased, the oscilloscope trace becomes smoother and the pulse is less distorted as shown in Figure 5.11 (c) at the maximum pump power of 180 mW.

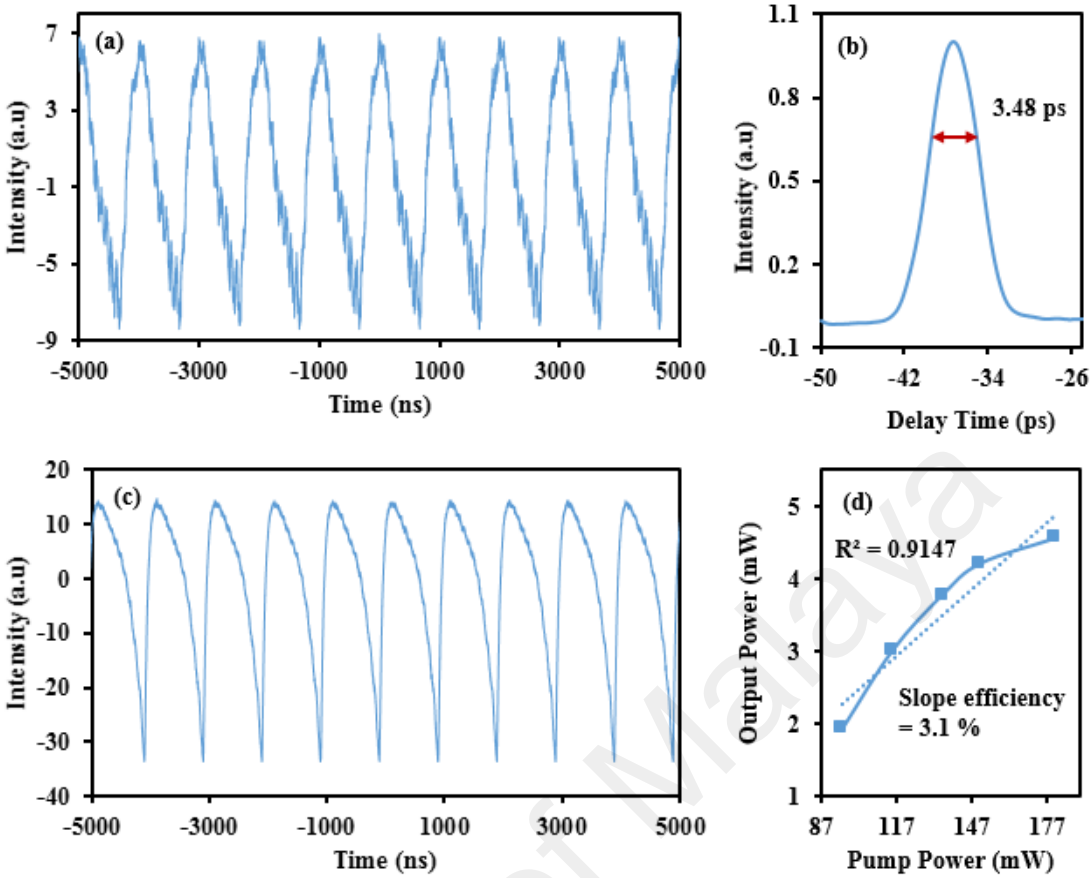

Figure 5.11: Characteristics of the dark pulse mode-locked fiber laser. (a) Pulse train of the dark pulse at pump power 98 mW (b) Autocorrelation trace with pulse duration of 3.48 ps (c) Pulse train of the dark pulse at pump power of 180 mW (d) Output power against pump power

The smooth pulse without any jitter and noise is due to the efficient saturable absorber, where it absorbs the low optical intensity like continuous wave and transform it to a short wave of pulse as increasing power intensity (Yang et al., 2005). Figure 5.11 (d) illustrates a slope efficiency of 3.1 % which is describes the relationship between output powers against pump power is less efficient due to high loss in cavity. Then, the regression trend line determines by R squared is 0.9147, verifies the good linearity and almost ideal for linear graph between both variables of powers. The maximum pump

power is 180 mW, taken right before the pulse became unstable and disappear. The output power and pulse energy measurement are 4.56 mW and 4.56 nJ, respectively.

5.5 Multiwavelength Dark Pulse Mode Locked Zr-EDFL with Black Phosphorus SA (BPSA)

To date, the most versatile SA is graphene, and it is well studied and established. It has outstanding optical properties as well as ultrafast recovery time and broad operational wavelength region (Sun, Hasan & Ferrari, 2012; Du et al., 2014). However, the zero band-gap causes a low absorption results and it limits the light-matter interaction which is critical for certain electronic applications (Jiang et al., 2015; Chen et al., 2015). Therefore, researchers are working to discover alternative material that can complement the drawback of graphene. Recently, a fascinating material, black phosphorus (BP) has attracted much attention due to its narrow direct band-gap. It observed to exhibit saturation of optical absorption under strong light illumination and has been experimentally demonstrated as SA to initiate pulsing in pulsed lasers (Sotor et al., 2015). In this section, a dark pulse mode-locked Zr-EDFL is demonstrated using a BP film as a SA in conjunction with simple ring configuration setup of Fig. 5.10. The performances of the pulsed laser with BP will be compared with the previously demonstrated graphene film based laser. The BP-based SA (BPSA) device was successfully incorporated into the laser cavity to produce dark pulse with the same repetition rate of 1 MHz, which corresponds to the total length cavity. To the best our knowledge, this is the first demonstration of dark pulse mode-locked fiber laser by using Zr-EDF with the utilization of BPSA.

5.5.1 Fabrication and Characteristic of BPSA

BPSA was prepared by using mechanically exfoliated method. The procedure starts by peeling process and ends by inserting prepared SA into the cavity as illustrated in Figure 5.12. All the preparation process take less than 3 minutes. Step 1, a base material of BPSA is peeled off several times from a commercially available BP crystal with purity of 99 % using a transparent scotch tape. The scotch tape containing the BP flakes is then pressed moderately onto the adhesive surface for 20 times in Step 2. In this process, BP flakes become thin enough for light to pass through with optimum performance. Lastly in Step 3, the obtained thin layer is cut into a small piece, about the minimum size of 9 μm to cover the fiber core and then it was transferred onto the fiber ferrule. The index matching gel is used as holding agent.

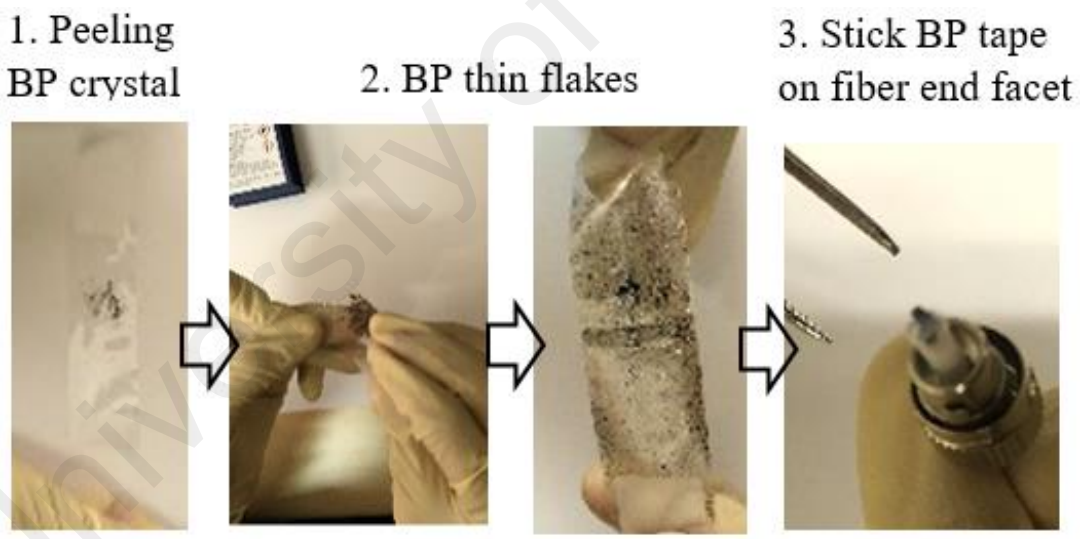

Figure 5.12: BPSA preparation process

Next, we demonstrate a nonlinear absorption profile of BP tape. This is important characteristics to determine the material's functionality as an SA. In measuring nonlinear absorption profile, a mode-locked laser is used as the input pulse source. The twin-detector measurement was applied, where we record the launched power and output power of the SA sample to obtain modulation depth of the material. By varying on the

input laser power, these two recorded powers are for normalization calculation in a function of incident peak intensity on the BP tape. With increasing peak intensity, the material absorption decreases as shown in Figure 5.13, confirming saturable absorption. The experimental data for absorption are fitted according to $\alpha(I) = [\alpha_s/(1+I/I_{sat})] + \alpha_{ns}$, a simple two-level SA model (Haris et al., 2015). The is $\alpha(I)$ the absorption, α_s is the modulation depth, I is the input intensity, I_{sat} is the saturation intensity, and α_{ns} is the non-saturable absorption. As shown in Figure 5.13, the modulation depth, non-saturable intensity, and saturation intensity are obtained to be 8 %, 57 % and 0.35 MW/cm^2, respectively. Taking into account its nonlinear optical response leading to absorption saturation at relatively low fluence, the mechanically exfoliated BP meets basic criteria of a passive SA for fiber lasers.

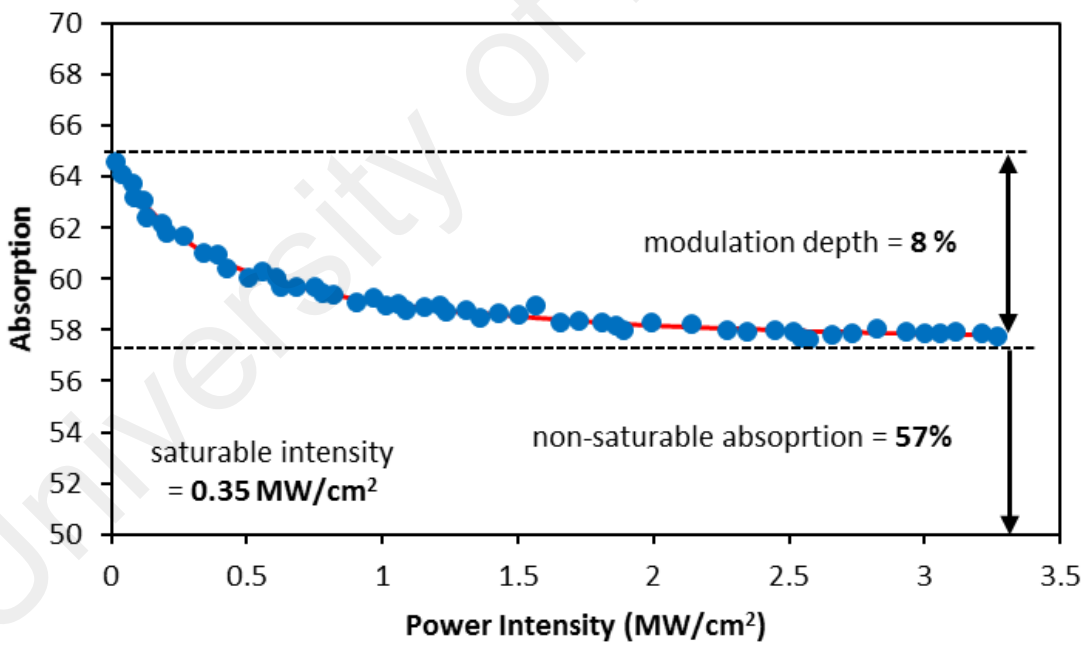

Figure 5.13: BPSA nonlinear absorption profile

Material characterization of prepared SA was performed by using field emission scanning electron microscope (FESEM), Raman spectroscopy, and energy dispersive spectroscopy (EDS). The presence of BP flakes on scotch tape surface is visibly seen in

the FESEM image as presented in Figure 5.14 (a). The composition of the transferred layers is confirmed by the EDS on the FESEM image. In Figure 5.14 (b), the higher peak phosphorus spectroscopy data confirms the presence of BP material on the scotch tape adhesive surface. We also performed Raman spectroscopy on the fabricated BP tape. Figure 5.14 (c) shows the Raman spectrum of BP tape has exhibits at A_g^1 of 360 cm^{-1}, B_{2g} of 438 cm^{-1}, and A_g^2 of 465 cm^{-1}, where define the vibration modes of layered BP (Li et al., 2015). About 50 mW (100 %) radiated power of 514 nm Argon laser was exposed onto the BP tape surface for 10 ms. The B_{2g} and A_g^2 modes define as in-plane oscillation of phosphorus atoms in BP layer. For the A_g^1, it related to the out-of-plane vibration.

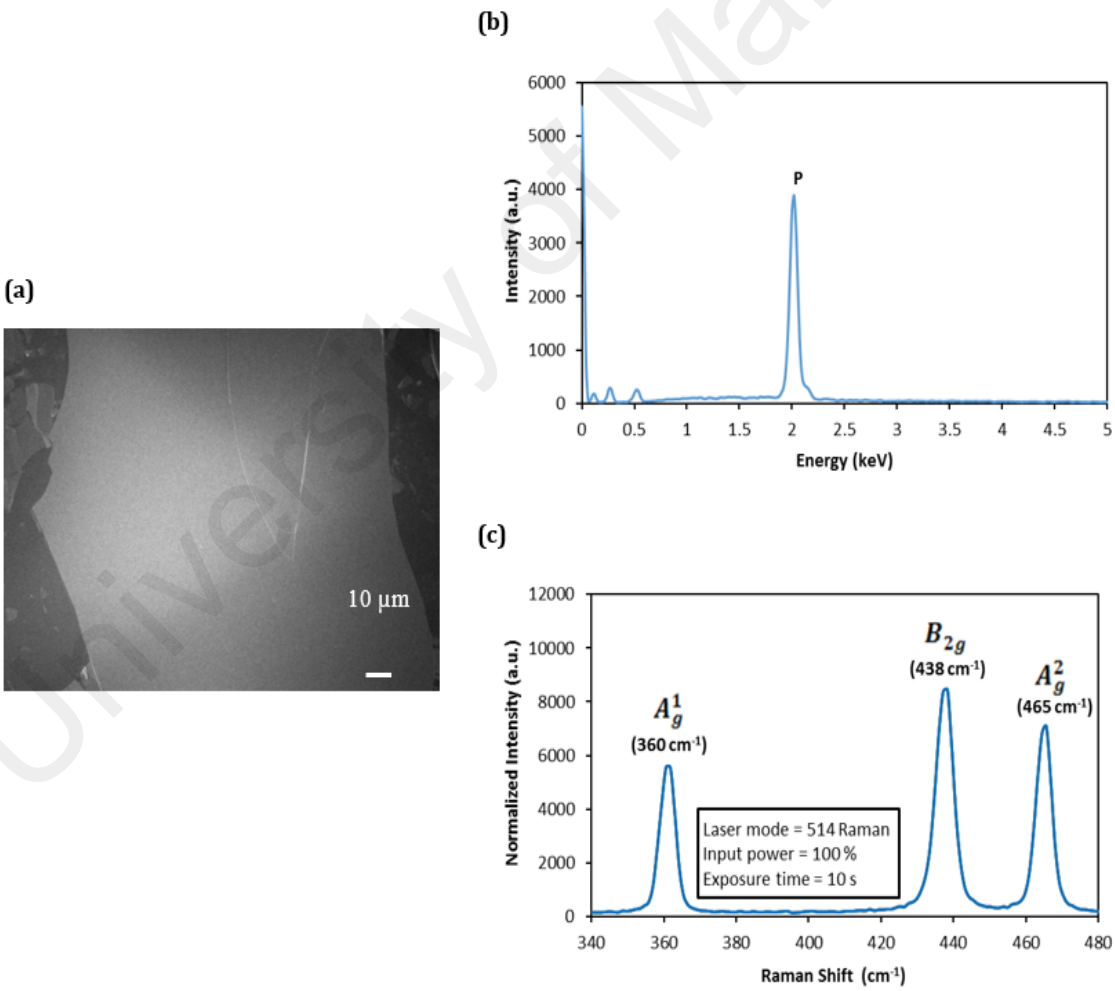

Figure 5.14: BPSA characteristics (a) FESEM image (b) EDS data. (c) Raman spectrum

5.5.2 Performance of Multiwavelength Dark Pulse Zr-EDFL

Then, the experiment is further carried out based on configuration of Figure 5.10 by replacing the saturable absorber with BPSA device. A stable self-starting fundamental mode-locking operation commences at around 90 mW and the multiwavelength optical spectrum is shown in Figure 5.15 (a). This multiwavelength Zr-EDFL generates five wavelengths at 1604.1 nm, 1603.5 nm, 1602.9 nm, 1602.3 nm and 1601.7 nm with a uniform channel spacing of 0.6 nm. The average and the highest peak power of laser are -21.5 dBm and -18.5 dBm. In our experiment, the multiwavelength is induced from the four-wave-mixing (FWM) effects that occurs from high nonlinearity SA (Luo et al., 2012). This shows that our fabricated BP has higher nonlinearity compared to the fabricated graphene film. The limitation number of lasing channels of multi-wavelength fiber laser is due to the mode-suppression and mode-competition in common EDF by the homogenous gain medium broadening at room temperature (Ahmad et al., 2012; Yang et al., 2005). Since use the same cavity, the stable obtained repetition rate is about 1 MHz. The different from graphene film may highlights in term of pump tunability and pulse train stability. As shown in Figure 5.15 (b), the SNR is observed to be 74.6 dB, which signifies that the pulsing behavior is rather stable in the cavity.

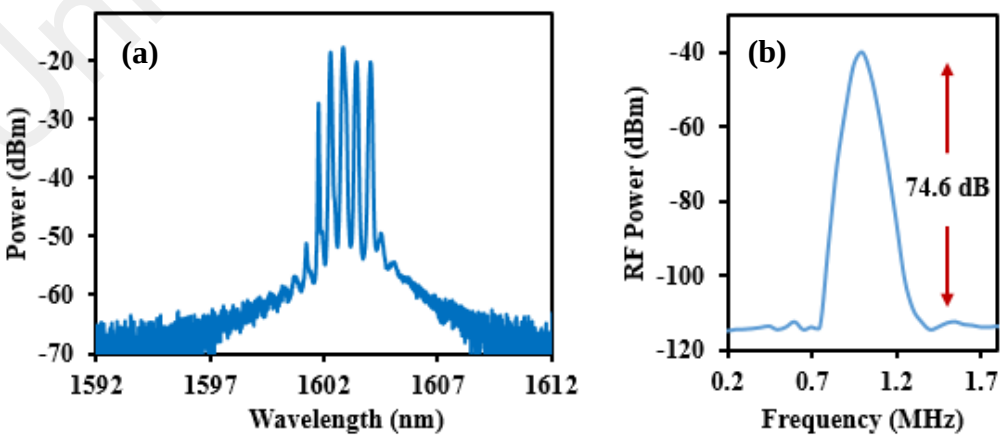

Figure 5.15: (a) Optical spectrum of multiwavelength Zr-EDFL by using BP as saturable absorber (b) RF spectrum at 1 MHz

Figure 5.16 (a) shows the oscilloscope trace of the laser, which indicates a dark pulse train with repetition rate of 1 MHz. An obvious stable mode-locking operation consist of dark pulse is obtained between pump power of 90 mW until 220 mW. As the pump power increases beyond the 220 mW, the pulse regime disappears. Meanwhile, the corresponding autocorrelation trace is shown in Figure 5.16 (b) and the measurement of pulse duration is 3.46 ps. The smooth dark pulse train is shown in Figure 5.16 (c) at pump power of 220 mW. Figure 5.16 (d) depicts the 6 % slope efficiency and 0.9928 regression trend line of BP cavity are better than graphene film as the relationship of output powers. At maximum pump power of 220 mW, the measurement of output power and pulse energy approximately around 9.89 mW and 9.89 nJ, respectively.

Unlike the autocorrelation trace of a common bright pulse which locates at the center with zero delay, the measured dark pulse of our pulsed laser is shifted from the center with delay of -37.7 ps and -37.3 ps respectively. The delay is due to the formation of dark pulse is initiated after the bright pulse has collapsed. But in our experiment, the formation of bright pulse with both saturable absorbers is not presence. The formation and propagation of dark pulse in the cavity is stabilized with the insertion of a spool of 180 m SMF. Without the spool of SMF, the pulse width of dark pulse are not measurable with autocorrelator. The dark pulse originates due to the high nonlinearity gain medium of 3 m long Zr-EDF and the fabricated BP. The generated dark pulse is further stabilized by the nonlinearity and birefringence from the 180 m long SMF spool.

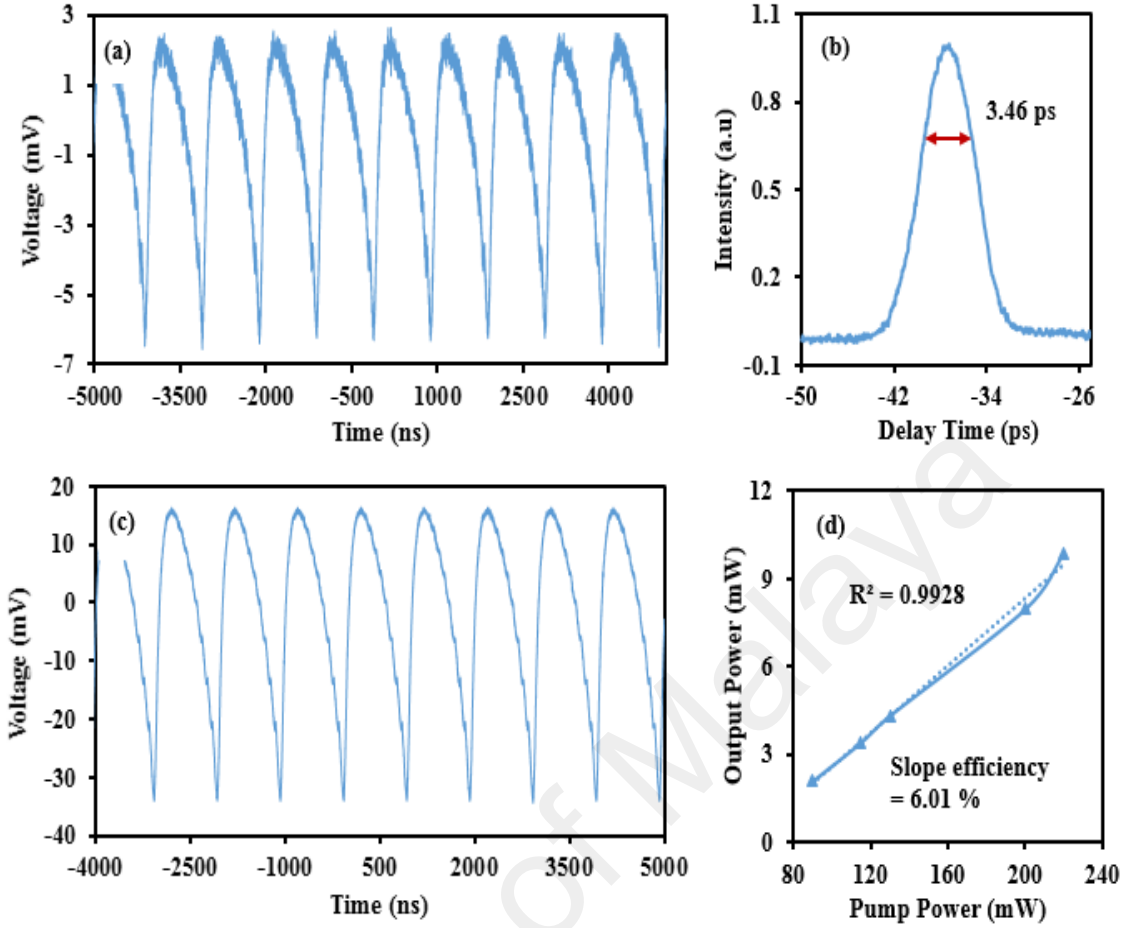

Figure 5.16: Characteristics of the dark pulse multiwavelength mode-locked fiber laser. (a) Pulse train of the dark pulse at pump power 90 mW. (b) Autocorrelation trace with pulse duration of 3.46 ps. (c) Pulse train of the dark pulse at pump power of 220 mW. (d) Output power against

5.6 Summary

The generation of soliton, multiwavelength and dark pulse of Zr-EDFL are successfully accomplished with passively mode-locking technique by using graphene oxide, graphene film and black phosphorus as saturable absorber. All the mode-locked pulses are function in L-band transmission bandwidth that ranging from 1567 nm to 1605 nm. This is because of the used of 3 m long Zr-EDF in cavity, that sufficient to amplify the signal and leads to the operational wavelength in L-band region. A Zr-EDFL with the

utilization of graphene oxide SA demonstrates a soliton mode-locking pulse with threshold pump power at 78 mW. The wavelength center and 3 dB spectral are 1577.46 nm and 5.4 nm with repetition rate of 13.9 MHz, corresponding to the total length cavity of 14.7 m. The pulse duration and optical signal-to-noise ratio (OSNR) are 0.6 ps and 43 dB while the TBP value is 0.48, which is slightly deviates from transform limit for $sech^2$-shaped laser pulses of 0.315. The pulse energy is 2.74 pJ at pump power of 84.1 mW.

Then, a further experiments are using the very same configuration setup with 203 m total cavity length via three different SAs; graphene oxide, graphene film and black phosphorus. Thus, all share the same repetition rate of 1 MHz, which is equivalents to the total length of cavity. Moreover, this experiments are successfully to generate dark pulse regime due to high nonlinearity gain medium of Zr-EDF, strong birefringence from a spool of 180 m SMF and high nonlinearity of 2D nanomaterial SAs. At first, a multiwavelength dark pulse mode-locking Zr-EDFL is demonstrates with the employment of GOSA. The threshold pump power is 65 mW to obtain five lasing lines of multiwavelength which operates at wavelength 1599.6 nm, 1600.1 nm, 1600.6 nm, 1601.1 nm and 1601.6 nm. The pulse duration, OSNR and pulse energy are 3.43 ps, 43 dB and 2.01 nJ.

Second, the dark pulse mode-locking Zr-EDFL is generated by using graphene film SA. The threshold pump and wavelength center are 98 mW and 1601.89 nm. The pulse duration, OSNR and pulse energy are 3.48 ps, 66.1 dB and 4.56 nJ. Finally, a multiwavelength dark pulse mode-locked Zr-EDFL is demonstrated with the employment of BPSA. The threshold pump power is 90 mW to develop five wavelengths at 1604.1 nm, 1603.5 nm, 1602.9 nm, 1602.3 nm and 1601.7 nm with a uniform channel spacing of 0.6 nm. The pulse duration, OSNR and pulse energy are 3.46 ps, 74.6 dB and 9.89 nJ. As observation, the performance of mode-locked fiber laser with the utilization of black phosphorus SA is more comparable than graphene oxide and graphene film. The reason

is, in term of the stability of mode-locking pulsed laser with five lines of multiwavelength spectrum, higher desired signal in cavity defines by OSNR value, high efficiency slope for output power against pump power and higher pulse energy.

CHAPTER 6: CONCLUSION AND FUTURE WORK

6.1 Conclusion

Optical fiber is one of the remarkable inventions that significantly important for various applications including the military, medical, telecommunication, networking and broadcasting industry. Erbium-doped fiber amplifier (EDFA) is one of the optical fiber devices that is widely used in communication systems. It is reliable, minimal loss, cost effective, simple and flexible to integrate in communication network and capable to produce high optical gain of more than 40 dB. A multiple stages of amplifier is required for long transmission distance in order to maintain the signals intensity over thousands of kilometres. However, accumulated gain fluctuation along these stages will cause additional noise, depreciate the total desired signal at receiver and thus, downgrades the overall wavelength division multiplexing (WDM) system performance. To overcome this problem, a gain medium with highly doped erbium concentration is necessary due to the capabilities to create an excellent population inversion that exceeds the noise figures, and consequently develop a high flat-gain in wideband transmission bandwidth. In this thesis, a new enhanced Erbium–Zirconia–Yttria–Aluminum Co-Doped Fiber (Zr-EDF) was characterized and investigated for both amplifier and pulsed laser applications. The Zr-EDF is obtained from a fiber preform, which is fabricated in a ternary glass host, zirconia-yttria-aluminium co-doped silica fiber using a MCVD in conjunction with solution doping process. The fiber consists of Er_2O_3-doped ZrO^2 rich nano-crystalline particles and thus it has a high erbium doping concentration with absorption pump power around 80.0 dB/m at 980 nm.

An efficient optical amplifier was successfully characterized and demonstrated using the Zr-EDF as a gain medium in Chapter 3. At the optimum length of 1 m, Zr-EDF amplifier (Zr-EDFA) produced a flat-gain of 27 dB from 1530 nm to 1565 nm wavelength

with gain fluctuation and noise figure were less than 3 dB and 6.9 dB by using a standard single pass configuration. The pump power and input signal are fixed at 130 mW and -30 dBm, respectively. With the same value of pump power and optimum length of Zr-EDF, a flat-gain of 19.6 dB is achieved from 1530 nm to 1570 nm with gain fluctuation of 0.27 dB and noise figure below than 11 dB for input signal fixed at -10 dBm. Again, by using optimum length of 1 m, the Zr-EDFA is successfully to obtain a high flat-gain of 38 dB from 1530 nm to 1565 nm with gain fluctuation less than 3 dB for double pass configuration. The pump power and input signal are maintained at 130 mW and -30 dBm, respectively. The Zr-EDFA was also presented an improved performance compare to previous Zr-EDFA with a lower erbium concentration, conventional Bi-EDFA and Si-EDFA.

Pulsed laser can be generated by using either passive or active technique. Passive technique is preferable especially for ultrashort pulsed laser, essentially due to the employment of saturable absorber (SA) which modulates the resonator much faster than any electronic modulator that is essential for an active mode-locking. There are two types of pulsed lasers; Q-switched and mode-locked. Normally, Q-switched develop pulse duration and repetition rate in nano- to micro-seconds and kilo- to micro-Hertz. Meanwhile mode-locked grows a spotlight due to its capabilities to develop ultrashort pulse duration and high repetition rate in the range of pico- to femto-seconds and Mega- to Tera-Hertz. In this work, the generation of pulsed lasers were demonstrated using passive methods such as nonlinear polarization rotation (NPR) and various types of SAs.

In Chapter 4, pulsed Zr-EDF lasers (Zr-EDFLs) were successfully demonstrated by using three different passive techniques such as NPR, thulium fiber SA and single-wall carbon nanotubes (SW-CNTs) SA. At first, a bright and dark pulse mode-locked Zr-EDFL was realized using an NPR technique with repetition rate and pulse duration of 14.1 MHz and 27 ns. Both of pulses can be obtained by only twisting the polarization

state of laser cavity. The bright and dark pulses are formed mainly due to the cross coupling between two-Eigen operation states of fiber laser through the nonlinear effects of optical fibers. Secondly, a simple Q-switched Zr-EDFL was demonstrated based on thulium-doped fiber as solid state saturable absorber fiber. The pulse duration and repetition rate were varied from 21.4 to 14.1 μs and 77.2 to 97.5 mW as increasing the pump power. Finally, a soliton mode-locked was obtainable based on SWCNTs SA to generate pulse train at repetition rate and pulse duration of 17.7 MHz and 770 fs, respectively. These results show that the new Zr-EDF has a potential to develop not only bright pulse, but also dark pulse regime of pulsed fiber laser.

Chapter 5 aimed to demonstrate the pulse generation in Zr-EDFL cavity using a two-dimensional nanomaterials as a SA. The new SA was developed using graphene oxide (GO), graphene film and black phosphorus (BP). A soliton mode-locked pulsed laser with repetition rate of 13.9 MHz and pulse width of 600 fs was firstly demonstrated by deployment of GO SA. Then, further experiments were carried out using the Zr-EDFL cavity with total cavity length of 203 m. The performance of the Zr-EDFL was investigated for three different 2D nanomaterials based SAs. It is observed that all the pulse train outputs from these lasers shared the same repetition rate of 1 MHz, which equivalents to the total length of cavity. With the utilization of GOSA, a multiwavelength dark pulse mode-locking with the pulse duration of 3.43 ps was obtained. As the SA was replaced with a graphene film, and the mode-locked Zr-EDFL produce a dark pulse with the pulse duration of 3.48 ps. A multi-wavelength dark pulse mode-locked laser was then obtained with pulse duration of 3.46 ps with the employment of BP SA. It is worthy to note that the BP based mode-locked Zr-EDFL shows a better mode-locking performance compared to other SA of graphene families in term of pulse stability, optical signal to noise ratio, slope efficiency and pulse energy. The generation of dark pulse is expected due to the high nonlinearity of Zr-EDF and the fabricated 2D nanomaterial SAs.

In conclusion, these results show that Zr-EDF is a suitable gain medium for the development of a compact flat-gain optical amplifier and ultrafast fiber lasers. 2D nanomaterials are found to have a great potential for use as SA for generating ultrafast mode-locked pulse train operating in both bright and dark regimes.

6.2 Future Works

The newly developed improved Zr-EDF gain medium shows excellent performances for both amplifier and pulsed laser applications. Thus, there are many more exploration should be done for either realizing flat-gain wide-band amplifiers or generating ultra-short pulse lasers. Various new techniques for mode-locking should be explored. For instance, a mode-locked fiber laser can be realized using a nonlinear polarization rotation technique by inserting optical components such as polarization beam splitter, dispersion-shifted fiber (DSF), dispersion-compensating fiber (DCF) and high nonlinear fiber inside the laser cavity. Other passive technique based on nonlinear optical loop mirror (NOLM) can also be explored. Besides, inelastic scattering phenomena such as stimulated Brillouin scattering and stimulated Raman scattering are also interesting to be investigated by using this special fiber.

With the development of ultrafast laser technology, the cavity length can be reduced and allows for the generation of ultrashort pulse down to femtoseconds with Mega- to Giga-Hertz repetition rate. The key component is a mode-locker where new nanomaterials such as Black phosphorus, Molybdenum disulfide (MoS_2) and topology insulator, TiO_2 and quantum dots. Besides, the solid state saturable absorber fiber can be further explored to obtain a mode-locking pulse. The fascinate generation of dark pulse can also be investigated with a short length cavity, high repetition rate and ultrashort pulse duration. The optimization of cavity dispersion and nonlinearity will lead to the formation of improved pulse train operating in dark regime.

REFERENCES

Agrawal, G. P. (2007). Nonlinear fiber optics. Academic press.

Ahmad, F., Harun, S. W., Nor, R. M., Zulkepely, N. R., Ahmad, H., & Shum, P. (2013). A passively mode-locked erbium-doped fiber laser based on a single-wall carbon nanotube polymer. *Chinese Physics Letters*, *30*(5), 054210.

Ahmad, H., Awang, N. A., Paul, M. C., Pal, M., Latif, A. A., & Harun, S. W. (2012). All fiber passively mode locked zirconium-based erbium-doped fiber laser. *Optics & Laser Technology*, *44*(3), 534-537.

Ahmad, H., Shahi, S., & Harun, S. W. (2010). Bismuth-based erbium-doped fiber as a gain medium for L-band amplification and Brillouin fiber laser. Laser physics, 20(3), 716-719.

Ahmad, H., Thambiratnam, K., Awang, N. A., Jemangin, M. H., & Harun, S. W. (2012). Stable zirconia-erbium doped multiwavelength fiber laser by precise control of polarization states. *Laser Physics*, *22*(5), 982-985.

Ahmad, H., Thambiratnam, K., Muhammad, F. D., Zulkifli, M. Z., Zulkifli, A. Z., Paul, M. C., & Harun, S. W. (2014). Q-Switching and Mode-Locking in Highly Doped Zr O–Al O–Er O-Doped Fiber Lasers Using Graphene as a Saturable Absorber. *Selected Topics in Quantum Electronics, IEEE Journal of*, *20*(1), 9-16.

Ahmad, H., Thambiratnam, K., Paul, M. C., Zulkifli, A. Z., Ghani, Z. A., & Harun, S. W. (2012). Fabrication and application of zirconia-erbium doped fibers. *Optical Materials Express*, *2*(12), 1690-1701.

Ahmad, H., Zulkifli, A. Z., Muhammad, F. D., Zulkifli, M. Z., Thambiratnam, K., & Harun, S. W. (2014). Mode-locked L-band bismuth–erbium fiber laser using carbon nanotubes. *Applied Physics B*, *115*(3), 407-412.

Ahmad, H., Zulkifli, A. Z., Thambiratnam, K., & Harun, S. W. (2013). Q-switched Zr-EDF laser using single-walled CNT/PEO polymer composite as a saturable absorber. *Optical Materials*, *35*(3), 347-352.

Ahmed, M. H. M., Latiff, A. A., Arof, H., & Harun, S. W. (2016). Mode-locking pulse generation with MoS 2–PVA saturable absorber in both anomalous and ultra-long normal dispersion regimes. *Applied Optics*, *55*(15), 4247-4252.

Aiso, K., Tashiro, Y., Suzuki, T., & Yagi, T. (2001, March). Erbium Lanthanum co-doped fiber for L-band amplifier with high efficiency, low non-linearity and low NF. In *Optical Fiber Communication Conference and Exhibit, 2001. OFC 2001* (Vol. 2, pp. TuA6-TuA6). IEEE.

Al-Taha, M. H., Idris, S. M., Jamaludin, M. Z., Al-Mansoori, M. H., & Abdullah, F. (2011, October). Gain improvement in L-band double-pass EDFA with incorporated CFBG. In *Photonics (ICP), 2011 IEEE 2nd International Conference on* (pp. 1-3). IEEE.

ANTHONY, R., & LAHIRI, R. (2012). PERFORMANCE ANALYSIS OF DIFFERENT ERBIUM DOPED FIBER BASED CO-DIRECTIONALLY PUMPED WDM

SYSTEMS OPERATING IN OPTICAL WIDE-BAND. *International Journal of Engineering Science and Technology (IJEST)*, *4*(02).

Arai, F., Tanimoto, M., Fukuda, T., Shimojima, K., Matsuura, H., & Negoro, M. (1996, April). Multimedia tele-surgery using high speed optical fiber network and its application to intravascular neurosurgery-system configuration and computer networked robotic implementation. In *Robotics and Automation, 1996. Proceedings., 1996 IEEE International Conference on* (Vol. 1, pp. 878-883). IEEE.

Barnoski, M. (Ed.). (2012). *Introduction to integrated optics*. Springer Science & Business Media.

Bass, M., DeCusatis, C., Enoch, J., Lakshminarayanan, V., Li, G., MacDonald, C., Mahajan, V., & Stryland, E. V. (2009). Handbook of Optics, Third Edition Volume V: Atmospheric Optics, Modulators, Fiber Optics, X-Ray and Neutron Optics. McGraw Hill Professional.

Becker, P. M., Olsson, A. A., & Simpson, J. R. (1999). *Erbium-doped fiber amplifiers: fundamentals and technology*. Academic press.

Birks, T. A., Knight, J. C., & Russell, P. S. J. (1997). Endlessly single-mode photonic crystal fiber. *Optics letters*, *22*(13), 961-963.

Bonaccorso, F., Sun, Z., Hasan, T., & Ferrari, A. C. (2010). Graphene photonics and optoelectronics. *Nature photonics*, *4*(9), 611-622.

Bufetov, I. A., & Dianov, E. M. (2009). Bi-doped fiber lasers. *Laser Physics Letters*, *6*(7), 487.

Cadek, M., Coleman, J. N., Barron, V., Hedicke, K., & Blau, W. J. (2002). Morphological and mechanical properties of carbon-nanotube-reinforced semicrystalline and amorphous polymer composites. *Applied physics letters*, *81*(27), 5123-5125.

Camargo, M. B., Kokta, M., Stultz, R. D., & Birnbaum, M. (1995). Co 2+: YSGG saturable absorber Q switch for infrared erbium lasers. *Optics letters*, *20*(3), 339-341.

Chang, K. F., Poopalan, P., Teyo, T. C., Subramaniam, T., & Ahmad, H. (2002, October). Gain Enhancement in Double-pass Erbium-doped Fiber Amplifier. In International Conference on Optical Communication and Networks–ICOCN, Singapore, paper 12D3 (pp. p77-79).

Chang, Y. M., Kim, H., Lee, J. H., & Song, Y. W. (2010). Multilayered graphene efficiently formed by mechanical exfoliation for nonlinear saturable absorbers in fiber mode-locked lasers. *Applied Physics Letters*, *97*(21), 211102.

Chen, Y., Jiang, G., Chen, S., Guo, Z., Yu, X., Zhao, C., ... & Fan, D. (2015). Mechanically exfoliated black phosphorus as a new saturable absorber for both Q-switching and Mode-locking laser operation. *Optics express*, *23*(10), 12823-12833.

Cheng, M. Y., Chang, Y. C., Galvanauskas, A., Mamidipudi, P., Changkakoti, R., & Gatchell, P. (2005). High-energy and high-peak-power nanosecond pulse

generation with beam quality control in 200-μm core highly multimode Yb-doped fiber amplifiers. *Optics letters*, *30*(4), 358-360.

Cheng, X. S., Hamida, B. A., Naji, A. W., Ahmad, H., & Harun, S. W. (2011). 67 cm long bismuth-based erbium doped fiber amplifier with wideband operation. Laser Physics Letters, 8(11), 814.

Cheng, X. S., Parvizi, R., Ahmad, H., & Harun, S. W. (2009). Wide-band bismuth-based erbium-doped fiber amplifier with a flat-gain characteristic. Photonics Journal, IEEE, 1(5), 259-264.

DeCusatis, C. (Ed.). (2013). *Handbook of fiber optic data communication: a practical guide to optical networking*. Academic Press.

Dianov, E. M. (2012). Bismuth-doped optical fibers: a challenging active medium for near-IR lasers and optical amplifiers. Light: Science & Applications, 1(5), e12.

Diebel, F., Leykam, D., Boguslawski, M., Rose, P., Denz, C., & Desyatnikov, A. S. (2014). All-optical switching in optically induced nonlinear waveguide couplers. Applied Physics Letters, 104(26), 261111.

Diebold, A., Emaury, F., Schriber, C., Golling, M., Saraceno, C. J., Südmeyer, T., & Keller, U. (2013). SESAM mode-locked Yb: CaGdAlO 4 thin disk laser with 62 fs pulse generation. Optics letters, 38(19), 3842-3845.

Digonnet, M. J. (Ed.). (2001). *Rare-earth-doped fiber lasers and amplifiers, revised and expanded*. CRC press.

Du, J., Wang, Q., Jiang, G., Xu, C., Zhao, C., Xiang, Y., ... & Zhang, H. (2014). Ytterbium-doped fiber laser passively mode locked by few-layer Molybdenum Disulfide (MoS2) saturable absorber functioned with evanescent field interaction. *Scientific reports*, *4*.

Dvoyrin, V. V., Mashinsky, V. M., & Dianov, E. M. (2007). Yb-Bi pulsed fiber lasers. *Optics letters*, *32*(5), 451-453.

Eda, G., & Chhowalla, M. (2010). Chemically derived graphene oxide: towards large-area thin-film electronics and optoelectronics. *Advanced Materials*, *22*(22), 2392-2415.

Eisenstein, G., Tucker, R. S., Koren, U., & Korotky, S. K. (1986). Active mode-locking characteristics of InGaAsP-single mode fiber composite cavity lasers. *IEEE journal of quantum electronics*, *22*, 142-148.

Emplit, P., Haelterman, M., Kashyap, R., & De Lathouwer, M. (1997). Fiber Bragg grating for optical dark soliton generation. *Photonics Technology Letters, IEEE*, *9*(8), 1122-1124.

Emplit, P., Hamaide, J. P., Reynaud, F., Froehly, C., & Barthelemy, A. (1987). Picosecond steps and dark pulses through nonlinear single mode fibers. *Optics communications*, *62*(6), 374-379.

Fang, F., & Xiao, Y. (2006). Stability of chirped bright and dark soliton-like solutions of the cubic complex Ginzburg–Landau equation with variable coefficients. *Optics communications*, *268*(2), 305-310.

Feng, M., Silverman, K. L., Mirin, R. P., & Cundiff, S. T. (2010). Dark pulse quantum dot diode laser. *Optics express*, *18*(13), 13385-13395.

Fermann, M. E., & Hartl, I. (2009). Ultrafast fiber laser technology. *Selected Topics in Quantum Electronics, IEEE Journal of*, *15*(1), 191-206.

Fermann, M. E., Galvanauskas, A., & Sucha, G. (Eds.). (2002). *Ultrafast lasers: technology and applications* (Vol. 80). CRC Press.

Ferrari, A. C., Meyer, J. C., Scardaci, V., Casiraghi, C., Lazzeri, M., Mauri, F., ... & Geim, A. K. (2006). Raman spectrum of graphene and graphene layers. *Physical review letters*, *97*(18), 187401.

Fujimoto, Y., & Nakatsuka, M. (2001). Infrared luminescence from bismuth-doped silica glass. Japanese Journal of Applied Physics, 40(3B), L279.

Gao, W., Liao, M., Kawashima, H., Suzuki, T., & Ohishi, Y. (2013). Dark-square-pulse generation in a ring cavity with a tellurite single-mode fiber. *Photonics Technology Letters, IEEE*, *25*(6), 546-549.

Gengler, J. J., Muratore, C., Roy, A. K., Hu, J., Voevodin, A. A., Roy, S., & Gord, J. R. (2010). Yttria-stabilized zirconia-based composites with adaptive thermal conductivity. *Composites Science and Technology*, *70*(14), 2117-2122.

Ghatak, A., & Thyagarajan, K. (1998). An introduction to fiber optics. Cambridge university press.

Giles, C. R., & Desurvire, E. (1991). Modeling erbium-doped fiber amplifiers. *Lightwave Technology, Journal of*, *9*(2), 271-283.

Gredeskul, S. A., & Kivshar, Y. S. (1989). Generation of dark solitons in optical fibers. *Physical review letters*, *62*(8), 977.

Hamida, B. A., Azooz, S. M., Jasim, A. A., Eltaif, T., Ahmad, H., Khan, S., & Harun, S. W. (2015). Flat-gain wide-band erbium doped fiber amplifier by combining two difference doped fibers. *Journal of the European Optical Society-Rapid publications*, *10*.

Hamida, B. A., Latiff, A. A., Cheng, X. S., Ismail, M. A., Naji, W., Khan, S., ... & Harun, S. W. (2012, May). Flat-Gain Single-Stage Amplifier Using High Concentration Erbium Doped Fibers in Single-Pass and Double-Pass Configurations. In Photonics and Optoelectronics (SOPO), 2012 Symposium on (pp. 1-5). IEEE.

Hamzah, A., Paul, M. C., Awang, N. A., Ahmad, H., Pal, M., Das, S., ... & Harun, S. W. (2013). Passively mode-locked erbium doped zirconia fiber laser using a nonlinear polarisation rotation technique. *Optics & Laser Technology*, *47*, 22-25.

Hamzah, A., Paul, M. C., Harun, S. W., Huri, N. A. D., Lokman, A., Pal, M., ... & Sahu, J. K. (2011). Compact fiber laser at L-band region using Erbium-doped Zirconia fiber. Laser Physics, 21(1), 176-179.

Haris, H., Harun, S. W., Anyi, C. L., Muhammad, A. R., Ahmad, F., Tan, S. J., ... & Arof, H. (2015). Generation of soliton and bound soliton pulses in mode-locked erbium-doped fiber laser using graphene film as saturable absorber. *Journal of Modern Optics*, 1-6.

Harumoto, M., Shigehara, M., & Suganuma, H. (2002). Gain-Flattening Filter Using Long-PeriodFiber Gratings. Journal of lightwave technology, 20(6), 1027.

Harun, S. W., & Ahmad, H. (2003). Gain-clamped two-stage L-band EDFA with a FBG laser in second stage. *Optics & Laser Technology*, *35*(8), 645-647.

Harun, S. W., & Ahmad, H. (2003). L-band erbium-doped fibre amplifier with clamped-and flattened-gain using FBG. Electronics Letters, 39(17), 1238-1240.

Harun, S. W., Akbari, R., Arof, H., & Ahmad, H. (2011). Mode-locked bismuth-based erbium-doped fiber laser with stable and clean femtosecond pulses output. *Laser Physics Letters*, *8*(6), 449.

Harun, S. W., Cheng, X. S., Saat, N. K., & Ahmad, H. (2005). S-band Brillouin erbium fibre laser. *Electronics Letters*, *41*(4), 174-176.

Harun, S. W., Dimyati, K., Jayapalan, K. K., & Ahmad, H. (2007). An overview on S-band erbium-doped fiber amplifiers. *Laser Physics Letters*, *4*(1), 10.

Harun, S. W., Parvizi, R., Cheng, X. S., Parvizi, A., Emami, S. D., Arof, H., & Ahmad, H. (2010). Experimental and theoretical studies on a double-pass C-band bismuth-based erbium-doped fiber amplifier. *Optics & Laser Technology*, *42*(5), 790-793.

Harun, S. W., Paul, M. C., Huri, N. A. D., Hamzah, A., Das, S., Pal, M., ... & Sahu, J. K. (2011). Double-pass erbium-doped zirconia fiber amplifier for wide-band and flat-gain operations. Optics & Laser Technology, 43(7), 1279-1281.

Harun, S. W., Poopalan, P., & Ahmad, H. (2002). Gain enhancement in L-band EDFA through a double-pass technique. Photonics Technology Letters, IEEE, 14(3), 296-297.

Harun, S. W., Rahman, F. A., Dimyati, K., & Ahmad, H. (2006). An efficient gain-flattened C-band Erbium-doped fiber amplifier. *Laser Physics Letters*, *3*(11), 536.

Harun, S. W., Saat, N. K., & Ahmad, H. (2005). An efficient S-band erbium-doped fiber amplifier using double-pass configuration. IEICE Electronics Express, 2(6), 182-185.

Harun, S. W., Sabran, M. B. S., Azooz, S. M., Zulkifli, A. Z., Ismail, M. A., & Ahmad, H. (2015). Q-switching and mode-locking pulse generation with graphene oxide paper-based saturable absorber. *The Journal of Engineering*, *1*(1).

Harun, S. W., Saidin, N., Zen, D. I. M., Ali, N. M., Ahmad, H., Ahmad, F., & Dimyati, K. (2013). Self-starting harmonic mode-locked thulium-doped fiber laser with carbon nanotubes saturable absorber. *Chinese Physics Letters*, *30*(9), 094204.

Haruna, T., Hirano, M., & Sasaki, T. (2009, March). Phosphorus and aluminum co-doped EDF insensitive to hydrogen exposure for extended L-band amplification. In *Optical Fiber Communication Conference* (p. OTuH8). Optical Society of America.

Hasegawa, A., & Tappert, F. (1973). Transmission of stationary nonlinear optical pulses in dispersive dielectric fibers. II. Normal dispersion. *Applied Physics Letters*, *23*(4), 171-172.

Hecht, J. (2004). City of light: the story of fiber optics. Oxford university press.

Hibino, Y. (2002). Recent advances in high-density and large-scale AWG multi/demultiplexers with higher index-contrast silica-based PLCs. *Selected Topics in Quantum Electronics, IEEE Journal of*, *8*(6), 1090-1101.

Hofer, M., Fermann, M. E., Haberl, F., Ober, M. H., & Schmidt, A. J. (1991). Mode locking with cross-phase and self-phase modulation. *Optics letters*, *16*(7), 502-504.

Hu, J., Feng, N. N., Carlie, N., Petit, L., Wang, J., Agarwal, A., ... & Kimerling, L. (2007). Low-loss high-index-contrast planar waveguides with graded-index cladding layers. *Optics express*, *15*(22), 14566-14572.

Huang, L., Jha, A., Shen, S., & Liu, X. (2004). Broadband emission in Er 3+-Tm 3+ codoped tellurite fibre. *Optics express*, *12*(11), 2429-2434.

Huang, P. L., Lin, S. C., Yeh, C. Y., Kuo, H. H., Huang, S. H., Lin, G. R., ... & Cheng, W. H. (2012). Stable mode-locked fiber laser based on CVD fabricated graphene saturable absorber. *Optics express*, *20*(3), 2460-2465.

Inoue, K., Kominato, T., & Toba, H. (1991). Tunable gain equalization using a Mach-Zehnder optical filter in multistage fiber amplifiers. Photonics Technology Letters, IEEE, 3(8), 718-720.

Ismail, M. A., Ahmad, F., Harun, S. W., Arof, H., & Ahmad, H. (2013). A Q-switched erbium-doped fiber laser with a graphene saturable absorber. Laser Physics Letters, 10(2), and 025102.

Ismail, M. A., Ahmad, H., & Harun, S. W. (2014). Soliton mode-locked erbium-doped fiber laser using non-conductive graphene oxide paper. Quantum Electronics, IEEE Journal of, 50(2), 85-87.

Ismail, M. A., Harun, S. W., Zulkepely, N. R., Nor, R. M., Ahmad, F., & Ahmad, H. (2012). Nanosecond soliton pulse generation by mode-locked erbium-doped fiber laser using single-walled carbon-nanotube-based saturable absorber. *Applied optics*, *51*(36), 8621-8624.

Ismail, M. A., Tan, S. J., Shahabuddin, N. S., Harun, S. W., Arof, H., & Ahmad, H. (2012). Performance comparison of mode-locked erbium-doped fiber laser with nonlinear polarization rotation and saturable absorber approaches. *Chinese Physics Letters*, *29*(5), 054216.

Jiang, T., Yin, K., Zheng, X., Yu, H., & Cheng, X. A. (2015). Black phosphorus as a new broadband saturable absorber for infrared passively Q-switched fiber lasers. *arXiv preprint arXiv:1504.07341*.

Kakui, M., Kashiwada, T., Onishi, M., Shigematsu, M., & Nishimura, M. (1998). Optical amplification characteristics around 1.58 mm of silica-based erbium-doped fibers containing phosphorous/alumina as codopants. *Tech. Dig. OAA*, 107-110.

Keiser, G. (2003). *Optical fiber communications*. John Wiley & Sons, Inc..

Kikuchi, N., Sekine, K., & Sasaki, S. (1997). Analysis of cross-phase modulation (XPM) effect on WDM transmission performance. *Electronics letters*, *33*(8), 653-654.

Kilmer, S. L., & Anderson, R. (1993). Clinical Use of the Q-Switched Ruby and the Q-Switched Nd: YAG (1064 nm and 532 nm) Lasers for Treatment of Tattoos. The Journal of dermatologic surgery and oncology, 19(4), 330-338.

Kim, H. S., Yun, S. H., Kim, H. K., Park, N., & Kim, B. Y. (1998). Actively gain-flattened erbium-doped fiber amplifier over 35nm by using all-fiber acoustooptic tunable filters.

Kivshar, Y. S. (1993). Dark solitons in nonlinear optics. Quantum Electronics, IEEE Journal of, 29(1), 250-264.

Kivshar, Y. S., Emplit, P., Hamaide, J. P., & Haelterman, M. (1994). Gordon–Haus effect on dark solitons. *Optics letters*, *19*(1), 19-21.

Kleine-Ostmann, T., & Nagatsuma, T. (2011). A review on terahertz communications research. *Journal of Infrared, Millimeter, and Terahertz Waves*,*32*(2), 143-171.

Kudin, K. N., Ozbas, B., Schniepp, H. C., Prud'Homme, R. K., Aksay, I. A., & Car, R. (2008). Raman spectra of graphite oxide and functionalized graphene sheets. *Nano letters*, *8*(1), 36-41.

Kurkov, A. S., Sholokhov, E. M., & Medvedkov, O. I. (2009). All fiber Yb-Ho pulsed laser. *Laser Physics Letters*, *6*(2), 135-138.

Lai, L. J., & Su, C. S. (2000). Luminescence excitation and near edge X-ray absorption spectra of Er 2 O 3 dopant on zirconia ceramics. *Materials chemistry and physics*, *62*(2), 148-152.

Laroche, M., Gilles, H., Girard, S., Passilly, N., & Aït-Ameur, K. (2006). Nanosecond pulse generation in a passively Q-switched Yb-doped fiber laser by Cr 4+: YAG saturable absorber. *Photonics Technology Letters, IEEE*, *18*(6), 764-766.

Lee, B. (2003). Review of the present status of optical fiber sensors. *Optical fiber technology*, *9*(2), 57-79.

Leuenberger, M. L., Mulas, M. W., Hata, T. R., Goldman, M. P., Fitzpatrick, R. E., & Grevelink, J. M. (1999). Comparison of the Q-switched alexandrite, Nd: YAG, and ruby lasers in treating blue-black tattoos. *Dermatologic surgery*, *25*(1), 10-14.

Li, D., Demirbas, U., Benedick, A., Sennaroglu, A., Fujimoto, J. G., & Kärtner, F. X. (2012). Attosecond timing jitter pulse trains from semiconductor saturable absorber mode-locked Cr: LiSAF lasers. *Optics express*, *20*(21), 23422-23435.

Li, D., Jussila, H., Karvonen, L., Ye, G., Lipsanen, H., Chen, X., & Sun, Z. (2015). Polarization and thickness dependent absorption properties of black phosphorus: new saturable absorber for ultrafast pulse generation. *Scientific reports*, *5*.

Li, H., Jin, Z., Li, N., Xu, Q., Gu, H., Lu, J., ... & Wang, L. (2011). A small-molecule-based device for data storage and electro-optical switch applications. *Journal of Materials Chemistry*, *21*(16), 5860-5862.

Li, X. H., Wang, Y. G., Wang, Y. S., Hu, X. H., Zhao, W., Liu, X. L., ... & Li, C. (2012). Wavelength-switchable and wavelength-tunable all-normal-dispersion mode-locked Yb-doped fiber laser based on single-walled carbon nanotube wall paper absorber. *Photonics Journal, IEEE*, *4*(1), 234-241.

Li, X., Tang, Y., Yan, Z., Wang, Y., Meng, B., Liang, G., ... & Wang, Q. J. (2014). Broadband saturable absorption of graphene oxide thin film and its application in pulsed fiber lasers. *Selected Topics in Quantum Electronics, IEEE Journal of*, *20*(5), 441-447.

Lichtenauer, J., Valstar, M., Shen, J., & Pantic, M. (2009, September). Cost-effective solution to synchronized audio-visual capture using multiple sensors. In *Advanced Video and Signal Based Surveillance, 2009. AVSS'09. Sixth IEEE International Conference on* (pp. 324-329). IEEE.

Lin, R. Y., Wang, Y. G., Yan, P. G., Zhang, G. L., Zhao, J. Q., Li, H. Q., ... & Duan, J. A. (2014). Bright and dark square pulses generated from a graphene-oxide mode-locked ytterbium-doped fiber laser. *Photonics Journal, IEEE*, *6*(3), 1-8.

Lin, Y. H., & Lin, G. R. (2013). Kelly sideband variation and self four-wave-mixing in femtosecond fiber soliton laser mode-locked by multiple exfoliated graphite nano-particles. Laser Physics Letters, 10(4), 045109.

Liu, H. H., & Chow, K. K. (2014). Dark pulse generation in fiber lasers incorporating carbon nanotubes. *Optics express*, *22*(24), 29708-29713.

Liu, X. (2011). Soliton formation and evolution in passively-mode-locked lasers with ultralong anomalous-dispersion fibers. Physical Review A, 84(2), 023835.

Liu, X., Han, D., Sun, Z., Zeng, C., Lu, H., Mao, D., ... & Wang, F. (2013). Versatile multi-wavelength ultrafast fiber laser mode-locked by carbon nanotubes. *Scientific reports*, *3*.

Liu, Z. B., He, X., & Wang, D. N. (2011). Passively mode-locked fiber laser based on a hollow-core photonic crystal fiber filled with few-layered graphene oxide solution. *Optics letters*, *36*(16), 3024-3026.

Lu, J., Yang, J. X., Wang, J., Lim, A., Wang, S., & Loh, K. P. ACS Nano 2009, 3, 2367–2375. *CrossRef| PubMed| CAS| Web of Science® Times Cited*, *64*.

Luo, Z. C., Liu, M., Guo, Z. N., Jiang, X. F., Luo, A. P., Zhao, C. J., ... & Zhang, H. (2015). Microfiber-based few-layer black phosphorus saturable absorber for ultra-fast fiber laser. *Optics express*, *23*(15), 20030-20039.

Luo, Z. C., Luo, A. P., Xu, W. C., Song, C. X., Gao, Y. X., & Chen, W. C. (2009). Sideband controllable soliton all-fiber ring laser passively mode-locked by nonlinear polarization rotation. *Laser Physics Letters*, *6*(8), 582.

M. Azadeh, "Fiber Optics Engineering (Optical Networks)," New York: Springer, (2009)

MacDonald, C. (2010). Handbook of Optics: Volume V-Atmospheric Optics, Modulators, Fibre Optics, X-Ray and Neutron Optic.

Maiman, T. H. (1960). Stimulated optical radiation in ruby.

Martinez, A., & Sun, Z. (2013). Nanotube and graphene saturable absorbers for fibre lasers. *Nature Photonics*, *7*(11), 842-845.

Martinez, A., Fuse, K., Xu, B., & Yamashita, S. (2010). Optical deposition of graphene and carbon nanotubes in a fiber ferrule for passive mode-locked lasing. *Optics express*, *18*(22), 23054-23061.

Matsas, V. J., Newson, T. P., Richardson, D. J., & Payne, D. N. (1992). Selfstarting passively mode-locked fibre ring soliton laser exploiting nonlinear polarisation rotation. *Electron. Lett*, *28*(15), 1391-1393.

Mears, R. J., Reekie, L., Jauncey, I. M., & Payne, D. N. (1987). Low-noise erbium-doped fibre amplifier operating at 1.54 μm. *Electronics Letters*, *23*(19), 1026-1028.

Méndez, A., & Morse, T. F. (Eds.). (2011). *Specialty optical fibers handbook*. Academic Press.

Milián, C., Skryabin, D. V., & Ferrando, A. (2009). Continuum generation by dark solitons. Optics letters, 34(14), 2096-2098.

Miniscalco, W. (1991). Erbium-doped glasses for fiber amplifiers at 1500 nm. Lightwave Technology, Journal of, 9(2), 234-250.

Mizuno, K., Nishi, Y., Mimura, Y., Iida, Y., Matsuura, H., Yoon, D., ... & Yo, A. (2000). Development of etalon-type gain-flattening filter. Furukawa Electric Review, 36-41.

Moghaddam, M. R. A., Harun, S. W., Akbari, R., & Ahmad, H. (2011). Stable mode-locked fiber laser using 49 cm long bismuth oxide based erbium doped fiber and slow saturable absorber. Laser Physics, 21(5), 913-918.

Mollenauer, L. F., & Smith, K. (1988). Demonstration of soliton transmission over more than 4000 km in fiber with loss periodically compensated by Raman gain. Optics letters, 13(8), 675-677.

Mollenauer, L. F., Neubelt, M. J., Evangelides, S. G., Gordon, J. P., Simpson, J. R., & Cohen, L. G. (1990). Experimental study of soliton transmission over more than 10,000 km in dispersion-shifted fiber. *Optics letters*, *15*(21), 1203-1205.

Mori, A. (2008). Tellurite-based fibers and their applications to optical communication networks. *Journal of the Ceramic Society of Japan*,*116*(1358), 1040-1051.

Myslinski, P., Nguyen, D., & Chrostowski, J. (1997). Effects of concentration on the performance of erbium-doped fiber amplifiers. Lightwave Technology, Journal of, 15(1), 112-120.

Naji, A. W., Hamida, B. A., Cheng, X. S., Mahdi, M. A., Harun, S., Khan, S., ... & Ahmad, H. (2011). Review of Erbium-doped fiber amplifier. *International Journal of Physical Sciences*, *6*(20), 4674-4689.

Nakazawa, M., & Suzuki, K. (1995). Generation of a pseudorandom dark soliton data train and its coherent detection by one-bit-shifting with a Mach-Zehnder interferometer. *Electronics Letters*, *31*(13), 1084-1085.

Nishizawa, N., & Goto, T. (2002). Characteristics of pulse trapping by ultrashort soliton pulse in optical fibers across zerodispersion wavelength. *Optics express*, *10*(21), 1151-1160.

Nisoli, M., De Silvestri, S., Svelto, O., Szipöcs, R., Ferencz, K., Spielmann, C., ... & Krausz, F. (1997). Compression of high-energy laser pulses below 5 fs. Optics letters, 22(8), 522-524.

Olsson, B. E., Ohlen, P., Rau, L., & Blumenthal, D. J. (2000). A simple and robust 40-Gb/s wavelength converter using fiber cross-phase modulation and optical filtering. IEEE Photonics Technology Letters, 12(7), 846-848.

Pal, M., Paul, M. C., Bhadra, S. K., Das, S., Yoo, S., Kalita, M. P., ... & Sahu, J. K. (2011). Study of multichannel amplification in erbium-doped zirconia-yttria-alumino-silicate fiber. *Journal of Lightwave Technology*, *29*(14), 2109-2115.

Parvez, K., Li, R., Puniredd, S. R., Hernandez, Y., Hinkel, F., Wang, S., ... & Müllen, K. (2013). Electrochemically exfoliated graphene as solution-processable, highly conductive electrodes for organic electronics. *ACS nano*, *7*(4), 3598-3606.

Paul, M. C., Dhar, A., Das, S., Pal, M., Bhadra, S. K., Markom, A. M., ... & Harun, S. W. (2015). Enhanced Erbium–Zirconia–Yttria–Aluminum Co-Doped Fiber Amplifier. *Photonics Journal, IEEE*, *7*(5), 1-7.

Paul, M. C., Harun, S. W., Huri, N. A. D., Hamzah, A., Das, S., Pal, M., ... & Boyland, A. J. (2010). Performance comparison of Zr-based and Bi-based erbium-doped fiber amplifiers. *Optics letters*, *35*(17), 2882-2884.

Paul, M. C., Harun, S. W., Huri, N. A. D., Hamzah, A., Das, S., Pal, M., ... & Boyland, A. J. (2010). Wideband EDFA based on erbium doped crystalline zirconia yttria alumino silicate fiber. *Journal of Lightwave Technology*, *28*(20), 2919-2924.

Paul, M. C., Sobon, G., Sotor, J., Abramski, K. M., Jagiello, J., Kozinski, R., ... & Pal, M. (2013). A graphene-based mode-locked nano-engineered zirconia–yttria–aluminosilicate glass-based erbium-doped fiber laser. *Laser Physics*, *23*(3), 035110.

Peng, J., Zhan, L., Gu, Z., Qian, K., Luo, S., & Shen, Q. (2012). Direct generation of 128-fs Gaussian pulses from a compensation-free fiber laser using dual mode-locking mechanisms. *Optics Communications*, *285*(5), 731-733.

Popa, D., Sun, Z., Hasan, T., Torrisi, F., Wang, F., & Ferrari, A. C. (2010). Graphene Q-switched, tunable fiber laser. *arXiv preprint arXiv:1011.0115*.

Ramaswami, R., Sivarajan, K., & Sasaki, G. (2009). *Optical networks: a practical perspective*. Morgan Kaufmann.

Rozhin, A. G., Sakakibara, Y., Namiki, S., Tokumoto, M., Kataura, H., & Achiba, Y. (2006). Sub-200-fs pulsed erbium-doped fiber laser using a carbon nanotube-polyvinylalcohol mode locker. *Applied physics letters*, *88*(5), 051118.

Set, S. Y., Yaguchi, H., Tanaka, Y., & Jablonski, M. (2004). Ultrafast fiber pulsed lasers incorporating carbon nanotubes. Selected Topics in Quantum Electronics, IEEE Journal of, 10(1), 137-146.

Singh, R. P., & Sapre, S. D. (2008). Communication Systems, 2E. Tata McGraw-Hill Education.

Singh, S. P. (2016). Hybrid Raman/Erbium-Doped Fiber Amplifiers for WDM Transmission Systems. Journal of Optoelectronics Engineering, 4(1), 1-4.

Singh, S. P., & Singh, N. (2007). Nonlinear effects in optical fibers: Origin, management and applications. *Progress In Electromagnetics Research*, *73*, 249-275.

Sobon, G., Sotor, J., Jagiello, J., Kozinski, R., Zdrojek, M., Holdynski, M., ... & Abramski, K. M. (2012). Graphene oxide vs. reduced graphene oxide as saturable absorbers for Er-doped passively mode-locked fiber laser. *Optics express*, *20*(17), 19463-19473.

Song, C., Xu, W., Luo, Z., Luo, A., & Chen, W. (2009). Switchable and tunable dual-wavelength ultrashort pulse generation in a passively mode-locked erbium-doped fiber ring laser. *Optics Communications*, *282*(22), 4408-4412.

Song, Y. F., Guo, J., Zhao, L. M., Shen, D. Y., & Tang, D. Y. (2014). 280 GHz dark soliton fiber laser. Optics letters, 39(12), 3484-3487.

Sotor, J., Sobon, G., Macherzynski, W., Paletko, P., & Abramski, K. M. (2015). Black phosphorus saturable absorber for ultrashort pulse generation. *Applied Physics Letters*, *107*(5), 051108.

Spühler, G. J., Paschotta, R., Kullberg, M. P., Graf, M., Moser, M., Mix, E., ... & Keller, U. (2001). A passively Q-switched Yb: YAG microchip laser. *Applied Physics B*, *72*(3), 285-287.

Stegeman, G. I., Hagan, D. J., & Torner, L. (1996). χ (2) cascading phenomena and their applications to all-optical signal processing, mode-locking, pulse compression and solitons. *Optical and Quantum electronics*, *28*(12), 1691-1740.

Sun, Z., Hasan, T., & Ferrari, A. C. (2012). Ultrafast lasers mode-locked by nanotubes and graphene. *Physica E: Low-dimensional Systems and Nanostructures*, *44*(6), 1082-1091.

Sun, Z., Hasan, T., Torrisi, F., Popa, D., Privitera, G., Wang, F., ... & Ferrari, A. C. (2010). Graphene mode-locked ultrafast laser. *ACS nano*, *4*(2), 803-810.

Sylvestre, T., Coen, S., Emplit, P., & Haelterman, M. (2002). Self-induced modulational instability laser revisited: normal dispersion and dark-pulse train generation. *Optics letters*, *27*(7), 482-484.

Tan, S. J., Harun, S. W., & Ahmad, H. (2013). Controllable stretched pulse and dissipative soliton emission using non-linear polarisation rotation and cavity loss tuning mechanism. IET Optoelectronics, 7(2), 38-41.

Tan, S. J., Harun, S. W., Arof, H., & Ahmad, H. (2013). Switchable Q-switched and mode-locked erbium-doped fiber laser operating in the L-band region. *Chinese Optics Letters*, *11*(7), 073201.

Tang, D. Y., Li, L., Song, Y. F., Zhao, L. M., Zhang, H., & Shen, D. Y. (2013). Evidence of dark solitons in all-normal-dispersion-fiber lasers. *Physical Review A*, *88*(1), 013849.

Tang, D., Guo, J., Song, Y., Zhang, H., Zhao, L., & Shen, D. (2014). Dark soliton fiber lasers. *Optics express*, *22*(16), 19831-19837.

Thyagarajan, K., & Kaur, J. (2000). A novel design of an intrinsically gain flattened erbium doped fiber. *Optics communications*, *183*(5), 407-413.

Tiu, Z. C. (2015). *Development of bright and dark pulsed fiber laser based on nonlinear polarization rotation/Tiu Zian Cheak* (Doctoral dissertation, University of Malaya).

Tiu, Z. C., Ahmad, F., Tan, S. J., Ahmad, H., & Harun, S. W. (2014). Passive Q-switched Erbium-doped fiber laser with graphene–polyethylene oxide saturable absorber in three different gain media. *Indian Journal of Physics*, *88*(7), 727-731.

Tiu, Z. C., Tan, S. J., Ahmad, H., & Harun, S. W. (2014). Dark pulse emission in nonlinear polarization rotation-based multiwavelength mode-locked erbium-doped fiber laser. Chinese Optics Letters, 12(11), 113202.

Tiu, Z. C., Tan, S. J., Zarei, A., Ahmad, H., & Harun, S. W. (2014). Nonlinear Polarization Rotation-Based Mode-Locked Erbium-Doped Fiber Laser with Three Switchable Operation States. *Chinese Physics Letters*, *31*(9), 094206.

Urick, V. J., Rogge, M. S., Bucholtz, F., & Williams, K. J. (2006). Wideband (0.045–6.25 GHz) 40 km analogue fibre-optic link with ultra-high (> 40 dB) all-photonic gain. *Electronics Letters*, *42*(9), 552-553.

V. Bobrovs, J. Jelinskis, G. Ivanovs and G. Lauks, "Research of Traffic Management in Fttx Optical Communication Systems," Latvian Journal of Physics and Technical Sciences. Volume 46, Issue 2, pp. 41–55, (2009)

Vadukumpully, S., Paul, J., & Valiyaveettil, S. (2009). Cationic surfactant mediated exfoliation of graphite into graphene flakes. *Carbon*, *47*(14), 3288-3294.

Vogel, A., Hentschel, W., Holzfuss, J., & Lauterborn, W. (1986). Cavitation bubble dynamics and acoustic transient generation in ocular surgery with pulsed neodymium: YAG lasers. *Ophthalmology*, *93*(10), 1259-1269.

Wang, J., Manga, K. K., Bao, Q., & Loh, K. P. (2011). High-yield synthesis of few-layer graphene flakes through electrochemical expansion of graphite in propylene carbonate electrolyte. *Journal of the American Chemical Society*, *133*(23), 8888-8891.

Wang, X., Zhou, P., Wang, X., Xiao, H., & Liu, Z. (2014). 2 μm bright–dark pulses in Tm-doped fiber ring laser with net anomalous dispersion. Applied Physics Express, 7(2), 022704.

Wei, D., Grande, L., Chundi, V., White, R., Bower, C., Andrew, P., & Ryhänen, T. (2012). Graphene from electrochemical exfoliation and its direct applications in enhanced energy storage devices. *Chemical Communications*, *48*(9), 1239-1241.

Wei, W., Wang, G., Yang, S., Feng, X., & Müllen, K. (2015). Efficient coupling of nanoparticles to electrochemically exfoliated graphene. *Journal of the American Chemical Society*, *137*(16), 5576-5581.

Xie, X. L., Mai, Y. W., & Zhou, X. P. (2005). Dispersion and alignment of carbon nanotubes in polymer matrix: a review. *Materials Science and Engineering: R: Reports*, *49*(4), 89-112.

Xing, G., Guo, H., Zhang, X., Sum, T. C., & Huan, C. H. A. (2010). The physics of ultrafast saturable absorption in graphene. *Optics express*, *18*(5), 4564-4573.

Xu, J., Liu, J., Wu, S., Yang, Q. H., & Wang, P. (2012). Graphene oxide mode-locked femtosecond erbium-doped fiber lasers. *Optics express*, *20*(14), 15474-15480.

Yamada, M., Kanamori, T., Terunuma, Y., Oikawa, K., Shimizu, M., Sudo, S., & Sagawa, K. (1996). Fluoride-based erbium-doped fiber amplifier with inherently flat gain spectrum. *Photonics Technology Letters, IEEE*, *8*(7), 882-884.

Yang, H., Hernandez, Y., Schlierf, A., Felten, A., Eckmann, A., Johal, S., ... & Palermo, V. (2013). A simple method for graphene production based on exfoliation of graphite in water using 1-pyrenesulfonic acid sodium salt. *Carbon*, *53*, 357-365.

Yang, X., Dong, X., Zhang, S., Lu, F., Zhou, X., & Lu, C. (2005). Multiwavelength erbium-doped fiber laser with 0.8-nm spacing using sampled Bragg grating and photonic crystal fiber. *Photonics Technology Letters, IEEE*, *17*(12), 2538-2540.

Yao, J., Yao, J., Wang, Y., Tjin, S. C., Zhou, Y., Lam, Y. L., ... & Lu, C. (2001). Active mode locking of tunable multi-wavelength fiber ring laser. *Optics Communications*, *191*(3), 341-345.

Yusoff, N. M., Bakar, M. A., Sheih, S. J., Adikan, F. M., & Mahdi, M. A. (2010). Gain-flattened erbium-doped fiber amplifier with flexible selective band for optical networks. Laser physics, 20(8), 1747-1751.

Z. Luo, M. Zhou, D. Wu, C. Ye, J. Weng, J. Dong, H. Xu, Z. Cai, and L. Chen, "Graphene-induced nonlinear four-wave-mixing and its application to multiwavelength Q-switched rare-earth-doped fiber lasers," Lightwave Technology, Journal of 29, 2732-2739 (2011)

Zen, D. I. M., Saidin, N., Damanhuri, S. S. A., Harun, S. W., Ahmad, H., Ismail, M. A., ... & Pal, M. (2013). Mode-locked thulium–bismuth codoped fiber laser using graphene saturable absorber in ring cavity. *Applied optics*, *52*(6), 1226-1229.

Zhang, H., Bao, Q., Tang, D., Zhao, L., & Loh, K. (2009). Large energy soliton erbium-doped fiber laser with a graphene-polymer composite mode locker. *Applied Physics Letters*, *95*(14), 141103.

Zhang, H., Tang, D. Y., Zhao, L. M., & Wu, X. (2009). Dark pulse emission of a fiber laser. *Physical Review A*, *80*(4), 045803.

Zhang, H., Tang, D. Y., Zhao, L. M., Wu, X., Bao, Q. L., & Loh, K. P. (2009). Dark soliton fiber laser. *arXiv preprint arXiv:0903.1968*.

Zhao, J. Q., Wang, Y. G., Yan, P. G., Ruan, S. C., Zhang, G. L., Li, H. Q., & Tsang, Y. H. (2013). An L-band graphene-oxide mode-locked fiber laser delivering bright and dark pulses. *Laser Physics*, *23*(7), 075105.

Zhao, W., & Bourkoff, E. (1992). Generation, propagation, and amplification of dark solitons. JOSA B, 9(7), 1134-1144.

Zhao, X., Liu, Z. B., Yan, W. B., Wu, Y., Zhang, X. L., Chen, Y., & Tian, J. G. (2011). Ultrafast carrier dynamics and saturable absorption of solution-processable few-layered graphene oxide. *Applied Physics Letters*, *98*(12), 121905.

Zhou, D. P., Wei, L., Dong, B., & Liu, W. K. (2010). Tunable passively-switched erbium-doped fiber laser with carbon nanotubes as a saturable absorber. *Photonics Technology Letters, IEEE*, *22*(1), 9-11.

Zhu, M. Q., Zhu, L., Han, J. J., Wu, W., Hurst, J. K., & Li, A. D. (2006). Spiropyran-based photochromic polymer nanoparticles with optically switchable luminescence. *Journal of the American Chemical Society*, *128*(13), 4303-4309.

APPENDIX

A selection of published works are attached in this appendix.